

Cohesin acetyltransferase Esco2 regulates SAC and kinetochore functions via maintaining H4K16 acetylation during mouse oocyte meiosis

Yajuan Lu, Xiaoxin Dai, Mianqun Zhang, Yilong Miao, Changyin Zhou, Zhaokang Cui and Bo Xiong*

College of Animal Science and Technology, Nanjing Agricultural University, Nanjing 210095, China

Received March 22, 2017; Revised June 13, 2017; Editorial Decision June 15, 2017; Accepted June 19, 2017

ABSTRACT

Sister chromatid cohesion, mediated by cohesin complex and established by the acetyltransferases Esco1 and Esco2, is essential for faithful chromosome segregation. Mutations in Esco2 cause Roberts syndrome, a developmental disease characterized by severe prenatal retardation as well as limb and facial abnormalities. However, its exact roles during oocyte meiosis have not clearly defined. Here, we report that Esco2 localizes to the chromosomes during oocyte meiotic maturation. Depletion of Esco2 by morpholino microinjection leads to the precocious polar body extrusion, the escape of metaphase I arrest induced by nocodazole treatment and the loss of BubR1 from kinetochores, indicative of inactivated SAC. Furthermore, depletion of Esco2 causes a severely impaired spindle assembly and chromosome alignment, accompanied by the remarkably elevated incidence of defective kinetochore-microtubule attachments which consequently lead to the generation of aneuploid eggs. Notably, we find that the involvement of Esco2 in SAC and kinetochore functions is mediated by its binding to histone H4 and acetylation of H4K16 both *in vivo* and *in vitro*. Thus, our data assign a novel meiotic function to Esco2 beyond its role in the cohesion establishment during mouse oocyte meiosis.

INTRODUCTION

Cohesin is a multi-subunit protein complex which appears to form a ring that can encircle DNA (1). This complex is composed of four subunits: Smc1, Smc3, Rad21 and SA1 or SA2 (2,3). Cohesin and its regulatory proteins function in an essential pathway enabling proper cohesion, segregation of sister chromatids, double-strand break repair and transcriptional regulation (4). Cohesion is established in S phase

at which time sister chromatids are generated by DNA replication and remain linked until their separation in anaphase. The establishment of cohesion is thought to be associated with the acetylation of the Smc3 subunit (5–8). In yeast, Smc3 acetylation is essential for viability and depends on an evolutionary conserved acetyltransferase, Eco1 (9,10). Mammalian genomes encode two Eco1 orthologs, Esco1 and Esco2 (11), both of which have been shown to acetylate Smc3 (12).

Mutations in Esco2 have been shown to cause Roberts syndrome in humans (9) that is characterized phenotypically by symmetrical limb reduction, craniofacial anomalies, growth retardation, mental retardation, cardiac and renal abnormalities, as well as spontaneous abortions in females (13). Deficiency in Esco2 leads to the termination of mouse embryogenesis in the pre-implantation period (14). In addition, Esco2 has been identified as a candidate regulator of meiosis by generating the transcripts with expression profiles similar to that of Stra8 (9,15). Despite numerous recent advances in the study of Esco2, its exact role during oocyte meiosis has still remained elusive.

In the current study, we document that Esco2 is required for proper spindle assembly, chromosome alignment and K-M attachment to ensure euploidy during mouse oocyte meiotic maturation. More importantly, we find that Esco2 is implicated in Spindle Assembly Checkpoint (SAC) activity by binding to histone H4 and regulating H4K16 acetylation. Our findings indicate that Esco2 exerts a novel function beyond its role in cohesion establishment via a different target during oocyte meiosis.

MATERIALS AND METHODS

Antibodies

Rabbit polyclonal anti-Esco2 antibody were purchased from Bethyl Laboratories (Cat#: A301-689A-T); mouse monoclonal anti- α -tubulin-FITC antibody was purchased from Sigma (Cat#: F2168, T7451 and T6557); human anti-centromere antibody was purchased from Antibod-

*To whom correspondence should be addressed. Tel: +86 25 8439 9605; Fax: +86 25 8439 9605; Email: xiongbo@njau.edu.cn

ies Incorporated (Cat#: CA95617); Rabbit polyclonal anti-histone H4 antibody and rabbit polyclonal anti-histone H4 (acetyl K16) antibody were purchased from Abcam (Cat#: ab177840, ab109463). Rabbit polyclonal anti-acetyl-histone H4 (Lys5) antibody was purchased from Cell Signaling Technology (Cat#: 9672).

Oocyte collection and culture

All experiments were approved by the Animal Care and Use Committee of Nanjing Agricultural University, China and were performed in accordance with institutional guidelines. Female ICR mice (4–6 weeks) were sacrificed by cervical dislocation after intraperitoneal injections of 5 IU PMSG for 46 h. GV oocytes were collected from ovaries in M2 medium (Sigma) and then cultured further in M16 medium (Sigma) under liquid paraffin oil at 37°C in an atmosphere of 5% CO₂ incubator for *in vitro* maturation. At different time points after culture, oocytes were collected for subsequent analysis.

cRNA construct and *in vitro* transcription

Wild-type and mutant Esco2 or mutant H4 cDNA was sub-cloned into pcDNA3.1 vector, respectively. Capped cRNA was synthesized from linearized plasmid using T7 mMessage mMachine kit (ThermoFisher), and purified with MEGAclear kit (ThermoFisher). Typically, 10–12 µl of 0.5–1.0 µg/µl cRNA was injected into oocytes and then arrested at the GV stage in M16 medium containing 2.5 µM milrinone for 6 h, allowing enough time for translation, followed by releasing into milrinone-free M16 medium for further study.

Morpholino knockdown

Esco2-targeting morpholino (5'-TCTTGGAGTAC AAGTTGCCATCATC-3') was obtained from Gene Tools LLC, and then diluted to 1mM as working concentration. For knockdown experiment, about 5–10 µl of morpholino was microinjected into the cytoplasm of GV oocytes. A non-targeting morpholino (5'-CCTCTTACCTCAGTTACAATTTATA-3') was injected as a control. In order to facilitate the morpholino-mediated inhibition of mRNA translation, oocytes were arrested at GV stage in M16 medium containing 2.5 µM milrinone for 20 h and then cultured in milrinone-free M16 medium for subsequent experiments.

Immunofluorescence and confocal microscopy

Oocytes were fixed in 4% paraformaldehyde in PBS (pH 7.4) for 30 min and permeabilized in 0.5% Triton-X-100 for 20 min at room temperature. Then, oocytes were blocked with 1% BSA-supplemented PBS for 1 h and incubated with anti-Esco2 (1:50), anti- α -tubulin-FITC (1:300), anti-centromere (1:200) or anti-histone H4 (acetyl K16) (1:100) antibodies at 4°C overnight. After washing in Phosphate Buffered Saline with Tween-20 (PBST), oocytes were incubated with an appropriate secondary antibody for 1 h at room temperature. Then oocytes were counterstained with PI or Hoechst for

10 min. Finally, oocytes were mounted on glass slides and observed under a confocal microscope (Carl Zeiss 700).

For measurement of immunofluorescent intensity, the signals from both control and experimental oocytes were acquired by performing the same immunostaining procedure and setting up the same parameters of confocal microscope. Data were analyzed by Image J software.

Immunoprecipitation and immunoblotting analysis

Immunoprecipitation was carried out using 800 oocytes according to the Instructions for ProFound Mammalian Co-Immunoprecipitation Kit (ThermoFisher).

For immunoblotting, oocytes were lysed in 4 × Lithium Dodecyl Sulfate (LDS) sample buffer (ThermoFisher) containing protease inhibitor, and then separated on 10% Bis-Tris precast gels and transferred onto PVDF membranes. The blots were blocked in TBST containing 5% low fat dry milk for 1 h at room temperature and then incubated with anti-Esco2 (1:1000), anti-histone H4 (acetyl K16) (1:500), anti-histone-H4 (1:1000) or anti-Gapdh (1:5000) antibodies overnight at 4°C. After wash in TBST, the blots were incubated with HRP-conjugated secondary antibodies for 1 h at room temperature. Chemiluminescence was detected with ECL Plus (GE Healthcare) and protein bands were visualized by Tanon-3900.

In vitro acetylation assay

Full-length Esco2 and mutant Esco2-W530G cDNAs were sub-cloned into pcDNA3.1/Flag vector, respectively, and then transfected into HEK293 cells for expression, followed by flag purification. Recombinant histone H4 was purchased from NEB (Cat#: M2504S). For the *in vitro* acetylation assay, 1 µg of recombinant histone H4 was incubated with 250 ng of purified Esco2-Flag or Esco2-W530G-Flag in 50 µl of acetyltransferase assay buffer (50 mM Tris-HCl pH8.0, 10% glycerol, 10 mM butyric acid, 0.1 mM ethylenediaminetetraacetic acid, 1 mM Dithiothreitol (DTT) and 1mM Phenylmethylsulfonyl fluoride (PMSF) with or without 10 µM Ac-CoA (Sigma) at 30°C for 1 h on a rotating platform. The reaction was then stopped by adding sodium dodecyl sulphate-polyacrylamide gel electrophoresis loading buffer and analyzed by western blotting with anti-H4K16ac antibody.

Statistical analysis

All percentages from at least three repeated experiments were expressed as mean ± SEM, and the number of oocytes observed was labeled in parentheses (n). Data were analyzed by paired-samples *t*-test, which was provided by GraphPad Prism5 statistical software. The level of significance was accepted as *P* < 0.05.

RESULTS

Esco2 localizes to the chromosomes during mouse oocyte meiotic maturation

To examine the subcellular localization of Esco2 in various developmental stages during oocyte meiotic maturation,

tion, immunofluorescent staining coupled with confocal microscopy was performed. The result showed that Esco2 appeared to accumulate on the chromosomes from GVBD (germinal vesicle breakdown) to metaphase II stages (Figure 1A). The close observation revealed that Esco2 predominantly distributed along the interstitial axes of chromosomes extending over centromere regions and arm regions both proximal and distal to chiasmata (Figure 1B). In addition, another pool of Esco2 was found in the periphery of sisters of homologs (Figure 1B). The chromosome arm localization pattern of Esco2 is consistent with the cohesin subunits such as Rec8 (16), but the periphery localization pattern indicates that Esco2 might have a unique function other than that in chromosome cohesion process.

In HeLa cells, Esco2 is absent in mitosis and reappears when the cells enter S phase of the next cell cycle (17). Inconsistent with this expression pattern, we showed that the protein level of Esco2 in oocyte meiosis was increasingly up-regulated from prophase I to metaphase II stages (Figure 1C), which suggests that the role of Esco2 is not restricted to S phase in germ cells.

Esco2 is required for meiotic progression and activation of SAC during oocyte meiosis

To clearly investigate the functional roles of Esco2 in oocytes, loss-of-function experiments via gene-targeting morpholino microinjection were carried out to deplete Esco2 in oocytes. A significant decrease of Esco2 protein level was shown in Esco2-depleted oocytes compared to controls by both western blot and immunofluorescence analysis (Figure 2A and Supplementary Figure S1), suggesting that Esco2 was successfully depleted by morpholino-based silencing approach. To test if Esco2 is required for the meiotic progression, GVBD and PBE (polar body extrusion), two critical developmental events during oocyte maturation, were examined after knockdown. The quantitative results showed that there were no distinguishable differences of GVBD rate between Esco2-depleted oocytes and controls ($71.78 \pm 1.97\%$, $n = 209$ versus $76.78 \pm 2.35\%$, $n = 222$ control; Figure 2B). However, at the time point of 6, 7 and 8 h post-GVBD, a significantly higher incidence of PBE was observed in Esco2-depleted oocytes than that in control oocytes ($6.23 \pm 0.85\%$, $n = 129$ versus $0.67 \pm 0.67\%$, $n = 138$ control, $P < 0.05$; $27.18 \pm 3.45\%$, $n = 129$ versus $12.18 \pm 1.26\%$, $n = 138$ control, $P < 0.05$; $50.52 \pm 3.83\%$, $n = 129$ versus $30.77 \pm 3.40\%$, $n = 138$ control, $P < 0.05$; Figure 2C and D), suggesting that meiotic progression was accelerated and SAC was inactivated in the absence of Esco2. To rule out the possibility that premature PBE we observed was due to the off-target effects of morpholino, we expressed the exogenous Esco2 by injecting its cRNA in Esco2-depleted oocytes to monitor the meiotic progression. As expected, in the rescue oocytes, the rates of PBE at the time point of 6, 7 and 8 h post-GVBD were decreased to the control comparable levels ($2.14 \pm 0.01\%$, $n = 140$; $14.97 \pm 2.05\%$, $n = 140$; $33.52 \pm 4.15\%$, $n = 140$; Figure 2C and D).

To further confirm the SAC control by Esco2, we tested whether oocytes depleted of Esco2 would override the metaphase I arrest induced by nocodazole treatment, indicative of SAC inactivation. The result showed that only

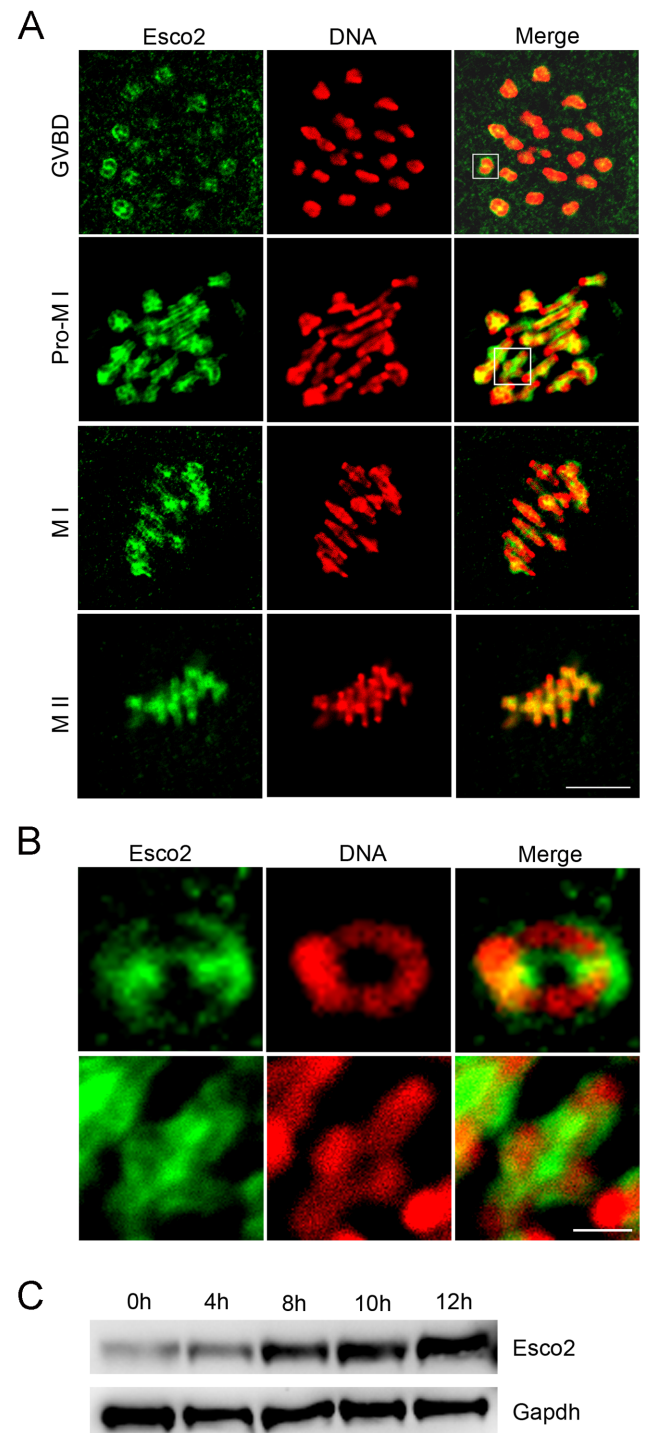


Figure 1. Subcellular localization and expression of Esco2 during mouse meiotic maturation. (A) Mouse oocytes at GVBD, prometaphase I, metaphase I and metaphase II stages were immunolabeled with anti-Esco2 antibody and counterstained with PI. Scale bar, 2.5 μm. (B) The magnified images from panel A. Scale bar, 0.5 μm. (C) Protein levels of Esco2 in oocytes corresponding to GV (0 h), GVBD (4 h), MI (8 h), ATI (10 h) and MII (12 h) stages were examined by western blot.

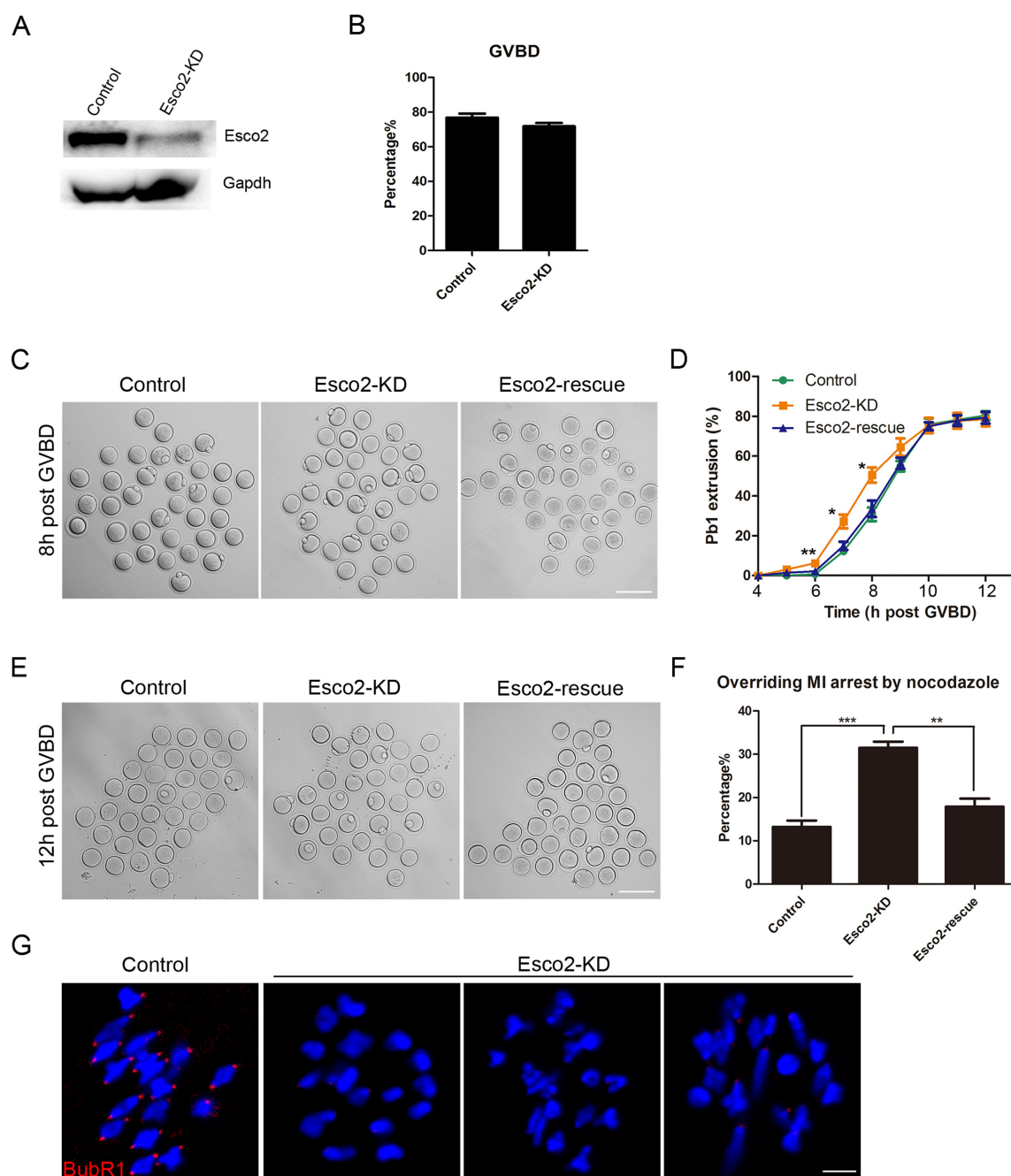


Figure 2. Effects of Esco2 depletion on the meiotic progression and SAC activity in mouse oocytes. (A) Protein levels of Esco2 in control and Esco2-KD oocytes at M I stage were examined by western blot. (B) Quantitative analysis of GVBD rate was shown in control and Esco2-KD oocytes. (C) Representative images of first polar body extrusion(PBE) in control, Esco2-KD and Esco2-rescue oocytes at the time point of 8 h post-GVBD. Scale bar, 200 μ m. (D) Quantitative analysis of PBE rate was shown in control, Esco2-KD and Esco2-rescue oocytes at consecutive time points of post-GVBD. (E) Representative images of first PBE in control, Esco2-KD and Esco2-rescue oocytes treated with low dose of nocodazole. Scale bar, 200 μ m. (F) The proportion of overriding M I arrest was recorded in control, Esco2-KD and Esco2-rescue oocytes. (G) Localization of BubR1 at prometaphase I stage in control and Esco2-KD oocytes. Scale bar, 2.5 μ m. Data of (B), (D) and (F) were presented as mean percentage (mean \pm SEM) of at least three independent experiments. Asterisk denotes statistical difference at a $P < 0.05$ level of significance.

about 13% of control oocytes could abrogate MI arrest and extrude the first polar body (Figure 2E and F). However, *Esco2*-depleted oocytes displayed a remarkably increased overriding incidence and around 31% of oocytes escaped the MI arrest to reach the MII stage ($31.49 \pm 1.44\%$, $n = 101$ versus $13.23 \pm 1.47\%$, $n = 99$ control, $P < 0.05$; Figure 2E and F). In the meantime, this increased rate of MI escape in *Esco2*-depleted oocytes could be rescued to the control indistinguishable level by expressing the exogenous *Esco2* ($17.88 \pm 1.87\%$, $n = 95$ rescue; Figure 2E and F).

Finally, we examined the SAC activity by immunostaining BubR1, an integral part of SAC complex, and its absence causes the loss of SAC control (18). As shown in Figure 2G, BubR1 was localized to the unattached kinetochores at prometaphase I stage in control oocytes. However, BubR1 was lost from most of kinetochores in *Esco2*-depleted oocytes, indicating that *Esco2* depletion impairs the SAC complex and activity.

Taken together, the above results indicate that *Esco2* is implicated in the activation of SAC during meiotic progression.

***Esco2* is necessary for spindle assembly and chromosome alignment during oocyte meiosis**

We next examined the spindle assembly and chromosome alignment in *Esco2*-depleted oocytes. To this end, mouse oocytes from control and *Esco2*-depleted groups were immunolabeled with anti- α -tubulin antibody to visualize the spindle morphologies and counterstained with PI to observe the chromosome alignment. We found a significant increased percentage of spindle defects ($76.60 \pm 4.51\%$, $n = 94$ versus $18.97 \pm 1.83\%$, $n = 95$ control, $P < 0.05$; Figure 3A and B) and chromosome misalignment ($76.67 \pm 2.46\%$, $n = 94$ versus $23.11 \pm 1.69\%$, $n = 95$ control, $P < 0.05$; Figure 3A and C) in *Esco2*-depleted oocytes, exhibiting diverse malformed spindle morphologies with several scattered or lagging chromosomes (Figure 3A). By striking contrast, control oocytes at MI stage usually show a typical barrel-shape spindle and well-aligned chromosomes at the equator (Figure 3A). In addition, we measured the width of chromosome plate at MI stage and found it remarkably wider in *Esco2*-depleted oocytes than the controls ($23.46 \pm 0.51\%$, $n = 94$ versus $13.01 \pm 0.39\%$, $n = 95$ control, $P < 0.05$; Figure 3D). Consistent with the defective MI spindle assembly, MII spindles also displayed a substantially higher rate of abnormality after *Esco2* depletion ($74.44 \pm 4.84\%$, $n = 90$ versus $21.11 \pm 2.94\%$, $n = 84$ control, $P < 0.05$; Supplementary Figure S2).

***Esco2* maintains the stability of K-MT attachments and prevents the incidence of aneuploidy in oocytes**

The high percentage of spindle/chromosome abnormalities predicts the compromised K-MT attachments in *Esco2*-depleted oocytes. To test it, oocytes were exposed to cold treatment for inducing depolymerization of microtubules that are not attached to kinetochores and then immunolabeled with CREST to show kinetochores, with anti- α -tubulin-FITC antibody to visualize microtubule fibers and counterstained with Hoechst to observe chromosomes as

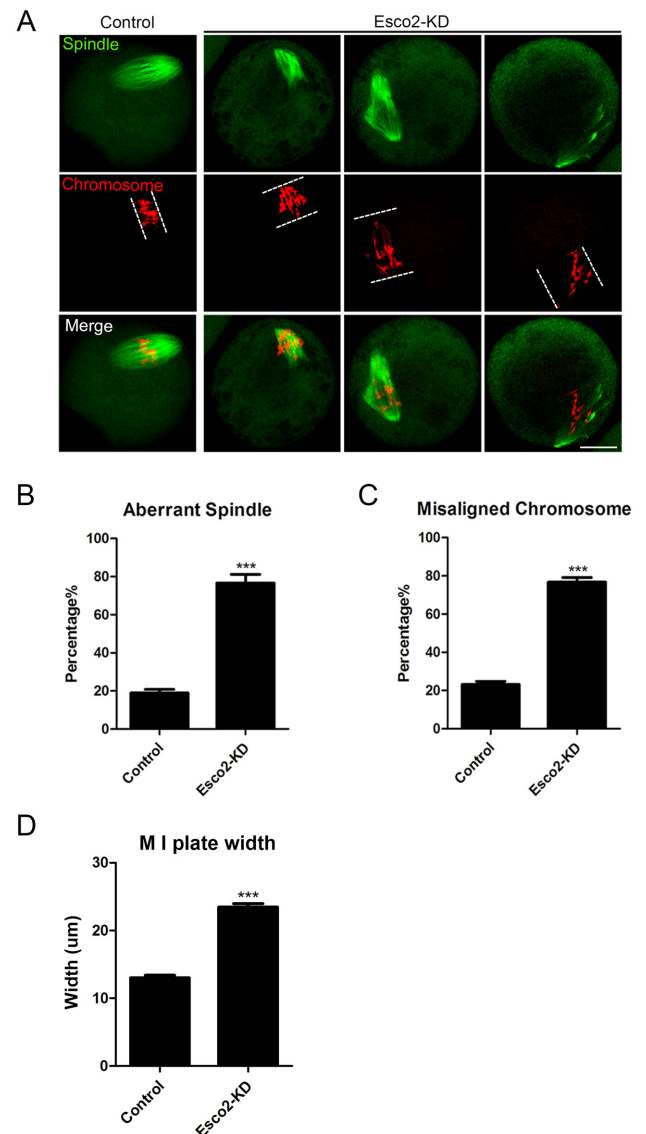


Figure 3. Depletion of *Esco2* causes spindle/chromosome abnormalities in mouse oocytes. (A) Representative images of spindle morphologies and chromosome alignment in control and *Esco2*-KD oocytes. Scale bar, 20 μ m. (B) The proportion of abnormal spindles was recorded in control and *Esco2*-KD oocytes. (C) The proportion of misaligned chromosomes was recorded in control and *Esco2*-KD oocytes. (D) The width of M I plate was measured in control and *Esco2*-KD oocytes. Data of (B–D) were presented as mean percentage (mean \pm SEM) of at least three independent experiments. Asterisk denotes statistical difference at a $P < 0.05$ level of significance.

described previously (19). We observed a prominently elevated frequency of kinetochores with very few cold-stable microtubules in *Esco2*-depleted oocytes (Figure 4A). By performing quantitative analysis, it was shown that depletion of *Esco2* substantially increased the proportion of impaired K-MT attachments compared to control oocytes to 78 from 29% ($78.59 \pm 1.81\%$, $n = 70$ versus $29.44 \pm 2.42\%$, $n = 64$ control, $P < 0.05$; Figure 4B). These K-MT attachment errors would inevitably result in the establishment of unstable chromosome biorientation, which is consistent

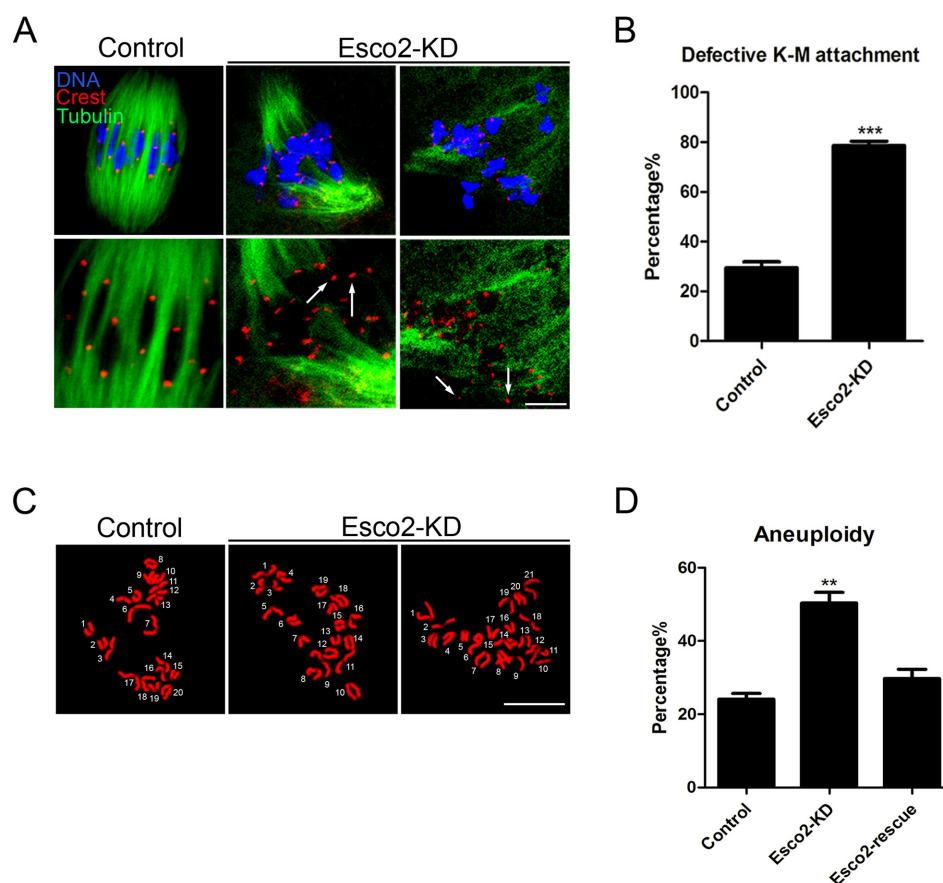


Figure 4. Depletion of Esco2 compromises K-M attachments and generates aneuploidy in mouse oocytes. (A) Representative images of kinetochore-microtubule attachments in control and Esco2-KD oocytes. Oocytes were immunostained with anti- α -tubulin-FITC antibody to visualize spindles, with CREST to visualize kinetochores and counterstained with Hoechst to visualize chromosomes. Scale bar, 5 μ m. (B) The rate of defective kinetochore-microtubule attachments was recorded in control and Esco2-KD oocytes. (C) Representative images of euploid and aneuploid MII eggs. Chromosome spread was performed to count the number of chromosomes in control and Esco2-KD oocytes. Chromosomes were counterstained with Hoechst. Scale bar, 2.5 μ m. (D) The rate of aneuploid eggs was recorded in control and Esco2-KD oocytes. Data of (B and D) were presented as mean percentage (mean \pm SEM) of at least three independent experiments. Asterisk denotes statistical difference at a $P < 0.05$ level of significance.

with the above observation of aneuploidy in the absence of Esco2.

To ask if the loss of Esco2 would generate aneuploidy in oocytes, karyotypic analysis of MII eggs was performed by chromosome spreading. We found that a large proportion of control oocytes had correct number of univalents to maintain the euploidy (Figure 4C). However, the incidence of aneuploid eggs that had more or less 20 univalents in Esco2-depleted oocytes increased about two fold compared to that in controls ($50.37 \pm 2.92\%$, $n = 49$ versus $24.13 \pm 1.56\%$, $n = 50$ control, $P < 0.05$, Figure 4D), suggesting that Esco2 is required to protect oocytes from aneuploidy. Consistently, in the rescue oocytes, the rate of aneuploidy was reduced to the normal level that was comparable to controls ($29.78 \pm 2.48\%$, $n = 37$; Figure 4D). Therefore, these observations reveal that loss of Esco2 inactivates SAC in oocytes, consequently generating aneuploid eggs.

Esco2 binds to histone H4 and is required for maintaining the acetylation status of H4K16 in oocytes

The involvement of Esco2 in activation of SAC and kine-

tochore functions prompted us to further explore the underlying mechanisms. On the other hand, it has been recently reported that H4K16 acetylation plays an important role in establishment of functional kinetochore in mouse oocytes (20,21), we thus hypothesized that Esco2 might participate in the SAC and kinetochore functions by maintaining the status of H4K16 acetylation during oocyte meiosis. To verify this possibility, we first examined the acetylation level of H4K16 by immunostaining analysis. The quantitative result of fluorescence intensity showed that signals of H4K16 acetylation were remarkably reduced in Esco2-depleted oocytes in comparison with controls (17.32 ± 2.07 , $n = 51$ versus 35.30 ± 3.31 , $n = 51$ control, $P < 0.05$; Figure 5A and B), but restored to the level indistinguishable from controls following the expression of exogenous Esco2 cRNA (30.04 ± 3.22 , $n = 45$; Figure 5A and B). However, the acetylation level of H4K16 could not be restored in Esco2-depleted oocytes exogenously expressing Esco2-W530G mutant cRNA (16.71 ± 2.23 , $n = 42$; Figure 5A and B), which corresponds to its conserved mutation Esco2-W539G in human cells that has been found to result in

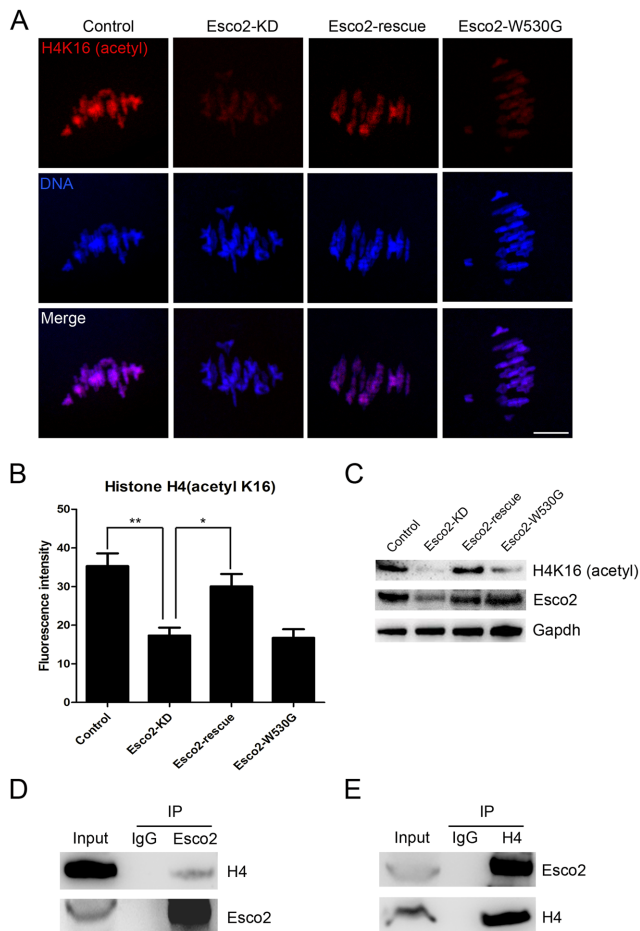


Figure 5. Esco2 binds to histone H4 to regulate the acetylation level of H4K16. (A) Representative images of acetylated H4K16 in control, Esco2-KD, Esco2-rescue and Esco2-W530G oocytes. Scale bar, 5 μ m. (B) The immunofluorescence intensity of acetylated H4K16 was recorded in control, Esco2-KD, Esco2-rescue and Esco2-W530G oocytes. Data were presented as mean percentage (mean \pm SEM) of at least three independent experiments. Asterisk denotes statistical difference at a $P < 0.05$ level of significance. (C) Acetylation levels of H4K16 in control, Esco2-KD, Esco2-rescue and Esco2-W530G oocytes were examined by western blotting. (D) IP was performed with the Esco2 antibody, and the blots of IP eluate were probed with anti-Esco2 and anti-histone H4 antibodies, respectively. (E) IP was performed with the histone H4 antibody, and the blots of IP eluate were probed with anti-Esco2 and anti-histone H4 antibodies, respectively.

loss of acetyltransferase activity (22,23). These observations were further confirmed by the western blotting analysis (Figure 5C), implying that H4K16 is the potential substrate of Esco2 in oocytes. We also detected the acetylation level of H4K5 by western blotting and found it unaffected in Esco2-depleted oocytes, suggesting that Esco2 specifically targets H4K16 (Supplementary Figure S3). Moreover, we carried out Co-IP to determine the interaction between Esco2 and histone H4. Immunoprecipitation was first performed with Esco2 antibody. The blot of IP eluate probed by Esco2 antibody showed that Esco2 was specifically present in the antibody group instead of IgG control group (Figure 5D), suggesting that the complex containing Esco2 was pulled down in the eluate. Meanwhile, the blot probed by H4 antibody also showed the exclusive presence of H4 in

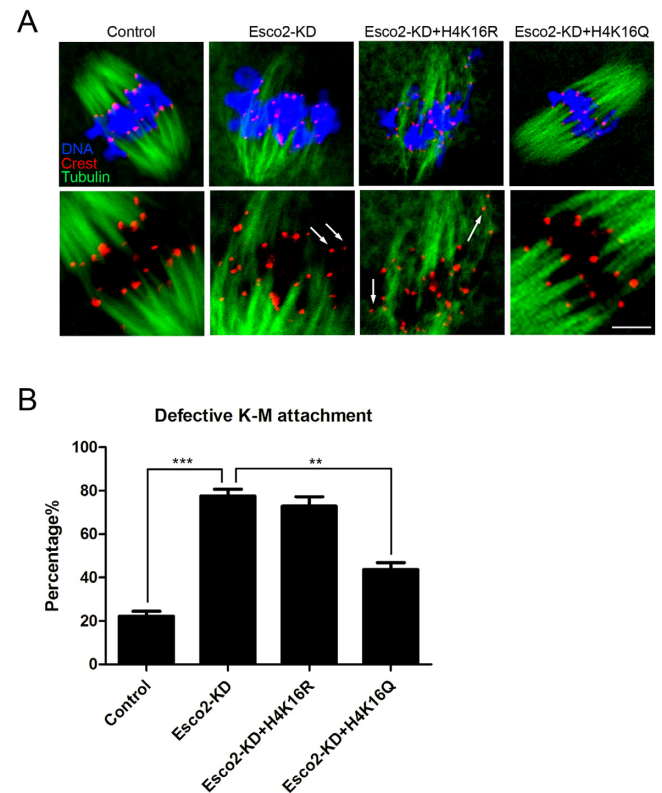


Figure 6. H4K16Q rescues the defect of K-M attachments in Esco2-depleted oocytes. (A) Representative images of kinetochore-microtubule attachments in control, Esco2-KD, Esco2-KD+H4K16R and Esco2-KD+H4K16Q oocytes. Scale bar, 5 μ m. (B) The rate of defective kinetochore-microtubule attachments was recorded in control, Esco2-KD, Esco2-KD+H4K16R and Esco2-KD+H4K16Q oocytes. Data were presented as mean percentage (mean \pm SEM) of at least three independent experiments. Asterisk denotes statistical difference at a $P < 0.05$ level of significance.

the antibody group (Figure 5D). Reciprocally, Esco2 was specifically present in the IP eluate which was pulled down by H4 antibody (Figure 5E), indicating that Esco2 associates with H4 in oocytes. Additionally, we tested whether acetylation status of H4K16 would affect the kinetochore-microtubule attachments in Esco2-depleted oocytes. The result showed that H4K16Q acetylmimic mutation but not H4K16R non-acetylatable mutation restored the impaired the kinetochore-microtubule attachments in the Esco2-depleted oocytes (Control: $22.22 \pm 2.22\%$ $n = 45$, Esco2-KD: $77.56 \pm 3.09\%$ $n = 40$, Esco2-KD + H4K16R: $72.84 \pm 4.36\%$ $n = 48$, Esco2-KD + H4K16Q: $43.73 \pm 3.16\%$ $n = 50$; Figure 6A and B). Collectively, the alteration of H4K16 acetylation in Esco2-depleted oocytes may perturb the chromatin conformation and kinetochore function, contributing, at least in part, to the spindle defects, chromosome misalignment and SAC activity during meiosis. Certainly we cannot rule out the possibility that Esco2 acts on other targets in this process. Future investigations will be required to uncover these details.

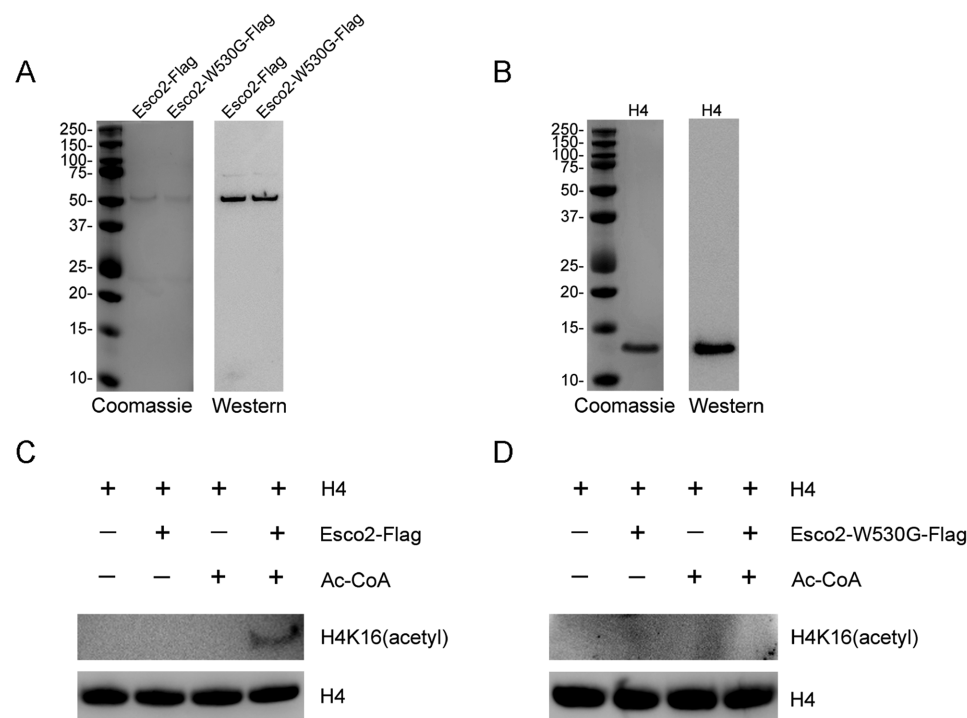


Figure 7. Esco2 acetylates histone H4 at Lys16 *in vitro*. (A) Flag purification of Esco2. Esco2 and enzymatically mutant Esco2-W530G were expressed in HEK293 cells and then purified according to the Flag purification procedure. Purified Esco2-Flag and Esco2-W530G-Flag were detected with sodium dodecyl sulphate-polyacrylamide gel electrophoresis followed by both coomassie staining and western blotting with anti-Esco2 antibody. (B) Commercially obtained recombinant histone H4 was identified by both coomassie staining and western blotting with anti-H4 antibody. (C) *In vitro* acetylation assay with Esco2-Flag. Recombinant histone H4 was incubated with or without purified Esco2-Flag and Ac-CoA in the acetyltransferase assay buffer at 30°C for 1 h. The reactions were analyzed by western blotting with anti-histone H4 (acetyl K16) antibody for acetylation levels of H4K16 and anti-histone H4 antibody as a loading control. (D) *In vitro* acetylation assay with Esco2-W530G-Flag. Recombinant histone H4 was incubated with or without purified Esco2-W530G-Flag and Ac-CoA in the acetyltransferase assay buffer at 30°C for 1 h. The reactions were analyzed by western blotting with anti-histone H4 (acetyl K16) antibody for acetylation levels of H4K16 and anti-histone H4 antibody as a loading control.

Esco2 acetylates histone H4 at Lys16 *in vitro*

To determine whether Esco2 can directly acetylate H4 at Lys16, both Esco2-Flag and enzymatically dead Esco2-W530G-Flag were purified from HEK293 cells by flag purification. In the coomassie stained gel, the bands in Esco2-Flag and Esco2-W530G-Flag lanes were specifically present in the same position which were further confirmed by western blotting with anti-Esco2 antibody (Figure 7A). Recombinant histone H4 was purified from *E. coli* and also identified by coomassie staining and western blotting analysis (Figure 7B).

We next performed *in vitro* acetylation assay using the purified proteins. We found that recombinant histone H4 was acetylated at Lys16 in the presence of both Esco2-Flag and Ac-CoA in an *in vitro* assay system (Figure 7C). By contrast, under the same conditions Esco2-W530G-Flag had no acetyltransferase activity toward the recombinant histone H4 (Figure 7D). Thus, this observation provides the direct evidence that Esco2 targets histone H4 at Lys16.

DISCUSSION

The well-known role of Esco2 is mediating the acetylation of cohesin subunit Smc3 to establish the chromosome cohesion in S phase, ensuring the proper chromosome segregation to maintain the genome stability. In mammalian

females, chromosome cohesion is established when meiotic DNA replication and recombination occur in fetal oocytes. After birth, oocytes arrest at the prolonged prophase I stage until recruited to grow into mature oocytes that divide at ovulation, but bivalent cohesion is maintained without detectable turnover (24,25). Thus, during the developmental window of oocyte meiotic maturation, chromosome cohesion does not require Esco2 to exert any function as the establishment factor. Because of the nature of acetyltransferase, Esco2 must have several unknown substrates that function in other biological processes. In the present study, we have determined a distinctive role of Esco2 during mouse oocyte meiotic maturation instead of a cohesion establishment factor.

Eco1 in budding yeast localizes to chromosomes throughout the cell cycle (26). In both HeLa cells and 293T cells, ~70% of the endogenous Esco2 associates with chromosomes and the rest are found in the soluble fractions that are contributed by the cytoplasmic Esco2 fractions (17). During meiosis Esco2 is reported to localize to the XY body in spermatocytes and accumulate to chromatin regions containing double-stranded breaks in the embryonic ovary (27). Our findings showed that Esco2 has two pools of localization patterns on the chromosomes during oocyte meiotic maturation. The localization along the interstitial axes of chromosomes is the same as the

cohesin subunits. The periphery of sisters of homologs localization which covers the region that the kinetochore localizes at the chromosome indicates that Esco2 might be involved in other biological events such as the regulation of kinetochore functions. In addition, the protein expression of Esco2 during oocyte meiosis is different from that in mitosis. Esco2 degrades in the remainder of cell cycle after S phase in mitotic cells (17). However, we found that the protein level of Esco2 increases from prophase I to metaphase II stages in mouse oocytes, which predicts that the Esco2 has the additional functions beyond S phase during oocyte meiosis.

To ask whether Esco2 has a distinctive role during oocyte maturation, we depleted Esco2 by the morpholino-based gene silencing in oocytes. We found that Esco2 is not indispensable for the meiotic progression but is required for SAC activation as depletion of Esco2 caused the premature PBE, the escape of M I arrest induced by nocodazole and the loss of BubR1 from kinetochores. These observations are in line with the previous studies in mouse oocytes that loss of SAC components leads to the strong acceleration of meiosis I and severe chromosome missegregations (18,28,29). Also, compared with mitosis, SAC is not very efficient in meiosis, and the presence of one or few incorrectly attached kinetochores with reduced K-MT tension escapes checkpoint detection in mouse oocytes (30–32). Since SAC inactivation is usually accompanied by the defects of spindle/chromosome abnormalities, we thus examined the spindle assembly and chromosome alignment in the absence of Esco2. The findings revealed that Esco2 plays a critical role in the maintenance of normal spindle formation, chromosome alignment and kinetochore-microtubule attachment, thereby ensuring euploidy during oocyte meiosis. It has been reported that SAC activity is dependent on the cohesin in the oocyte but not in zygote, suggesting that this dependence is a feature specific to the oocyte (33,34). Our data further demonstrates that cohesin regulator Esco2 is also involved in the regulation of SAC in the oocyte. Then another question is raised: what is the downstream effector of Esco2 that mediates this process? Because acetylation of H4K16 has been shown to participate in the establishment of functional kinetochores in mouse oocytes (20,21), we then tested whether Esco2 acts as a SAC regulator via maintaining the acetylation level of H4K16. Our findings manifested that Esco2 associates with histone H4 and is required for H4K16 acetylation. WT but not catalytically dead mutation of Esco2 could rescue the reduced acetylation level of H4K16 in depletion of Esco2. Also, H4K16Q acetylmimic mutation but not H4K16R non-acetylatable mutation restored the compromised the kinetochore-microtubule attachment in the Esco2-depleted oocytes. More importantly, we performed the *in vitro* acetylation assay using the purified proteins to show that Esco2 can directly acetylate histone H4 at Lys16. Therefore, we demonstrate that Esco2 maintains the acetylation status of H4K16 to take part in the kinetochore functions.

Collectively, we provide a body of evidence that Esco2 plays an important role in the kinetochore functions for SAC activity to ensure the euploidy via binding to histone H4 to regulate H4K16 acetylation status in mouse oocytes.

These observations uncover a novel meiotic function to Esco2 beyond its role in chromosome cohesion.

SUPPLEMENTARY DATA

Supplementary Data are available at NAR Online.

ACKNOWLEDGEMENTS

We thank Dr Shaochen Sun for extensive advice and constructive comments on the manuscript.

FUNDING

National Natural Science Foundation of China [31571545]; Natural Science Foundation of Jiangsu Province [BK20150677]. Funding for open access charge: National Natural Science Foundation of China [31571545].
Conflict of interest statement. None declared.

REFERENCES

- Xiong, B. and Gerton, J.L. (2010) Regulators of the cohesin network. *Annu. Rev. Biochem.*, **79**, 131–153.
- Onn, I., Heidinger-Pauli, J.M., Guacci, V., Unal, E. and Koshland, D.E. (2008) Sister chromatid cohesion: a simple concept with a complex reality. *Annu. Rev. Cell Dev. Biol.*, **24**, 105–129.
- Nasmyth, K. and Haering, C.H. (2009) Cohesin: its roles and mechanisms. *Annu. Rev. Genet.*, **43**, 525–558.
- Saito, Y., Zhou, H. and Kobayashi, J. (2016) Chromatin modification and NBS1: their relationship in DNA double-strand break repair. *Genes Genet. Syst.*, **90**, 195–208.
- Rolef Ben-Shahar, T., Heeger, S., Lehane, C., East, P., Flynn, H., Skehel, M. and Uhlmann, F. (2008) Eco1-dependent cohesin acetylation during establishment of sister chromatid cohesion. *Science*, **321**, 563–566.
- Unal, E., Heidinger-Pauli, J.M., Kim, W., Guacci, V., Onn, I., Gygi, S.P. and Koshland, D.E. (2008) A molecular determinant for the establishment of sister chromatid cohesion. *Science*, **321**, 566–569.
- Rowland, B.D., Roig, M.B., Nishino, T., Kurze, A., Uluocak, P., Mishra, A., Beckouet, F., Underwood, P., Metson, J., Imre, R. *et al.* (2009) Building sister chromatid cohesion: smc3 acetylation counteracts an antiestablishment activity. *Mol. Cell*, **33**, 763–774.
- Sutani, T., Kawaguchi, T., Kanno, R., Itoh, T. and Shirahige, K. (2009) Budding yeast Wpl1(Rad61)-Pds5 complex counteracts sister chromatid cohesion-establishing reaction. *Curr. Biol.*, **19**, 492–497.
- Vega, H., Waisfisz, Q., Gordillo, M., Sakai, N., Yanagihara, I., Yamada, M., van Gosliga, D., Kayserili, H., Xu, C., Ozono, K. *et al.* (2005) Roberts syndrome is caused by mutations in ESCO2, a human homolog of yeast ECO1 that is essential for the establishment of sister chromatid cohesion. *Nat. Genet.*, **37**, 468–470.
- Cao, Q., Wang, Y., Chen, F., Xia, Y., Lou, J., Zhang, X., Yang, N., Sun, X., Zhang, Q., Zhuo, C. *et al.* (2014) A novel signal transduction pathway that modulates rhl quorum sensing and bacterial virulence in *Pseudomonas aeruginosa*. *PLoS Pathog.*, **10**, e1004340.
- Whelan, G., Kreidl, E., Peters, J.M. and Eichele, G. (2012) The non-redundant function of cohesin acetyltransferase Esco2: some answers and new questions. *Nucleus*, **3**, 330–334.
- Nishiyama, T., Ladurner, R., Schmitz, J., Kreidl, E., Schleiffer, A., Bhaskara, V., Bando, M., Shirahige, K., Hyman, A.A., Mechtler, K. *et al.* (2010) Sororin mediates sister chromatid cohesion by antagonizing Wapl. *Cell*, **143**, 737–749.
- Goh, E.S., Li, C., Horsburgh, S., Kasai, Y., Kolomietz, E. and Morel, C.F. (2010) The Roberts syndrome/SC phocomelia spectrum—a case report of an adult with review of the literature. *Am. J. Med. Genet. A*, **152**, 472–478.
- Whelan, G., Kreidl, E., Wutz, G., Egner, A., Peters, J.M. and Eichele, G. (2012) Cohesin acetyltransferase Esco2 is a cell viability factor and is required for cohesion in pericentric heterochromatin. *EMBO J.*, **31**, 71–82.

15. Hogarth, C.A., Mitchell, D., Evanoff, R., Small, C. and Griswold, M. (2011) Identification and expression of potential regulators of the mammalian mitotic-to-meiotic transition. *Biol. Reprod.*, **84**, 34–42.
16. Rong, M., Matsuda, A., Hiraoka, Y. and Lee, J. (2016) Meiotic cohesin subunits RAD21L and REC8 are positioned at distinct regions between lateral elements and transverse filaments in the synaptonemal complex of mouse spermatocytes. *J. Reprod. Dev.*, **62**, 623–630.
17. Hou, F. and Zou, H. (2005) Two human orthologues of Eco1/Ctf7 acetyltransferases are both required for proper sister-chromatid cohesion. *Mol. Biol. Cell*, **16**, 3908–3918.
18. Touati, S.A., Buffin, E., Cladiere, D., Hached, K., Rachez, C., van Deursen, J.M. and Wassmann, K. (2015) Mouse oocytes depend on BubR1 for proper chromosome segregation but not for prophase I arrest. *Nat. Commun.*, **6**, 6946–6958.
19. Ma, R., Hou, X., Zhang, L., Sun, S.C., Schedl, T., Moley, K. and Wang, Q. (2014) Rab5a is required for spindle length control and kinetochore-microtubule attachment during meiosis in oocytes. *FASEB J.*, **28**, 4026–4035.
20. Choy, J.S., Acuna, R., Au, W.C. and Basrai, M.A. (2011) A role for histone H4K16 hypoacetylation in *Saccharomyces cerevisiae* kinetochore function. *Genetics*, **189**, 11–21.
21. Ma, P. and Schultz, R.M. (2013) Histone deacetylase 2 (HDAC2) regulates chromosome segregation and kinetochore function via H4K16 deacetylation during oocyte maturation in mouse. *PLoS Genet.*, **9**, e1003377.
22. van der Lelij, P., Godthelp, B.C., van Zon, W., van Gosliga, D., Oostra, A.B., Steltenpool, J., de Groot, J., Scheper, R.J., Wolthuis, R.M., Waisfisz, Q. *et al.* (2009) The cellular phenotype of Roberts syndrome fibroblasts as revealed by ectopic expression of ESCO2. *PLoS One*, **4**, e6936.
23. Gordillo, M., Vega, H., Trainer, A.H., Hou, F., Sakai, N., Luque, R., Kayserili, H., Basaran, S., Skovby, F., Hennekam, R.C. *et al.* (2008) The molecular mechanism underlying Roberts syndrome involves loss of ESCO2 acetyltransferase activity. *Hum. Mol. Genet.*, **17**, 2172–2180.
24. Burkhardt, S., Borsos, M., Szydłowska, A., Godwin, J., Williams, S.A., Cohen, P.E., Hirota, T., Saitou, M. and Tachibana-Konwalski, K. (2016) Chromosome cohesion established by Rec8-cohesin in fetal oocytes is maintained without detectable turnover in oocytes arrested for months in mice. *Curr. Biol.*, **26**, 678–685.
25. Tachibana-Konwalski, K., Godwin, J., van der Weyden, L., Champion, L., Kudo, N.R., Adams, D.J. and Nasmyth, K. (2010) Rec8-containing cohesin maintains bivalents without turnover during the growing phase of mouse oocytes. *Genes Dev.*, **24**, 2505–2516.
26. Toth, A., Ciosk, R., Uhlmann, F., Galova, M., Schleiffer, A. and Nasmyth, K. (1999) Yeast cohesin complex requires a conserved protein, Eco1p(Ctf7), to establish cohesion between sister chromatids during DNA replication. *Genes Dev.*, **13**, 320–333.
27. Evans, E.B., Hogarth, C., Evanoff, R.M., Mitchell, D., Small, C. and Griswold, M.D. (2012) Localization and regulation of murine Esco2 during male and female meiosis. *Biol. Reprod.*, **87**, 61–68.
28. Hached, K., Xie, S.Z., Buffin, E., Cladiere, D., Rachez, C., Sacras, M., Sorger, P.K. and Wassmann, K. (2011) Mps1 at kinetochores is essential for female mouse meiosis I. *Development*, **138**, 2261–2271.
29. McGuinness, B.E., Anger, M., Kouznetsova, A., Gil-Bernabe, A.M., Helmhart, W., Kudo, N.R., Wuensche, A., Taylor, S., Hoog, C., Novak, B. *et al.* (2009) Regulation of APC/C activity in oocytes by a Bub1-dependent spindle assembly checkpoint. *Curr. Biol.*, **19**, 369–380.
30. Nagaoka, S.I., Hodges, C.A., Albertini, D.F. and Hunt, P.A. (2011) Oocyte-specific differences in cell-cycle control create an innate susceptibility to meiotic errors. *Curr. Biol.*, **21**, 651–657.
31. Lane, S.I., Yun, Y. and Jones, K.T. (2012) Timing of anaphase-promoting complex activation in mouse oocytes is predicted by microtubule-kinetochore attachment but not by bivalent alignment or tension. *Development*, **139**, 1947–1955.
32. Gui, L. and Homer, H. (2012) Spindle assembly checkpoint signalling is uncoupled from chromosomal position in mouse oocytes. *Development*, **139**, 1941–1946.
33. Percival, S.M. and Parant, J.M. (2016) Observing mitotic division and dynamics in a live zebrafish embryo. *J. Vis. Exp.*, **113**, e54218.
34. Tachibana-Konwalski, K., Godwin, J., Borsos, M., Rattani, A., Adams, D.J. and Nasmyth, K. (2013) Spindle assembly checkpoint of oocytes depends on a kinetochore structure determined by cohesin in meiosis I. *Curr. Biol.*, **23**, 2534–2539.

Melatonin protects oocyte quality from Bisphenol A-induced deterioration in the mouse

Mianqun Zhang | Xiaoxin Dai | Yajuan Lu | Yilong Miao | Changyin Zhou |
Zhaokang Cui | Honglin Liu | Bo Xiong 

College of Animal Science and
Technology, Nanjing Agricultural
University, Nanjing, China

Correspondence

Bo Xiong, College of Animal Science
and Technology, Nanjing Agricultural
University, Nanjing, China.
Email: xiongbo@njau.edu.cn

Funding information

This work was supported by the
National Natural Science Foundation
of China (31571545) and the Natural
Science Foundation of Jiangsu Province
(BK20150677)

Abstract

Bisphenol A (BPA) has been reported to adversely affect the mammalian reproductive system in both sexes. However, the underlying mechanisms regarding how BPA disrupts the mammalian oocyte quality and how to prevent it have not been fully defined. Here, we document that BPA weakens oocyte quality by impairing both oocyte meiotic maturation and fertilization ability. We find that oral administration of BPA (100 µg/kg body weight per day for 7 days) compromises the first polar body extrusion (78.0% vs 57.0%, $P < .05$) by disrupting normal spindle assembly, chromosome alignment, and kinetochore-microtubule attachment. This defect could be remarkably ameliorated (76.7%, $P < .05$) by concurrent oral administration of melatonin (30 mg/kg body weight per day for 7 days). In addition, BPA administration significantly decreases the fertilization rate of oocytes (87.2% vs 41.1%, $P < .05$) by reducing the number of sperm binding to the zona pellucida, which is consistent with the premature cleavage of ZP2 as well as the mis-localization and decreased protein level of ovastacin. Also, the localization and protein level of Juno, the sperm receptor on the egg membrane, are strikingly impaired in BPA-administered oocytes. Finally, we show that melatonin administration substantially elevates the in vitro fertilization rate (63.0%, $P < .05$) by restoring above defects of fertilization proteins and events, which might be mediated by the improvement of oocyte quality via reduction of ROS levels and inhibition of apoptosis. Collectively, our data reveal that melatonin has a protective action against BPA-induced deterioration of oocyte quality in mice.

KEYWORDS

Bisphenol A, fertilization, Juno, melatonin, oocyte maturation, ovastacin, spindle assembly

1 | INTRODUCTION

Bisphenol A (BPA), a widely used chemical in the production of polycarbonate plastics and epoxy resins, is found extensively in food containers, adhesives, and dental sealants¹⁻⁴ and has been detected in food and water consumed by animals and humans.⁵ BPA has been demonstrated to be carcinogenic for causing aneuploidy in both cell culture and animal models.⁴⁻⁸ Human exposure to BPA through the food chain is widespread and continuous,⁹ because BPA is released by

food and beverage containers, especially when heated⁹ or cleaned with harsh detergents or when they contain acidic, and it can accumulate in the body fat.¹⁰ Accumulating experimental evidence has shown that BPA has adverse effects on the female reproductive system. It has been reported that BPA is an ovarian toxicant that is likely to act through multiple pathways including lipid peroxidation and generation of free radicals causing oxidative stress and apoptosis.¹¹ Low dose of BPA exposure during the pre-implantation period significantly reduces the pregnancy rate in the mouse.¹² BPA

also alters oviduct morphology and gene expression, which might impair development and transport of the conceptus from the oviduct to the uterus.¹³ Furthermore, BPA affects uterine morphology and function and may transmit these changes for several generations through mechanisms that involve cell proliferation and receptivity.^{14,15}

Melatonin (5-methoxy-*N*-acetyltryptamine) is a natural hormone that is primarily released by the pineal gland to the circulation.¹⁶ It participates in the circadian and circannual rhythms such as the sleep/wake cycle and regulates seasonal reproductive activity.¹⁷⁻¹⁹ In addition, numerous studies have revealed that melatonin and its derivatives exert various biological activities such as antioxidative,²⁰⁻²³ anti-inflammatory,²⁴⁻²⁷ and anti-apoptotic effects,²⁸⁻³⁰ as well as the regulation of cytoskeletal organization.³¹ As a robust antioxidant, melatonin readily scavenges the most toxic free radical, hydroxyl radical, peroxy radical, peroxyxynitrite anion, nitric oxide, and singlet oxygen to prevent the deterioration of cellular membranes and reduce the lipid peroxidation.³²⁻³⁶ Notably, melatonin also plays an important role in regulation of follicle development and ovarian function in different mammalian species.^{20,22,37-40} In fact, melatonin has been found in the human follicle fluid and may be produced from the ovary and granulosa cells.⁴¹ It is necessary to maintain high concentrations of melatonin in large pre-ovulatory follicles to protect oocytes from oxidative stress that accompanies ovulation, a process known to generate free oxygen radicals.⁴²⁻⁴⁴

Despite a number of studies that have reported the potential toxic effects of BPA and potential protective effects of melatonin on the female reproductive system in the past years, whether melatonin is able to protect the oocytes against BPA-induced damage is still unknown. Therefore, in this study, we evaluated the oocyte quality from control, BPA-exposed, and “BPA+melatonin”-administered groups by investigating their oocyte meiotic maturation and fertilization ability. We examined the critical events during meiotic maturation including germinal vesicle breakdown, first polar body extrusion, spindle assembly, chromosome alignment, and kinetochore-microtubule attachment. We also tested two key regulators ovastacin and Juno during fertilization. Based on these investigations, we revealed that melatonin has a protective role in preventing the BPA-induced deterioration of oocyte quality.

2 | MATERIALS AND METHODS

2.1 | Animals and feeding treatment

All mice were handled in accordance with the Animal Research Institute Committee guidelines of Nanjing Agricultural University, China. The ICR mice were kept at controlled condition of temperature (20-23°C) and

illumination (12 hours light-dark cycle) and had free access to food and water throughout the period of the study. Male mice were used for sperm collection, and female mice were used for oocyte collection.

2.2 | Oocyte collection and culture

Fully grown oocytes arrested at prophase of meiosis I were collected from ovaries in M2 medium (Sigma, St. Louis, MO, USA). Only those immature oocytes displaying a germinal vesicle (GV) were cultured further in M16 medium under liquid paraffin oil at 37°C in an atmosphere of 5% CO₂ incubator for in vitro maturation. At different time points after culture, oocytes were collected for subsequent analysis.

2.3 | BPA and melatonin treatment

Female ICR mice (4-6 week old) were randomly assigned to three or four groups: a control group, a BPA-exposed group, and one or two “BPA+melatonin” groups. No “melatonin without BPA” group was included. On average, mice received BPA of daily oral doses of 100 µg/kg body weight and/or melatonin of daily oral doses of 15 or 30 mg/kg body weight in a corn oil carrier at 9:00 AM everyday for 7 days preceding oocyte collection and analysis. The data analysts were blind to the experimental treatments.

2.4 | Immunofluorescence and confocal microscopy

Mouse oocytes were fixed in 4% paraformaldehyde in PBS (pH 7.4) for 30 minutes and permeabilized in 0.5% Triton X-100 for 20 minutes at room temperature. Then, oocytes were blocked with 1% BSA-supplemented PBS for 1 hour and incubated at 4°C overnight or at room temperature for 4 hours with anti- α -tubulin-FITC antibody (1:200, Sigma), anticontromere CREST antibody (1:50, Antibodies Incorporated, CA, USA), rat monoclonal anti-mouse Folr4-FITC antibody (1:100, BioLegend, CA, USA), or rabbit polyclonal anti-mouse ovastacin antibody (1:100, obtained from Dr. Jurrien Dean). After washing four times (5 minutes each) in PBS containing 1% Tween-20 and 0.01% Triton X-100, oocytes were incubated with an appropriate secondary antibody for 1 hours at room temperature. After washing three times, oocytes were counterstained with Hoechst 33342 (10 µg/ml) for 10 minutes. Finally, oocytes were mounted on glass slides and viewed under a confocal laser scanning microscope (Carl Zeiss LSM 700 META).

2.5 | Chromosome spread

Oocytes were exposed to Tyrode's buffer (pH 2.5) for about 30 seconds at 37°C to remove zona pellucida. After recovery

in M2 medium for 10 minutes, oocytes were fixed in a drop of 1% paraformaldehyde with 0.15% Triton X-100 on a glass slide. After air drying, chromosomes were counterstained with PI and examined under a laser scanning confocal microscope.

2.6 | In vitro fertilization

Caudae epididymides from 12-week-old male mice were lanced in a dish of human tubal fluid (HTF) medium under mineral oil (EMD Millipore, Billerica, MA, USA) to release sperm, followed by being capacitated for 1 hour (37°C, 5% CO₂), and added to ovulated oocytes at a concentration of 4×10^5 /mL sperm in 100 μ L HTF for 5 hour at 37°C, 5% CO₂. The presence of two pronuclei was scored as successful fertilization.

2.7 | Sperm binding assay

Caudae epididymal sperm were isolated from wild-type ICR mice and placed under oil (Sigma) in HTF medium previously equilibrated with 5% CO₂ and capacitated by an additional 1 hour of incubation at 37°C. Sperm binding to ovulated oocytes or two-cell embryos isolated from control, BPA-exposed, and melatonin-treated mice was observed using capacitated sperm and control two-cell embryos as a negative wash control. Samples were fixed in 4% PFA for 30 minutes, stained with Hoechst 33342. Bound sperm were quantified from z projections acquired by confocal microscopy, and results reflect the mean \pm SEM from at least three independently obtained samples, each containing 10–12 mouse oocytes/embryos.

2.8 | Western blot analysis

Mouse eggs or two-cell embryos were lysed in 4 \times LDS sample buffer with 10 \times reducing reagent (ThermoFisher, Waltham, MA, USA) and heated at 95°C for 5 minutes. Proteins were separated on 12% Bis-Tris precast gels, transferred to PVDF membranes, blocked in 5% nonfat milk in TBS (Tris-buffered saline, pH 7.4) with 0.1% Tween-20 (TBST) for 1 hour at room temperature, and then probed with 1:500 dilution of M2c.2 antibody (obtained from Dr. Jurrien Dean), rat monoclonal anti-mouse Folr4 antibody (1:1000, BioLegend, CA, USA), or rabbit polyclonal anti-mouse ovastacin antibody (1:1000) at 4°C overnight. After washing three times in TBST (10 minutes each), blots were incubated for 1 hour with a 1:5000 dilution of HRP (horseradish peroxidase) conjugated goat anti-rat or goat anti-rabbit IgG secondary antibodies (Santa Cruz, TX, USA). Chemiluminescence was performed with ECL Plus (Pierce), and signals were acquired by Tanon-3900.

2.9 | Determination of ROS generation

To determine the levels of intracellular ROS production, cumulus-denuded oocytes were incubated with the oxidation-sensitive fluorescent probe dichlorodihydrofluorescein (DCFH) for 30 minutes at 37°C in D-PBS that contained 10 μ mol/L DCFH diacetate (DCFH-DA) (Beyotime Institute of Biotechnology, China). Then, oocytes were washed three times in D-PBS containing 0.1% BSA and then placed on glass slides. The measurement of the fluorescent intensity in each oocyte was carried out by a Zeiss LSM 700 META confocal system with the same scanning settings.

2.10 | Annexin-V staining

According to the manufacturer's instruction (Beyotime Institute of Biotechnology, Hangzhou, China), mouse oocytes were stained with the Annexin-V staining kit. After washing twice in PBS, the viable oocytes were stained for 30 minutes in the dark with 90 μ L of binding buffer containing 10 μ L of Annexin-V-FITC. Fluorescent signals were measured by the confocal microscope with the same scanning settings (Zeiss LSM 700 META).

2.11 | Statistical analysis

The data were expressed as mean \pm SEM and analyzed by one-way ANOVA, followed by LSD's post hoc test, which was provided by SPSS16.0 statistical software. The level of significance was accepted as $P < .05$.

3 | RESULTS

3.1 | Melatonin promotes the meiotic progression in BPA-exposed oocytes

We first examined the meiotic progression in oocytes following BPA administration. The rates of germinal vesicle breakdown (GVBD) and polar body extrusion (PBE), two critical developmental events during meiosis, were calculated. The quantitative results showed that BPA exposure did not affect GVBD ($81.7 \pm 1.5\%$, $n=112$ vs $80.7 \pm 0.9\%$, $n=109$, $P < .05$; Figure 1A,B) but markedly decreased the PBE rate compared to controls ($78.0 \pm 2.0\%$, $n=98$ vs $57.0 \pm 4.9\%$, $n=119$, $P < .05$; Figure 1C,D), suggesting that BPA causes the meiotic arrest during maturation. To ask whether melatonin has the protective effect against BPA-induced meiotic arrest, we administered BPA-exposed mice with a low dose (15 mg/kg) or a high dose (30 mg/kg) of melatonin. Expectedly, melatonin significantly increased the proportion of PBE in BPA-exposed oocytes to the control comparable level, especially in the high-dose group ($76.7 \pm 2.6\%$, $n=121$, $P < .05$; Figure 1C,D). Thus, the high-dose administration of melatonin was used in the subsequent study.

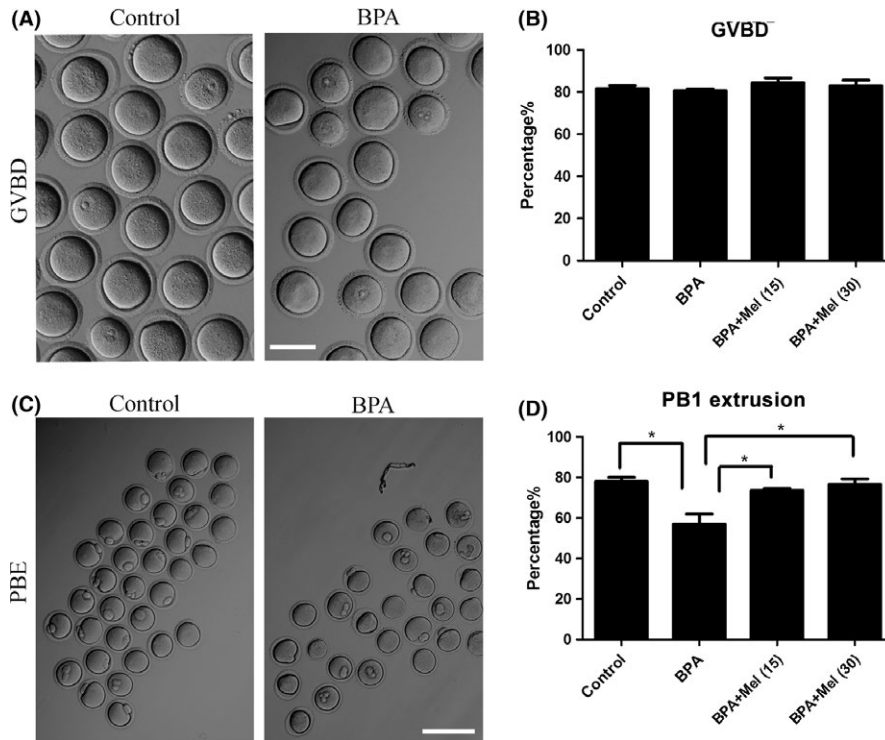


FIGURE 1 Effect of melatonin on the meiotic progression in BPA-exposed oocytes. A, Representative images of oocytes which had undergone GVBD (germinal vesicle breakdown) in control and BPA-exposed groups. Scale bar, 100 μ m. B, GVBD rates were recorded in control, BPA-exposed, low dose of melatonin-treated and high dose of melatonin-treated oocytes. The concentrations of low dose and high dose of melatonin are 15 and 30 mg/kg, respectively. C, Representative images of oocytes which extruded the first polar body (PB1) in control and BPA-exposed groups. Scale bar, 200 μ m. D, PBE (polar body extrusion) rates were recorded in control, BPA-exposed, low dose of melatonin-treated and high dose of melatonin-treated oocytes. Data were presented as mean percentage (mean \pm SEM) of at least three independent experiments. Asterisk denotes statistical difference at a $P < .05$.

3.2 | Melatonin restores the spindle defects and chromosome misalignment in BPA-exposed oocytes

As meiotic arrest is largely due to the defective spindle organization, we then observed the formation of spindle apparatus in BPA-exposed oocytes. To this end, oocytes were immunostained with anti- α -tubulin-FITC antibody to observe the spindle morphologies and counterstained with Hoechst to visualize the chromosome alignment. The results showed that most of control oocytes exhibited a typical barrel-shape spindle apparatus with a well-aligned chromosome on the equatorial plate (Figure 2A). In striking contrast, a majority of disorganized spindle morphologies and misaligned chromosomes was observed in BPA-exposed oocytes (Figure 2A). Statistically, more than 70% of oocytes displayed the disrupted spindles and about 80% of oocytes exhibited misaligned chromosomes, and melatonin administration reduced the abnormal rates to a level indistinguishable from controls (spindle: $11.8 \pm 1.0\%$, $n=132$ vs $77.8 \pm 3.2\%$, $n=96$ vs $22.6 \pm 2.1\%$, $n=101$, $P < .05$; chromosome: $13.5 \pm 1.4\%$, $n=127$ vs $80.6 \pm 6.5\%$, $n=89$ vs $29.0 \pm 2.0\%$, $n=97$, $P < .05$; Figure 2B-D).

3.3 | Melatonin restores the defective kinetochore-microtubule attachment to maintain the euploidy in BPA-exposed oocytes

Aberrant spindle formation and incorrect chromosome alignment are highly correlated with the defective interaction between kinetochores and microtubules; thus, we next

tested the stability of kinetochore-microtubule attachments following BPA administration. For this purpose, metaphase I oocytes were briefly chilled to induce the depolymerization of microtubules that are not attached to kinetochores and then immunostained with CREST to detect kinetochores, with anti- α -tubulin-FITC antibody to visualize the microtubules and counterstained with Hoechst to observe the chromosomes. It was shown that in a variety of control oocytes, kinetochores were fully attached by microtubules and chromosomes were well-aligned (Figure 3A). However, a prominently increased frequency of kinetochores without attachment by microtubules was observed in BPA-exposed oocytes, whereas the melatonin administration significantly reduced the abnormalities ($19.7 \pm 1.8\%$, $n=92$ vs $76.1 \pm 6.1\%$, $n=99$ vs $30.8 \pm 10.5\%$, $n=123$, $P < .05$; Figure 3A,B).

As impaired kinetochore-microtubule attachment is often coupled with the aneuploidy, we then analyzed the karyotype of metaphase II oocytes by chromosome spreading. Normally, the number of single chromosomes (univalents) is 20, which is a prerequisite for genomic integrity. However, a significantly higher frequency of aneuploid oocytes that had more or less than 20 univalents was found in BPA-exposed oocytes compared to controls, and melatonin administration, expectedly, decreased the aneuploidy rate induced by BPA ($3.7 \pm 3.7\%$, $n=82$ vs $42.6 \pm 1.8\%$, $n=94$ vs $22.7 \pm 5.3\%$, $n=111$, $P < .05$; Figure 3C,D).

Taken together, these observations suggest that melatonin is able to, at least partially, restore the BPA-induced defects of spindle assembly, chromosome alignment, and kinetochore-microtubule attachment to maintain the euploidy during mouse oocyte meiotic progression.

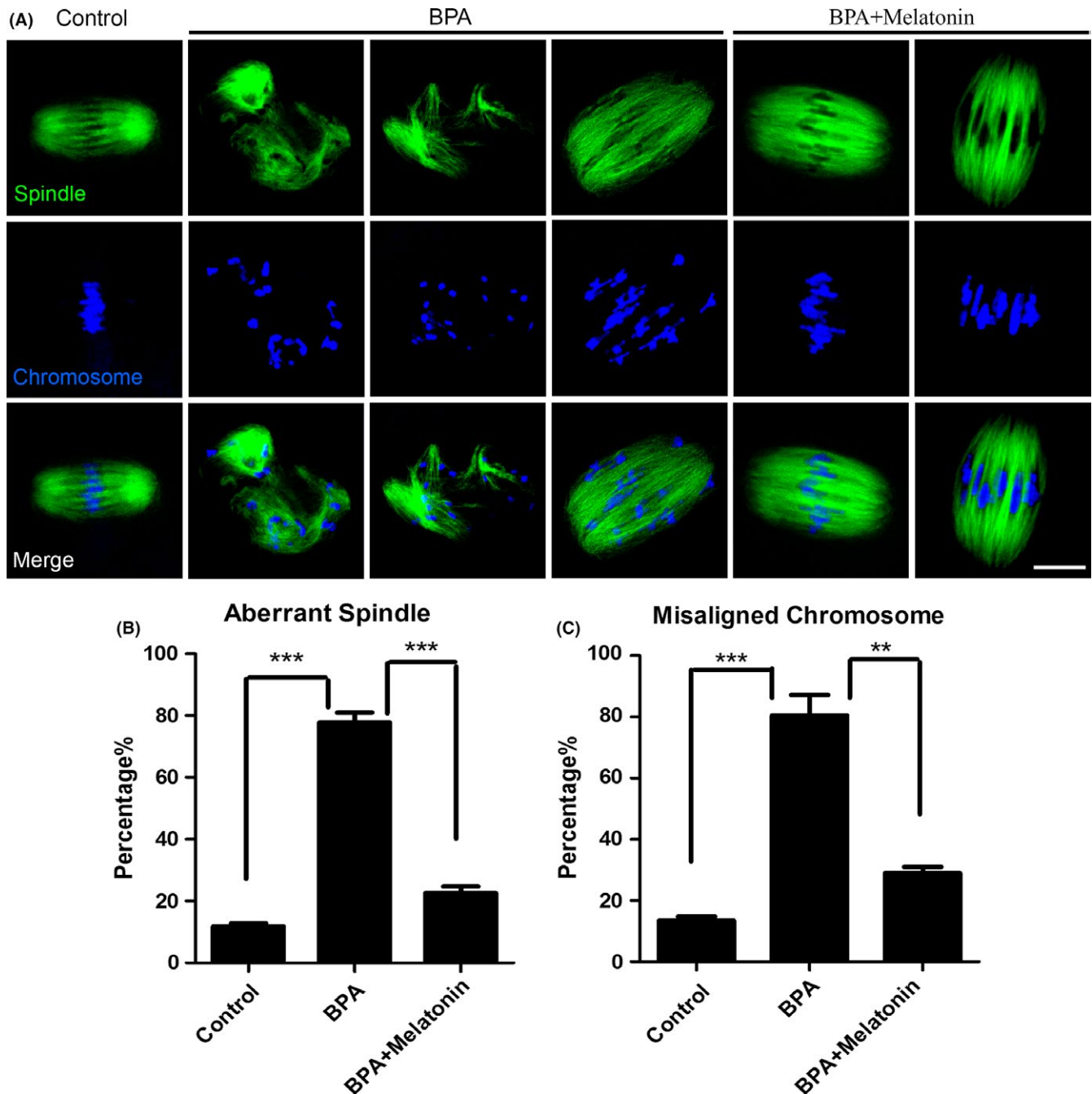


FIGURE 2 Effect of melatonin on the spindle assembly and chromosome alignment in BPA-exposed oocytes. A, Representative images of spindle morphologies and chromosome alignment in control, BPA-exposed, and melatonin-treated oocytes. Oocytes were immunostained with α -tubulin-FITC antibody to visualize the spindles and counterstained with Hoechst to visualize the chromosomes. Scale bar, 10 μ m. B, The rates of aberrant spindles were recorded in control, BPA-exposed, and melatonin-treated oocytes. C, The rates of misaligned chromosomes were recorded in control, BPA-exposed, and melatonin-treated oocytes. Data were presented as mean percentage (mean \pm SEM) of at least three independent experiments. Asterisk denotes statistical difference at a $P<.05$ level of significance.

3.4 | Melatonin improves fertilization ability of BPA-exposed mouse eggs

We next asked whether BPA administration would impair the fertilization potential of mouse eggs. As shown in Figure 4A, most of control eggs were able to be fertilized and develop to 2-cell embryos, while BPA-exposed eggs had significantly

reduced fertilization rates ($87.2\pm0.9\%$, $n=72$ vs $41.1\pm1.5\%$, $n=65$, $P<.05$; Figure 4A,B). To further determine the effect of melatonin on the fertilization of BPA-exposed eggs, a low dose and a high dose of melatonin (15 and 30 mg/kg) were administered, respectively. As expected, in the groups of melatonin-administered eggs, the rates of fertilization were increased. In particular, a high dose of melatonin significantly

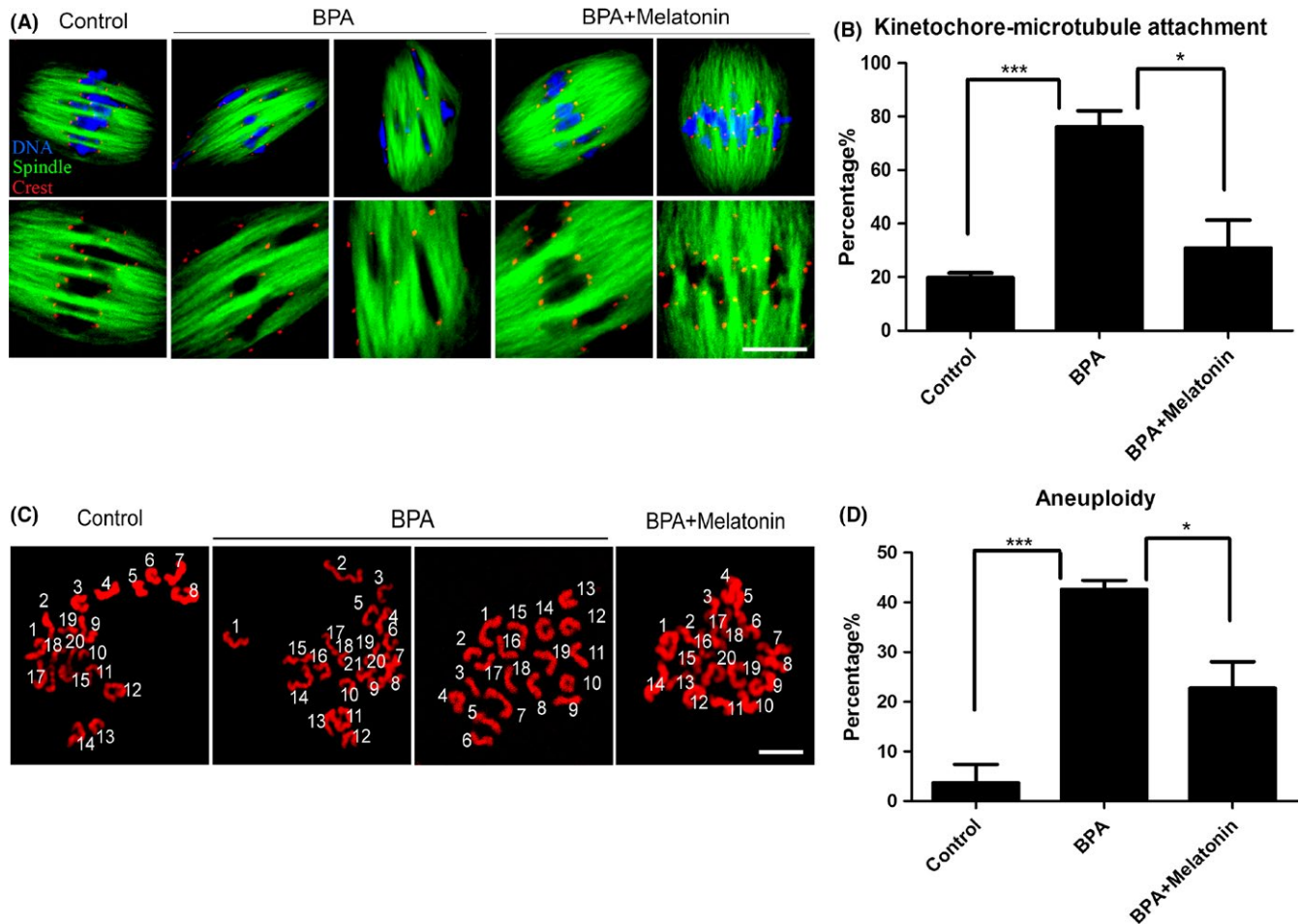


FIGURE 3 Effect of melatonin on the kinetochore-microtubule attachment and euploidy in BPA-exposed oocytes. A, Representative images of kinetochore-microtubule attachment in control, BPA-exposed, and melatonin-treated oocytes. Oocytes were immunostained with α -tubulin-FITC antibody to visualize the spindles, with Crest to visualize the kinetochores, and counterstained with Hoechst to visualize the chromosomes. Scale bar, 5 μ m. B, The rates of defective kinetochore-microtubule attachments were recorded in control, BPA-exposed, and melatonin-treated oocytes. C, Representative images of euploid and aneuploid MII eggs. Chromosome spread was performed to calculate the number of chromosomes. Chromosomes were counterstained with PI. Scale bar, 2.5 μ m. D, The rates of aneuploid eggs were recorded in control, BPA-exposed, and melatonin-treated oocytes. Data were presented as mean percentage (mean \pm SEM) of at least three independent experiments. Asterisk denotes statistical difference at a $P<.05$ level of significance.

increased the fertilization rate from 41% in BPA-exposed group to 63% ($63.0\pm2.6\%$, $n=80$, $P<.05$; Figure 4B). Collectively, these results indicate that melatonin is able to improve the fertilization capability of BPA-exposed eggs.

3.5 | Melatonin elevates the sperm binding ability of BPA-exposed eggs

Successful fertilization depends on a series of sperm-egg interaction events. First of all, sperm should bind to zona pellucida surrounding oocytes; thus, we tested whether fertilization failure in BPA-exposed eggs is due to the defects in this process. We stained the sperm head with Hoechst to count the number of sperm binding to the zona pellucida. In control unfertilized eggs, zona pellucida supported numerous sperm binding, and in 2-cell embryos, due to the loss of

sperm binding site, zona pellucida no longer supported any sperm binding (Figure 5A). However, in BPA-exposed eggs, the number of sperm binding to the zona pellucida remarkably reduced compared to the control eggs (Figure 5A,B), but significantly increased in the melatonin-administered group (128.3 ± 6.7 , $n=32$ vs 34.2 ± 5.3 , $n=32$ vs 91.3 ± 5.0 , $n=32$, $P<.05$; Figure 5A,B). Taken together, the above results imply that melatonin is able to rescue the disrupted sperm binding ability of BPA-exposed eggs.

3.6 | Melatonin relieves ZP2 cleavage level in BPA-exposed eggs

Because sperm binding to zona pellucida is determined by the cleavage status of N-terminus of ZP2, the sperm binding site, we used the antibody M2c.2 that recognizes the C-terminus

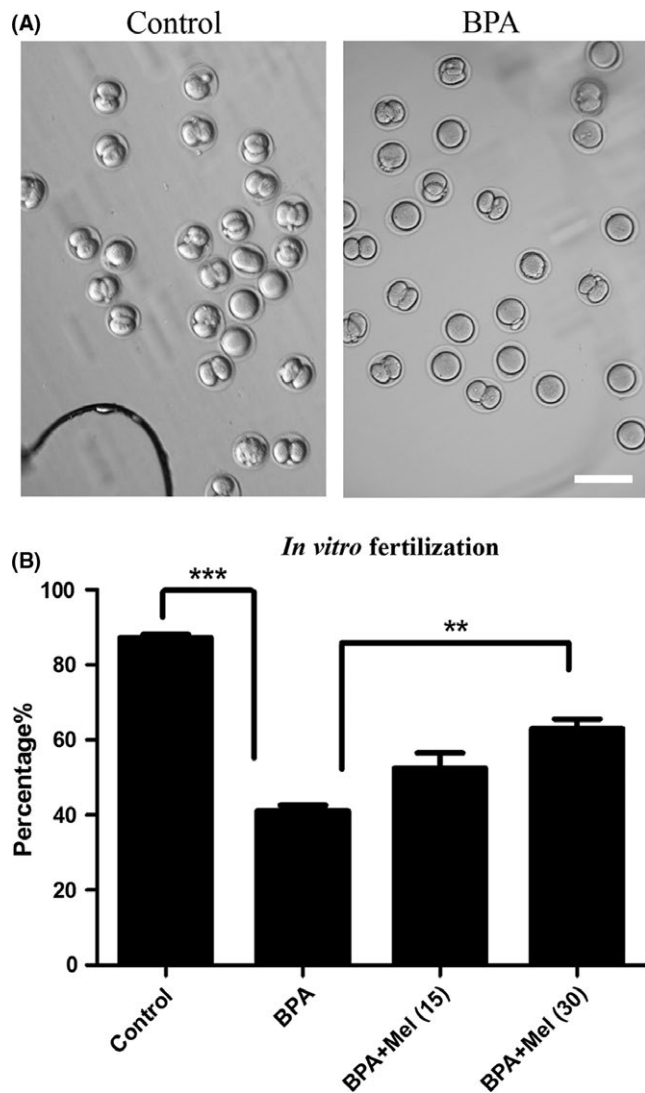


FIGURE 4 Effect of melatonin on the in vitro fertilization of BPA-exposed eggs. A, Representative images of fertilized eggs in control and BPA-exposed groups. Scale bar, 200 μ m. B, In vitro fertilization rates were recorded in control, BPA-exposed, low dose of melatonin-treated, and high dose of melatonin-treated eggs. The concentrations of low dose and high dose of melatonin are 15 and 30 mg/kg, respectively. Data were presented as mean percentage (mean \pm SEM) of at least three independent experiments. Asterisk denotes statistical difference at a $P < .05$.

of mouse ZP2 to detect the cleavage by Western blotting. In controls, ZP2 remained intact around 120kD in unfertilized eggs and became cleaved about 90kD in 2-cell embryos (Figure 5C). Strikingly, cleaved ZP2 was present even in unfertilized eggs in BPA-administered group (Figure 5C), which indicates that BPA exposure renders eggs lose the sperm binding sites. Also, this observation is consistent with the above sperm binding assay showing that BPA-exposed eggs have less sperm binding to the zona pellucida. As melatonin is able to partially restore the sperm binding capability of BPA-exposed eggs, theoretically it can also restore

the ZP2 cleavage level. As expected, although ZP2 was also cleaved in melatonin-administered group, the cleavage level was lower compared to BPA-exposed eggs (Figure 5C).

3.7 | Melatonin rescues localization and protein level of ovastacin in BPA-exposed eggs

To further explore the possible reason causing the failure of sperm binding to the zona pellucida surrounding BPA-exposed eggs, we examined the localization and protein level of ovastacin, an oocyte-specific metalloprotease in the cortical granules which is responsible for postfertilization cleavage of N-terminus of ZP2. Immunostaining results showed that ovastacin was localized under the oocyte subcortical region and excluded in cortical granule free domain (CGFD) in controls (Figure 6A). By striking contrast, various types of abnormal localization of ovastacin were observed in BPA-exposed eggs, and these abnormalities could be rescued by melatonin (Figure 6A). Statistically, the frequency of abnormal ovastacin in BPA-exposed eggs was significantly higher than that in controls, but was markedly reduced in the melatonin-administered group ($22.5 \pm 0.7\%$, $n=99$ vs $82.5 \pm 3.2\%$, $n=97$ vs $52.8 \pm 6.7\%$, $n=99$, $P < .05$; Figure 6B). We then examined the protein level of ovastacin by Western blotting. The data showed that the protein amount of ovastacin indeed substantially decreased in BPA-exposed eggs (Figure 6C), suggesting that a part of ovastacin has been prematurely exocytosed to the extracellular matrix to cleave ZP2 prior to fertilization. However, the melatonin administration restored the protein level indistinguishable from controls (Figure 6C). Collectively, these data indicate that BPA exposure of eggs would result in the mis-localization and premature exocytosis of ovastacin, which might be one of the critical factors leading to the sperm binding defect and fertilization failure.

3.8 | Melatonin rescues the protein level of Juno on the membrane in BPA-exposed eggs

After sperm bind to and penetrate zona pellucida, sperm should fuse with egg membrane to complete the fertilization. Juno is a recently found receptor on the egg membrane which binds to Izumo1 in the sperm head to mediate the sperm-egg fusion; thus, we further examined the behavior of Juno on the egg membrane. We performed the immunostaining of Juno to observe its localization. As shown in Figure 7A, Juno evenly distributed on the egg membranes in controls, but partly or entirely lost its localization in BPA-exposed eggs (Abnormal rates: $23.0 \pm 7.4\%$, $n=84$ vs $76.2 \pm 3.1\%$, $n=109$, $P < .05$; Figure 7B). These mis-localization patterns of Juno in BPA-exposed eggs could be rescued by the melatonin administration ($39.3 \pm 10.3\%$, $n=92$, $P < .05$; Figure 7B). We then measured the immunofluorescent intensity of Juno, and the result showed that signals in BPA-exposed eggs were

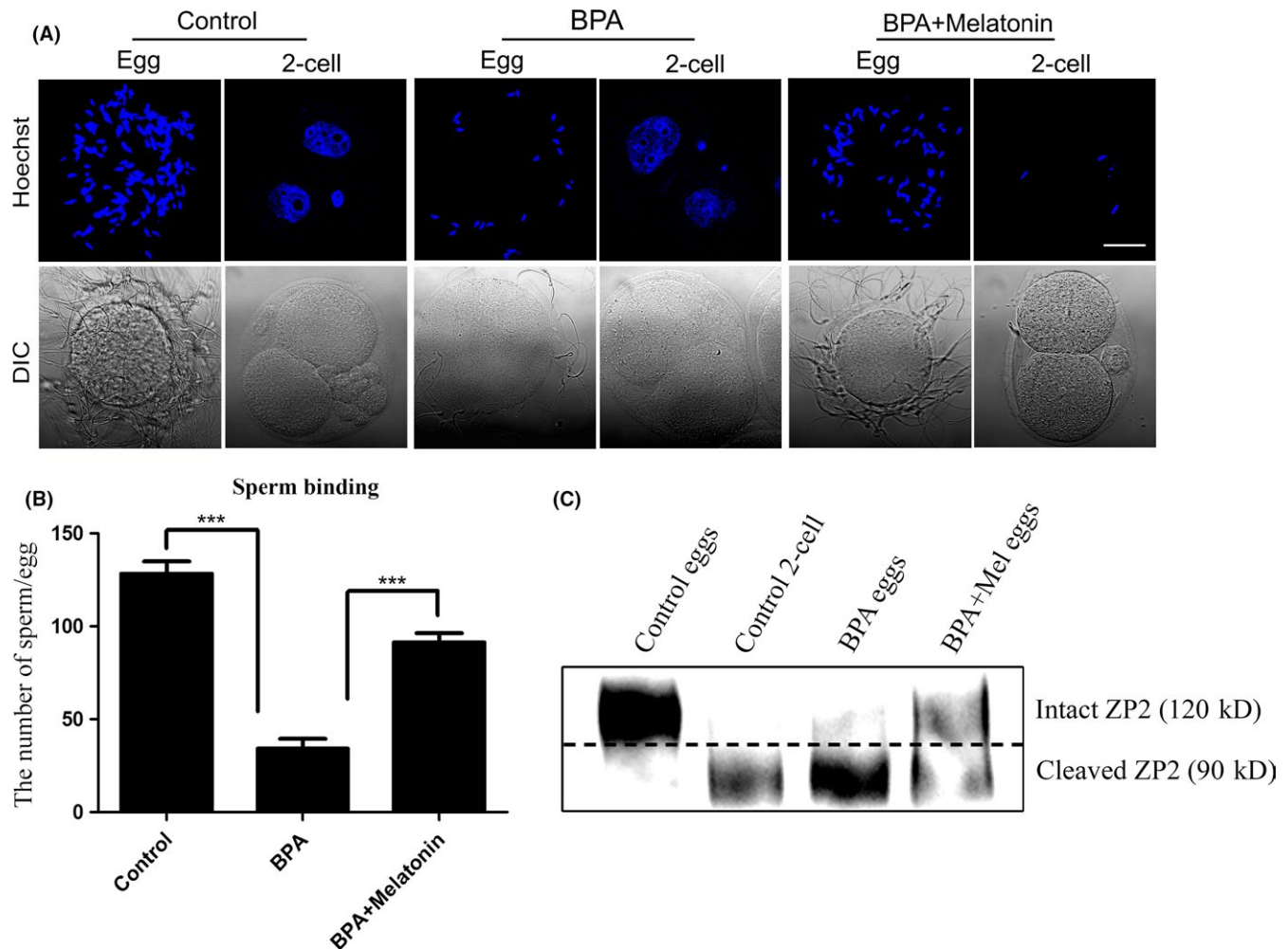


FIGURE 5 Effect of melatonin on sperm binding to the zona pellucida of BPA-exposed eggs. A, Eggs and two-cell embryos from control, BPA-exposed, and melatonin-treated groups were incubated with capacitated sperm for 1 h. After washing with a wide-bore pipette to remove all but two to six sperm on normal two-cell embryos (negative control), eggs and embryos with sperm were fixed and stained with Hoechst 33342. Scale bar, 20 μ m. B, The number of sperm binding to the surface of zona pellucida surrounding eggs from control, BPA-exposed, and melatonin-treated groups was record. Data were presented as mean percentage (mean \pm SEM) of at least three independent experiments. Asterisk denotes statistical difference at a $P<.05$. C, Western blot of ZP2 cleavage status was performed in eggs and/or two-cell embryos from control, BPA-exposed, and melatonin-treated groups using M2c.2 antibody that recognizes the C-terminus of cleaved ZP2. The size of intact ZP2 is 120 kD; the size of the cleaved C-terminal fragment of ZP2 is 90 kD.

prominently decreased compared to control eggs (Figure 7C). Meanwhile, melatonin administration to some extent restored the signals of Juno on the egg membrane (40.0 ± 2.0 , $n=84$ vs 16.5 ± 1.1 , $n=109$ vs 35.3 ± 2.2 , $n=92$, $P<.05$; Figure 7C). Therefore, the reduced amount of Juno on the egg membrane might be one of the important causes leading to the compromised fertilization ability of mouse BPA-exposed eggs.

3.9 | Melatonin decreases ROS level and suppresses early apoptosis in BPA-exposed oocytes

To determine how melatonin acts as an antioxidant to influence the oocyte meiotic progression and fertilization, we hypothesized that BPA exposure would induce the oxidative

stress which accelerates the apoptosis of mouse oocytes and thereby leads to the deterioration of critical regulators and events during oocyte meiotic progression and fertilization. Then, we assessed the ROS level and apoptosis in different groups. In BPA-exposed oocytes, the fluorescence intensity of ROS was apparently increased compared to controls (153.8 ± 7.7 , $n=138$ vs 70.9 ± 3.1 , $n=96$, $P<.05$; Figure 8A,B). Notably, melatonin administration was able to reduce the level of ROS comparable to controls (73.4 ± 12.7 , $n=51$, $P<.05$; Figure 8A,B).

Next, we examined the early apoptosis by Annexin-V staining. The result showed that green fluorescent signals were hardly detected in control oocytes, but clearly found on the membrane in BPA-exposed oocytes (Figure 8C). The rate of apoptotic oocytes was dramatically higher in BPA-exposed

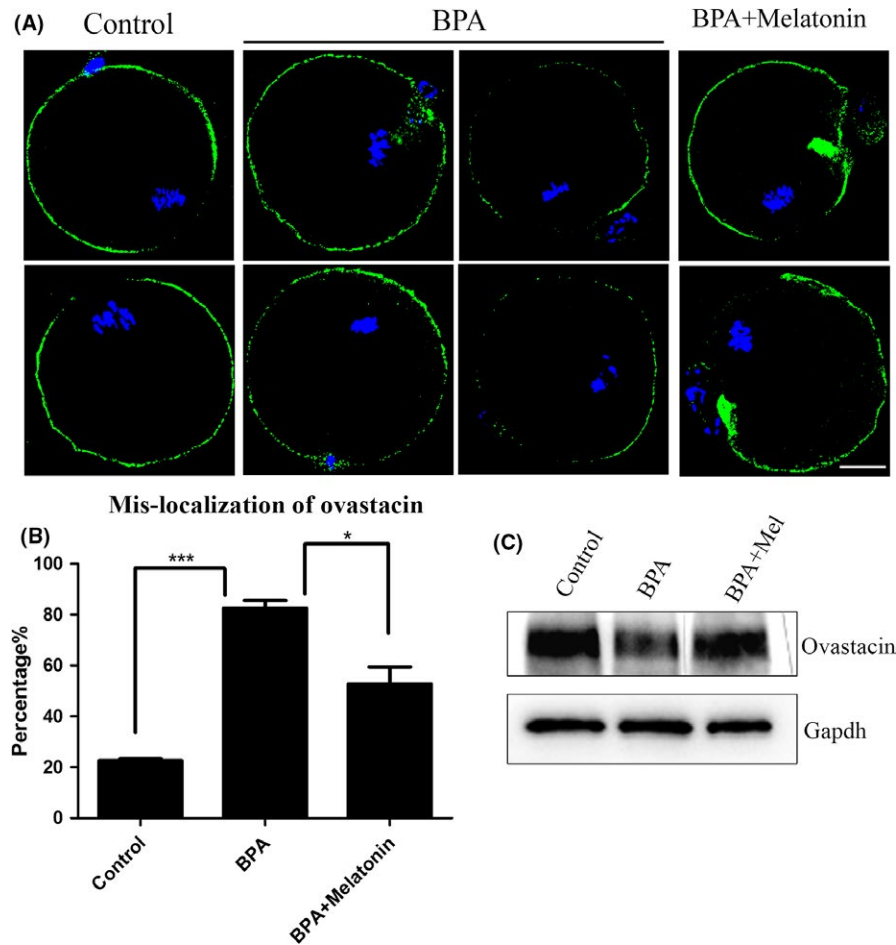


FIGURE 6 Effect of melatonin on the localization and protein level of ovastacin in BPA-exposed eggs. A, Representative images of ovastacin in control, BPA-exposed, and melatonin-treated eggs. Ovastacin was immunostained with rabbit polyclonal anti-mouse ovastacin antibody and examined by confocal microscopy. Scale bar, 20 μ m. B, Abnormal rates of ovastacin localization were recorded in control, BPA-exposed, and melatonin-treated eggs. Data were presented as mean percentage (mean \pm SEM) of at least three independent experiments. Asterisk denotes statistical difference at a $P<.05$ level of significance. C, Protein levels of ovastacin examined by Western blot in control, BPA-exposed, and melatonin-treated eggs.

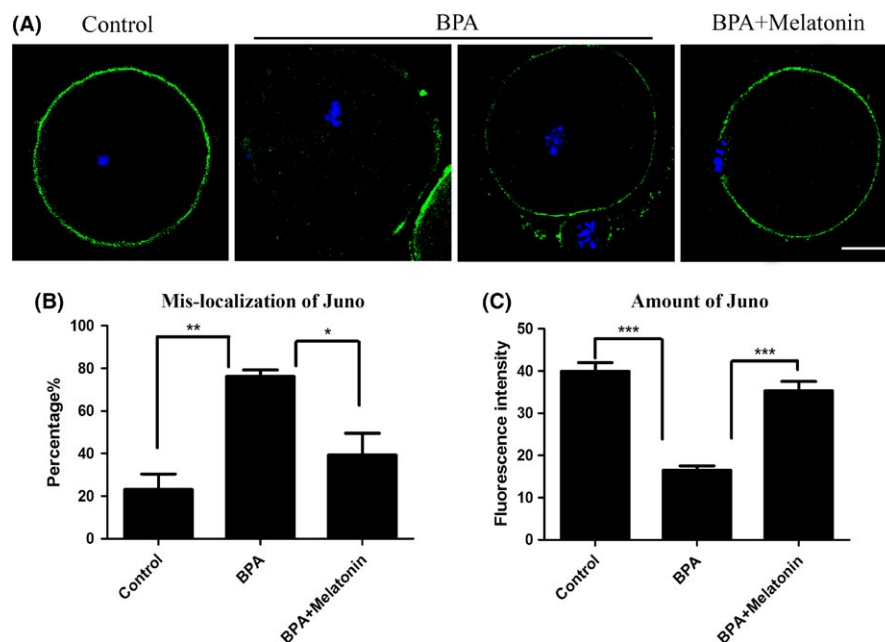


FIGURE 7 Effect of melatonin on the localization and protein level of Juno in BPA-exposed eggs. A, Representative images of Juno in control, BPA-exposed, and melatonin-treated eggs. Juno was immunostained with rat monoclonal anti-mouse Folr4 antibody and examined by confocal microscopy. Scale bar, 20 μ m. B, Abnormal rates of Juno localization in control, BPA-exposed, and melatonin-treated eggs. Data were presented as mean percentage (mean \pm SEM) of at least three independent experiments. Asterisk denotes statistical difference at a $P<.05$ level of significance. C, The immunofluorescence intensity of Juno signals was recorded in control, BPA-exposed, and melatonin-treated eggs. Data were presented as mean percentage (mean \pm SEM) of at least three independent experiments. Asterisk denotes statistical difference at a $P<.05$ level of significance.

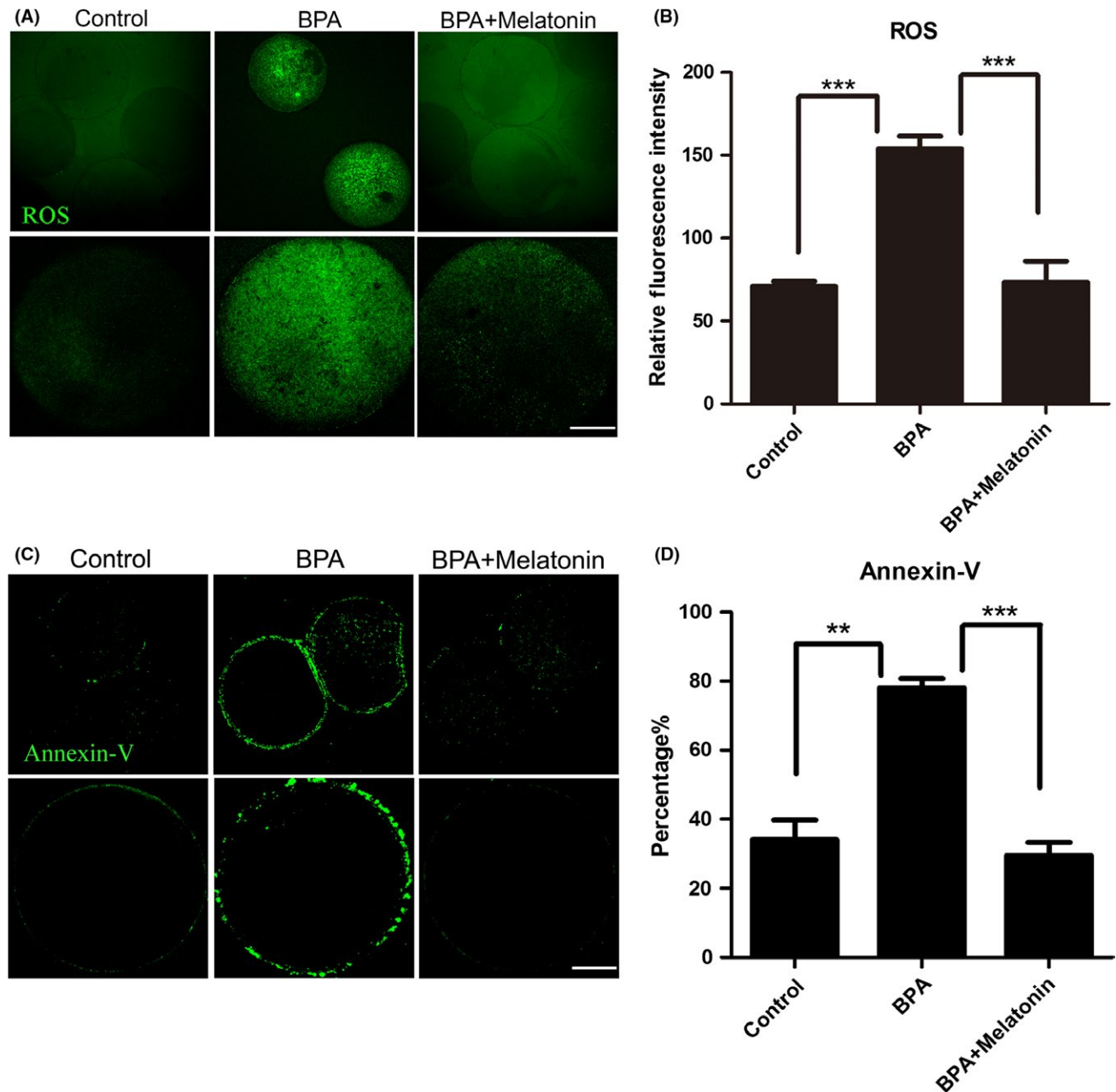


FIGURE 8 Effect of melatonin on ROS levels and early apoptosis in BPA-exposed oocytes. A, Representative images of ROS levels in control, BPA-exposed, and melatonin-treated oocytes. Scale bar, 20 μ m. B, Fluorescence intensities of ROS in control, BPA-exposed and melatonin-treated oocytes were measured by confocal microscopy using identical settings and parameters. C, Representative images of apoptotic oocytes in control, BPA-exposed, and melatonin-treated groups. Oocytes were immunostained with Annexin-V-FITC. Scale bar, 20 μ m. D, The rate of early apoptosis was recorded in control, BPA-exposed, and melatonin-treated oocytes. Data in (B) and (D) were presented as mean percentage (mean \pm SEM) of at least three independent experiments. Asterisk denotes statistical difference at a $P < .05$ level of significance.

group than that in controls, but reduced in melatonin-administered group ($29.6 \pm 3.7\%$, $n=94$ vs $78.2 \pm 2.6\%$, $n=82$ vs $34.1 \pm 5.6\%$, $n=111$, $P < .05$; Figure 8D).

4 | DISCUSSION

Increasing evidence has shown that BPA adversely impacts the mammalian reproductive system by generation of free

radicals⁴⁴⁻⁴⁸ and that melatonin is able to scavenge the most toxic free radical as a robust antioxidant.²⁸ We thus propose that melatonin could ameliorate BPA-induced oocyte deterioration. To test this, we examined the mouse oocyte meiotic progression, one key indicator of high-quality oocytes, as well as the spindle assembly and chromosome alignment following BPA administration in mice. In agreement with previous studies,⁴⁸ BPA exposure caused the oocyte meiotic arrest by damaging spindle organization and chromosome

alignment. As expected, melatonin treatment via oral administration substantially restored the spindle/chromosome structural defects to promote the meiotic progression, suggesting that melatonin indeed has the potential to ameliorate the oocyte quality. Because kinetochore attaches chromosomes to spindle microtubules and maintains the attachment to growing or disassembling microtubules to drive chromosome segregation,^{49,50} spindle/chromosome abnormalities are always accompanied by the errors of kinetochore-microtubule attachments.^{17,51,52} We further determined the effect of melatonin on the stability of kinetochore-microtubule attachments in BPA-exposed oocytes. Our findings showed that melatonin significantly elevated proportion of stable kinetochore-microtubule attachments in BPA-exposed oocytes. As a result of chromosome misalignment, aneuploidy, an abnormal number of chromosomes, occurred frequently in BPA-exposed oocytes and was recovered by melatonin administration.

Fertilization is a unique and multistep event that initiates the onset of development.^{53,54} Fertilization ability is another key indicator of high-quality oocytes. Our findings revealed that melatonin restored the declined fertilization potential resulted from BPA exposure, and we also discovered the underlying mechanisms. During mammalian fertilization, capacitated sperm must bind to and penetrate the specialized extracellular matrix of the egg, known as zona pellucida, and then fuse with the oolemma to become the fertilized oocytes.⁵⁵ Thus, sperm-egg interaction begins with the sperm binding to the zona pellucida surrounding oocytes. We found that BPA exposure dramatically reduced the number of sperm binding to the zona pellucida, which perturbed the fertilization capability at the first step. The mouse genetic studies have defined the N-terminal domain of ZP2 as the sperm binding site in the zona pellucida, and the sperm binding to oocytes but not two-cell embryos is determined by the only documented biochemical change which is ZP2 cleavage status.^{53,56,57} In unfertilized oocytes, ZP2 remains intact to be ready for sperm binding. However, once the fertilization occurs, ovastacin in the CGs is released to the extracellular space to cleave ZP2 at the N-terminus for block to polyspermy, and the zona pellucida surrounding fertilized oocytes and embryos no longer support the sperm binding. Based on the fact that less sperm binding was observed in BPA-exposed oocytes, we then investigated the ZP2 cleavage status to determine the loss of sperm binding ability. In agreement with sperm binding assay, even in the unfertilized oocytes in BPA-administered group, ZP2 was partially cleaved, suggesting that a part of sperm binding sites had been removed.

Ovastacin, as a first identified component of mammalian cortical granules, is responsible for the postfertilization cleavage of ZP2 to prevent polyspermy.⁵⁸ However, if a large amount of ovastacin is exocytosed before fertilization, ZP2 will be prematurely cleaved, leading to less or no sperm binding and the fertilization failure. Thus, we further examined

the localization and protein amount of ovastacin in the oocytes following postovulatory aging. Our data showed that ovastacin was mislocalized and precociously released before fertilization, which were consistent with the previous observations that ZP2 was prematurely cleaved and sperm binding was lost in unfertilized BPA-exposed oocytes.

Egg membrane sits interior to the ZP and fuses with the ZP-penetrated sperm to complete sperm-egg interaction. It has been shown that Juno, an egg membrane protein, is essential for fertilization due to its interaction with Izumo1 which is the fusion protein on the sperm head.⁵⁹ Mice lack either Juno or Izumo1 exhibit sex-specific sterility because their gametes cannot fuse to their wild-type partner's cells.^{59,60} To ascertain whether the fertilization failure caused by BPA exposure to some extent results from the impairment of fusion process, we examined the localization and the amount of Juno on the egg membrane. The data revealed that the localization of Juno on the plasma membrane was compromised and the amount was reduced in BPA-exposed oocytes. More importantly, we found that melatonin could, at least partially, restore all the defects related to the fertilization failure caused by the BPA exposure via stabilizing ovastacin and Juno. Collectively, we provide a body of evidence demonstrating that melatonin improves the quality of oocyte exposed to BPA by promoting meiotic progression and maintaining the fertilization ability through inhibiting BPA-induced oxidative stress and apoptosis.

In human clinical studies, the use of 3 mg melatonin has been demonstrated to improve the oocyte maturation, the fertilization rate, the quality of embryos and the pregnancy outcomes without any obvious physiologic side effects.⁶¹ In our study, the dose of 30 mg/kg body weight of melatonin used in mice is equal to 2.5 mg for human use according to the dose conversion between mouse and human.⁶² Therefore, our findings provide an implication that melatonin has a potential role in preventing the deterioration of human oocytes exposed to BPA when supplied concurrently, but whether it can reverse the adverse effects of BPA that have already accumulated in oocytes needs the future investigations.

ACKNOWLEDGEMENTS

We thank Dr. Jurrien Dean very much for providing antibodies.

CONFLICT OF INTEREST

The authors have no conflicts of interest to disclose.

REFERENCES

1. Brotons JA, Olea-Serrano MF, Villalobos M, et al. Xenoestrogens released from lacquer coatings in food cans. *Environ Health Perspect.* 1995;103:608–612.

2. Fung EY, Ewoldsen NO, ST GERMAIN HA Jr, et al. Pharmacokinetics of bisphenol A released from a dental sealant. *J Am Dent Assoc.* 2000;131:51–58.
3. Krishnan AV, Stathis P, Permuth SF, et al. Bisphenol-A: an estrogenic substance is released from polycarbonate flasks during autoclaving. *Endocrinology.* 1993;132:2279–2286.
4. Tsutsui T, Tamura Y, Suzuki A, et al. Mammalian cell transformation and aneuploidy induced by five bisphenols. *Int J Cancer.* 2000;86:151–154.
5. Rashid H, Ahmad F, Rahman S, et al. Iron deficiency augments bisphenol A-induced oxidative stress in rats. *Toxicology.* 2009;256:7–12.
6. Tsutsui T, Tamura Y, Yagi E, et al. Bisphenol-A induces cellular transformation, aneuploidy and DNA adduct formation in cultured Syrian hamster embryo cells. *Int J Cancer.* 1998;75:290–294.
7. Ochi T. Induction of multiple microtubule-organizing centers, multipolar spindles and multipolar division in cultured V79 cells exposed to diethylstilbestrol, estradiol-17 β and bisphenol A. *Mutat Res.* 1999;431:105–121.
8. Pfeiffer E, Rosenberg B, Deuschel S, et al. Interference with microtubules and induction of micronuclei in vitro by various bisphenols. *Mutat Res.* 1997;390:21–31.
9. Vandenberg LN, Chahoud I, Padmanabhan V, et al. Biomonitoring studies should be used by regulatory agencies to assess human exposure levels and safety of bisphenol A. *Environ Health Perspect.* 2010;118:1051–1054.
10. Fernandez MF, Arrebola JP, Taoufik J, et al. Bisphenol-A and chlorinated derivatives in adipose tissue of women. *Reprod Toxicol.* 2007;24:259–264.
11. Korkmaz A, Ahbab MA, Kolankaya D, et al. Influence of vitamin C on bisphenol A, nonylphenol and octylphenol induced oxidative damages in liver of male rats. *Food Chem Toxicol.* 2010;48:2865–2871.
12. Berger RG, Hancock T, Decatanzaro D. Influence of oral and subcutaneous bisphenol-A on intrauterine implantation of fertilized ova in inseminated female mice. *Reprod Toxicol.* 2007;23:138–144.
13. Erler C, Novak J. Bisphenol a exposure: human risk and health policy. *J Pediatr Nurs.* 2010;25:400–407.
14. Vom Saalfs FS, Welshons WV, Hansen LG. Organochlorine residues and breast cancer. *N Engl J Med.* 1998;338:988–991.
15. Sakaue M, Ago Y, Murakami C, et al. Involvement of benzodiazepine binding sites in an antiaggressive effect by 5-HT(1A) receptor activation in isolated mice. *Eur J Pharmacol.* 2001;432:163–166.
16. Chern CM, Liao JF, Wang YH, et al. Melatonin ameliorates neural function by promoting endogenous neurogenesis through the MT2 melatonin receptor in ischemic-stroke mice. *Free Radic Biol Med.* 2012;52:1634–1647.
17. Reiter RJ, Mayo JC, Tan DX, et al. Melatonin as an antioxidant: under promises but over delivers. *J Pineal Res.* 2016;61:253–278.
18. Huang MD, Sun X, Cao X, et al. The protective effect of melatonin on auditory cortex toxicity induced by cis-platinum. *Zhongguo Ying Yong Sheng Li Xue Za Zhi.* 2009;25:539–542.
19. Tan DX, Manchester LC, Terron MP, et al. One molecule, many derivatives: a never-ending interaction of melatonin with reactive oxygen and nitrogen species? *J Pineal Res.* 2007;42:28–42.
20. Zhang HM, Zhang Y. Melatonin: a well-documented antioxidant with conditional pro-oxidant actions. *J Pineal Res.* 2014;57:131–146.
21. Yang Y, Duan W, Jin Z, et al. JAK2/STAT3 activation by melatonin attenuates the mitochondrial oxidative damage induced by myocardial ischemia/reperfusion injury. *J Pineal Res.* 2013;55:275–286.
22. Galano A, Tan DX, Reiter RJ. Melatonin as a natural ally against oxidative stress: a physicochemical examination. *J Pineal Res.* 2011;51:1–16.
23. Giacomo CG, Antonio M. Melatonin in cardiac ischemia/reperfusion-induced mitochondrial adaptive changes. *Cardiovasc Hematol Disord Drug Targets.* 2007;7:163–169.
24. Shim DW, Shin HJ, Han JW, et al. A novel synthetic derivative of melatonin, 5-hydroxy-2'-isobutyl-streptochlorin (HIS), inhibits inflammatory responses via regulation of TRIF-dependent signaling and inflammasome activation. *Toxicol Appl Pharmacol.* 2015;284:227–235.
25. Song J, Kang SM, Lee KM, et al. The protective effect of melatonin on neural stem cell against LPS-induced inflammation. *Biomed Res Int.* 2015;2015:854359.
26. Mauriz JL, Collado PS, Veneroso C, et al. A review of the molecular aspects of melatonin's anti-inflammatory actions: recent insights and new perspectives. *J Pineal Res.* 2013;54:1–14.
27. Russcher M, Koch B, Nagtegaal E, et al. The role of melatonin treatment in chronic kidney disease. *Front Biosci (Landmark Ed).* 2012;17:2644–2656.
28. Amin AH, El-Missiry MA, Othman AI. Melatonin ameliorates metabolic risk factors, modulates apoptotic proteins, and protects the rat heart against diabetes-induced apoptosis. *Eur J Pharmacol.* 2015;747:166–173.
29. El-Missiry MA, Othman AI, Al-Abdan MA, et al. Melatonin ameliorates oxidative stress, modulates death receptor pathway proteins, and protects the rat cerebrum against bisphenol-A-induced apoptosis. *J Neurol Sci.* 2014;347:251–256.
30. Zhou L, Zhao D, An H, et al. Melatonin prevents lung injury induced by hepatic ischemia-reperfusion through anti-inflammatory and anti-apoptosis effects. *Int Immunopharmacol.* 2015;29:462–467.
31. Benitez-King G. Melatonin as a cytoskeletal modulator: implications for cell physiology and disease. *J Pineal Res.* 2006;40:1–9.
32. Hardeland R. Antioxidative protection by melatonin: multiplicity of mechanisms from radical detoxification to radical avoidance. *Endocrine.* 2005;27:119–130.
33. Reiter RJ, Tan DX, Mayo JC, et al. Melatonin as an antioxidant: biochemical mechanisms and pathophysiological implications in humans. *Acta Biochim Pol.* 2003;50:1129–1146.
34. Schaefer M, Hardeland R. The melatonin metabolite N-acetyl-5-methoxykynuramine is a potent singlet oxygen scavenger. *J Pineal Res.* 2009;46:49–52.
35. Tan DX, Chen LD, Poeggeler B, et al. Melatonin: a potent, endogenous hydroxyl radical scavenger. *Endocr J.* 1993;1:57–60.
36. Tan DX, Reiter RJ, Manchester LC, et al. Chemical and physical properties and potential mechanisms: melatonin as a broad spectrum antioxidant and free radical scavenger. *Curr Top Med Chem.* 2002;2:181–197.
37. Adriaens I, Jacquet P, Cortvrindt R, et al. Melatonin has dose-dependent effects on folliculogenesis, oocyte maturation capacity and steroidogenesis. *Toxicology.* 2006;228:333–343.
38. Manjunatha BM, Devaraj M, Gupta PS, et al. Effect of taurine and melatonin in the culture medium on buffalo in vitro embryo development. *Reprod Domest Anim.* 2009;44:12–16.

39. Kang JT, Koo OJ, Kwon DK, et al. Effects of melatonin on in vitro maturation of porcine oocyte and expression of melatonin receptor RNA in cumulus and granulosa cells. *J Pineal Res.* 2009;46:22–28.
40. Bandyopadhyay D, Biswas K, Bandyopadhyay U, et al. Melatonin protects against stress-induced gastric lesions by scavenging the hydroxyl radical. *J Pineal Res.* 2000;29:143–151.
41. Itoh MT, Ishizuka B, Kuribayashi Y, et al. Melatonin, its precursors, and synthesizing enzyme activities in the human ovary. *Mol Hum Reprod.* 1999;5:402–408.
42. Nakamura Y, Tamura H, Takayama H, et al. Increased endogenous level of melatonin in preovulatory human follicles does not directly influence progesterone production. *Fertil Steril.* 2003;80:1012–1016.
43. Tamura H, Takasaki A, Miwa I, et al. Oxidative stress impairs oocyte quality and melatonin protects oocytes from free radical damage and improves fertilization rate. *J Pineal Res.* 2008;44:280–287.
44. Sato EF, Kobuchi H, Edashige K, et al. Dynamic aspects of ovarian superoxide dismutase isozymes during the ovulatory process in the rat. *FEBS Lett.* 1992;303:121–125.
45. Hunt PA, Koehler KE, Susiarjo M, et al. Bisphenol A exposure causes meiotic aneuploidy in the female mouse. *Curr Biol.* 2003;13:546–553.
46. Kundakovic M, Gudsnuik K, Franks B, et al. Sex-specific epigenetic disruption and behavioral changes following low-dose in utero bisphenol A exposure. *Proc Natl Acad Sci USA.* 2013;110:9956–9961.
47. Vomsaal FS, Cooke PS, Buchanan DL, et al. A physiologically based approach to the study of bisphenol A and other estrogenic chemicals on the size of reproductive organs, daily sperm production, and behavior. *Toxicol Ind Health.* 1998;14:239–260.
48. Dessi-Fulgheri F, Porrini S, Farabollini F. Effects of perinatal exposure to bisphenol A on play behavior of female and male juvenile rats. *Environ Health Perspect.* 2002;110(Suppl 3):403–407.
49. Wynne DJ, Funabiki H. Kinetochore function is controlled by a phospho-dependent coexpansion of inner and outer components. *J Cell Biol.* 2015;210:899–916.
50. Nijenhuis W, Vallardi G, Teixeira A, et al. Negative feedback at kinetochores underlies a responsive spindle checkpoint signal. *Nat Cell Biol.* 2014;16:1257–1264.
51. Liu H. Insights into centromeric transcription in mitosis. *Transcription.* 2016;7:21–25.
52. Shomper M, Lappa C, Fitzharris G. Kinetochore microtubule establishment is defective in oocytes from aged mice. *Cell Cycle.* 2014;13:1171–1179.
53. Aydin H, Sultana A, Li S, et al. Molecular architecture of the human sperm IZUMO1 and egg JUNO fertilization complex. *Nature.* 2016;534:562–565.
54. Ohto U, Ishida H, Krayukhina E, et al. Structure of IZUMO1-JUNO reveals sperm-oocyte recognition during mammalian fertilization. *Nature.* 2016;534:566–569.
55. Bleil JD, Beall CF, Wassarman PM. Mammalian sperm-egg interaction: fertilization of mouse eggs triggers modification of the major zona pellucida glycoprotein, ZP2. *Dev Biol.* 1981;86:189–197.
56. Avella MA, Xiong B, Dean J. The molecular basis of gamete recognition in mice and humans. *Mol Hum Reprod.* 2013;19:279–289.
57. Clark GF. The molecular basis of mouse sperm-zona pellucida binding: a still unresolved issue in developmental biology. *Reproduction.* 2011;142:377–381.
58. Burkart AD, Xiong B, Baibakov B, et al. Ovastacin, a cortical granule protease, cleaves ZP2 in the zona pellucida to prevent polyspermy. *J Cell Biol.* 2012;197:37–44.
59. Bianchi E, Doe B, Goulding D, et al. Juno is the egg Izumo receptor and is essential for mammalian fertilization. *Nature.* 2014;508:483–487.
60. Han L, Nishimura K, Sadat AL, Hosseini H, et al. Divergent evolution of vitamin B9 binding underlies Juno-mediated adhesion of mammalian gametes. *Curr Biol.* 2016;26:R100–R101.
61. Fernando S, Rombauts L. Melatonin: shedding light on infertility? A review of the recent literature. *J Ovarian Res.* 2014;7:98.
62. Nair AB, Jacob S. A simple practice guide for dose conversion between animals and human. *J Basic Clin Pharm.* 2016;7:27–31.

How to cite this article: Zhang M, Dai X, Lu Y, et al. Melatonin protects oocyte quality from Bisphenol A-induced deterioration in the mouse. *J Pineal Res.* 2017;62:e12396. <https://doi.org/10.1111/jpi.12396>

RESEARCH ARTICLE

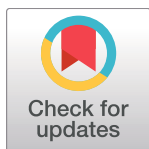
A Unique Egg Cortical Granule Localization Motif Is Required for Ovastacin Sequestration to Prevent Premature ZP2 Cleavage and Ensure Female Fertility in Mice

Bo Xiong^{1*}, Yangu Zhao, Stephanie Beall, Anna Burkart Sadusky, Jurrien Dean^{2*}

Laboratory of Cellular and Developmental Biology, NIDDK, National Institutes of Health, Bethesda, Maryland, United States of America

¹ Current address: College of Animal Science and Technology, Nanjing Agricultural University, Nanjing, China

* xiongbo@njau.edu.cn (BX); jurrien.dean@nih.gov (JD)



OPEN ACCESS

Citation: Xiong B, Zhao Y, Beall S, Sadusky AB, Dean J (2017) A Unique Egg Cortical Granule Localization Motif Is Required for Ovastacin Sequestration to Prevent Premature ZP2 Cleavage and Ensure Female Fertility in Mice. PLoS Genet 13(1): e1006580. doi:10.1371/journal.pgen.1006580

Editor: Paula E. Cohen, Cornell University, UNITED STATES

Received: October 26, 2016

Accepted: January 12, 2017

Published: January 23, 2017

Copyright: This is an open access article, free of all copyright, and may be freely reproduced, distributed, transmitted, modified, built upon, or otherwise used by anyone for any lawful purpose. The work is made available under the [Creative Commons CC0](https://creativecommons.org/licenses/by/4.0/) public domain dedication.

Data Availability Statement: All relevant data are within the paper and its Supporting Information files.

Funding: SB was supported by the Combined Federal Fellowship in Reproductive Endocrinology and Infertility and the research was funded by the intramural program of NIH, NIDDK (DK015603). The funders had no role in study design, data collection and analysis, decision to publish, or preparation of the manuscript.

Abstract

Monospermic fertilization is mediated by the extracellular zona pellucida composed of ZP1, ZP2 and ZP3. Sperm bind to the N-terminus of ZP2 which is cleaved after fertilization by ovastacin (encoded by *Astl*) exocytosed from egg cortical granules to prevent sperm binding. *Astl*^{Null} mice lack the post-fertilization block to sperm binding and the ability to rescue this phenotype with *Astl*^{mCherry} transgenic mice confirms the role of ovastacin in providing a definitive block to polyspermy. During oogenesis, endogenous ovastacin traffics through the endomembrane system prior to storage in peripherally located cortical granules. Deletion mutants of ovastacin^{mCherry} expressed in growing oocytes define a unique 7 amino acid motif near its N-terminus that is necessary and sufficient for cortical granule localization. Deletion of the 7 amino acids by CRISPR/Cas9 at the endogenous locus (*Astl*^Δ) prevents cortical granule localization of ovastacin. The misdirected enzyme is present within the endomembrane system and ZP2 is prematurely cleaved. Sperm bind poorly to the zona pellucida of *Astl*^{Δ/Δ} mice with partially cleaved ZP2 and female mice are sub-fertile.

Author Summary

Monospermic fertilization is essential for the onset of development. Egg cortical granules exocytose their contents after fertilization to prevent polyspermy by modifying the extracellular zona pellucida (ZP1, ZP2, ZP3). Little is known about the biology of these subcellular organelles which are unique to oocytes. Ovastacin, a zinc metalloendoprotease that cleaves ZP2 to prevent sperm binding, is a pioneer marker of mammalian cortical granules. ZP2 remains uncleaved in transgenic mice lacking ovastacin and sperm bind to the zona matrix independent of fertilization and cortical granule exocytosis. After documenting the rescue of the null phenotype with transgenic mice expressing fluorescently-tagged ovastacin, we defined a unique, well conserved, cortical granule localization motif using cRNA deletion mutants microinjected into mouse oocytes. The importance of the motif

Competing Interests: The authors have declared that no competing interest exist.

for localization to cortical granules was confirmed *in vivo* by deleting DNA encoding 7 amino acids of the endogenous locus with CRISPR/Cas9. Unexpectedly, mutant female mice were sub-fertile due to partial cleavage of ZP2 in the zona pellucida which prevented sperm from binding to ovulated eggs *in vitro* and *in vivo*. These observations offer unique insight into the molecular basis for translocation of proteins to cortical granules which is needed for successful, monospermic fertilization.

Introduction

In mammals, gamete recognition initiates fertilization and the onset of development. Although an overwhelming number of sperm are deposited in the lower female reproductive tract at coitus, a limited number progress to encounter the one, or relatively few, ovulated eggs. For fertilization, sperm must bind and penetrate the extracellular zona pellucida to fuse with eggs in the ampulla of the oviduct. Equally important are mechanisms that limit fertilization to a single sperm to avoid polyspermy which is embryonic lethal. Following fertilization, there is an immediate block to gamete fusion at the egg plasma membrane [1, 2] that is independent of cortical granule exocytosis [3, 4]. Subsequent cortical granule exocytosis [5] blocks sperm binding to the zona pellucida [6], but the underlying molecular mechanisms remain obscure and we have little understanding of these subcellular organelles in mice.

Mammalian cortical granules, first described in hamster [7], are detected in mice starting in unilaminar follicles where immature oocytes are surrounded by a single layer of cuboidal granulosa cells. During oocyte-growth, cortical granules continuously arise from the Golgi apparatus [8] and require microfilaments to migrate to the periphery [9]. Concomitant with oocyte growth, the number of cortical granules increases to 6,000–8,000 and are uniformly distributed in the subcortex of full-grown, 80 μm oocytes [10]. However, cortical granule exocytosis is not yet enabled in these germinal vesicle (GV, nucleus) intact oocytes [11]. During meiosis I, a substantial cortical granule free domain appears in mice (25–40% of surface area), the first polar body is extruded and cortical granules decrease to ~4,000 [12]. Rather than early exocytosis, this cortical granule free domain reflects a redistribution of granules that is triggered by the peripheral migration of chromatin during meiosis I and formation of an actin cap [13]. Cortical granules become fully competent for exocytosis after completion of the first meiotic division in MII eggs [11, 14].

The egg is activated at fertilization and cortical granule exocytosis is triggered by release of Ca^{+2} from proximate, peripherally located stores in the endoplasmic reticulum [15]. Although precise details remain under investigation, cortical granule fusion with the egg plasma membrane involves SNARE-protein mediated pathways [16, 17]. Unlike regulated secretory granules in somatic cells (e.g., synaptic vesicles of neurons, zymogen granules of pancreatic acinar cells), cortical granules in oocytes are not renewed after exocytosis. Cortical granules contain a discrete set of proteins, albeit varying by report [18–20], including trypsin-like proteases [21–23], ovoperoxidase [24], N-acetylglucosaminidase [25], a 75 kD protein of unknown function [26] and, most recently, an astacin-like metalloendoprotease encoded by *Astl* [27]. The only documented function ascribed to cortical granules is the post-fertilization zona block to polyspermy that prevents sperm binding and penetration through the zona pellucida [22, 28].

The zona pellucida, composed of three (mouse) or four (human) glycoproteins (ZP1–4), surrounds growing oocytes, ovulated eggs and pre-implantation embryos [29, 30]. The N-terminus of ZP2^{51–149} has been defined as the zona ligand for sperm binding based on gain- and loss-of-function assays in transgenic mice [31, 32]. Ovastacin (435 amino acids) is an

oocyte-specific member of the astacin-like family of Zn^{+2} metalloendoproteases that is synthesized as a zymogen with a signal peptide (1–23 aa) to direct it into the endomembrane system for ultimate storage in cortical granules. For enzymatic activity, astacins require removal of an N-terminal prosegment (24–85 aa) that runs in opposite direction to the future protein substrate [33]. The enzymatic active site of ovastacin is formed by glutamate and a single zinc atom complexed to three adjacent histidine residues (underlined, ¹⁸²HELMHVLGFWH¹⁹²). Following fertilization, ovastacin is exocytosed from egg cortical granules and cleaves ZP2 at ¹⁶⁶LA[↓]DE¹⁶⁹ after which sperm no longer bind. Ablation of *Astl* that encodes ovastacin, or mutation of the ZP2 cleavage site (*Zp2^{Mut}*), prevents post-fertilization cleavage of ZP2 and sperm bind to the surface of the zona pellucida of 2-cell embryos despite fertilization and cortical granule exocytosis [27, 34].

Using mouse transgenesis, we rescue the *Astl^{Null}* phenotype by ectopic expression of *Astl^{mCherry}* and define a 7 amino acid motif required for ovastacin trafficking to cortical granules. Deletion of the cortical granule localization signal at the endogenous locus with CRISPR/Cas9 unexpectedly leads to premature modification of the egg's zona pellucida and female sub-fertility.

Results and Discussion

Astl^{mCherry} transgenic mice provide an authentic biological marker for cortical granules

The zona pellucida and ovastacin proteins transverse the endomembrane system during oogenesis during which passage ZP2 remains intact [27]. Secreted ZP2 is incorporated into the extracellular zona pellucida surrounding ovulated eggs and is cleaved in the zona matrix surrounding 2-cell embryos [28]. In addition to a rapid, cortical-granule independent, post-fertilization block to gamete fusion [1, 2], ZP2 cleavage provides a definitive block to polyspermy in that sperm that do not bind cannot penetrate the zona matrix nor fuse with the egg plasma membrane [34].

The single copy *Astl* gene encodes ovastacin (435 aa), an oocyte-specific metalloendoprotease [35] that has been located by immunohistochemistry in cortical granules at the periphery of growing oocytes and ovulated eggs. In *Astl^{Null}* mice that lack ovastacin, ZP2 remains intact in the zona surrounding 2-cell embryos [27]. To confirm that these observations reflect the absence of ovastacin, we established *Astl^{mCherry}* transgenic mice expressing ovastacin tagged with fluorescent mCherry at the C-terminus (Fig 1a, S1a and S1b Fig) and documented ovary-specific expression by RT-PCR (S1c Fig). The biological authenticity of the *Astl^{mCherry}* transgene *in vivo* was investigated by crossing *Astl^{mCherry}* with *Astl^{Null}* mice to generate a 'rescue' mouse line. The null phenotype was reversed in mice expressing the *Astl^{mCherry}* transgene in the *Astl^{Null}* background and ZP2 was cleaved in the zona pellucida surrounding 2-cell embryos (Fig 1b).

Sperm bind to the zona pellucida if ZP2 is uncleaved, independent of fertilization and cortical granule exocytosis [27, 34]. Thus, sperm did not bind to the zona matrix surrounding wild-type embryos (Fig 1c), but did bind to *Astl^{Null}* derived embryos (Fig 1d) in which ZP2 remains intact. However, sperm did not bind to 2-cell embryos derived from 'rescue' female mice (Fig 1e) in which ZP2 was cleaved (Fig 1b). The ability of *Astl^{mCherry}* transgene to rescue the *Astl^{Null}* phenotype is consistent with ovastacin acting as the cortical granule protease responsible for the post-fertilization cleavage of ZP2 that prevents sperm binding and provides a block to polyspermy. The *Astl^{mCherry}* mice also offer a useful platform for live-imaging that should provide additional insights into cortical granule biology.

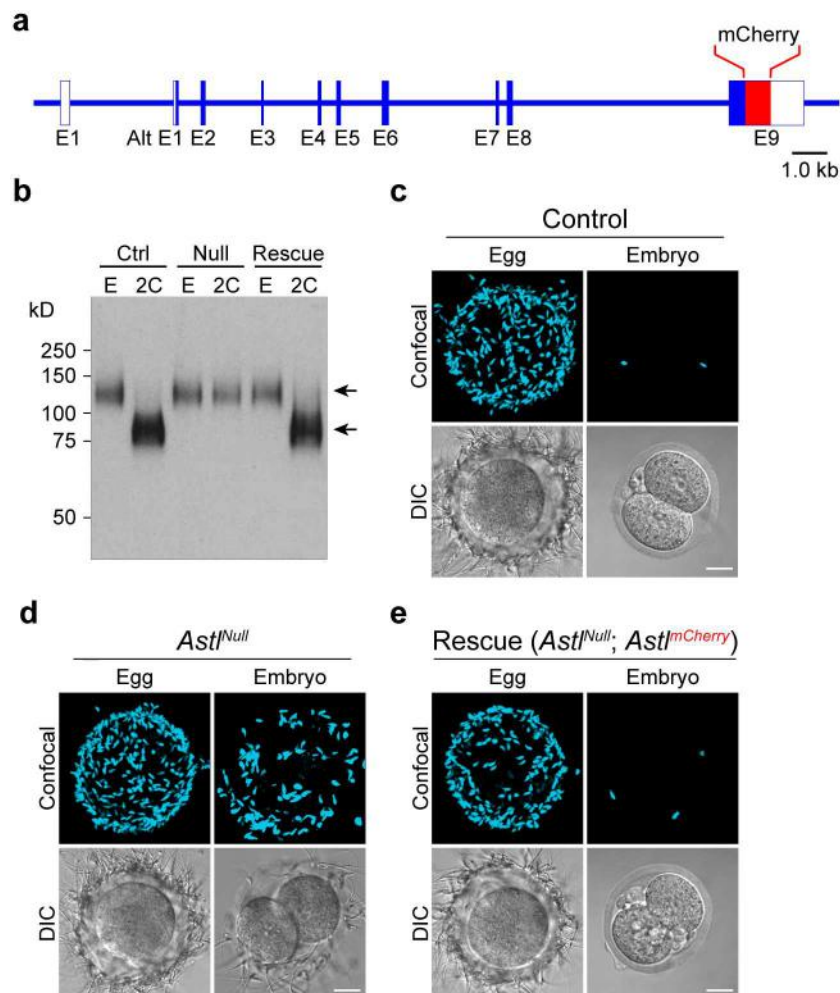


Fig 1. *Astl*^{mCherry} rescues the *Astl*^{Null} phenotype. (a) Schematic of the *Astl*^{mCherry} transgene. (b) Immunoblot of eggs (E) and 2-cell embryos (2C) from wild-type (Ctrl), *Astl*^{Null} (Null) and *Astl*^{Null}; *Astl*^{mCherry} (Rescue) mice (10–15 eggs or embryos per lane). Primary antibody (M2c.2) binds to the C-terminus of ZP2 and detected intact (upper arrow) and cleaved (lower arrow) protein. Molecular mass (kD) on left. (c–e) Mouse sperm binding to eggs and two-cell embryos from: (c), wild-type; (d), *Astl*^{Null}, and (e), *Astl*^{mCherry} rescue mice. Confocal projections (upper) and DIC (lower) images were obtained after fixation and staining with Hoechst. Scale bar, 20 μ m.

doi:10.1371/journal.pgen.1006580.g001

Localization of cortical granules before and after fertilization

Prior to germinal vesicle (nucleus) breakdown (GVBD), cortical granules are uniformly present in the subcortex of fully grown oocytes [27]. To validate the intracellular trafficking of ovastacin to the cortex *in vivo*, intraovarian oocytes (up to 70 μ m diameter) were isolated from *Astl*^{mCherry} transgenic mice and placed in an environmental chamber where confocal microscopy was used to obtain live images during GVBD. Most of the fluorescent signal was detected in peripherally located cortical granules. However, by increasing the sensitivity, ovastacin^{mCherry} was detected throughout the first 2 hr of culture in the peri-nuclear region where the endoplasmic reticulum (ER) is located (Fig 2a, left panel). Subsequently, during the early phases of GVBD, ovastacin^{mCherry} was present in close proximity to the dissolving nuclear membrane (Fig 2a, middle panel), but by 4 hr it was primarily located in the subcortex in the periphery of oocytes (Fig 2a, right panel). These observations were complemented

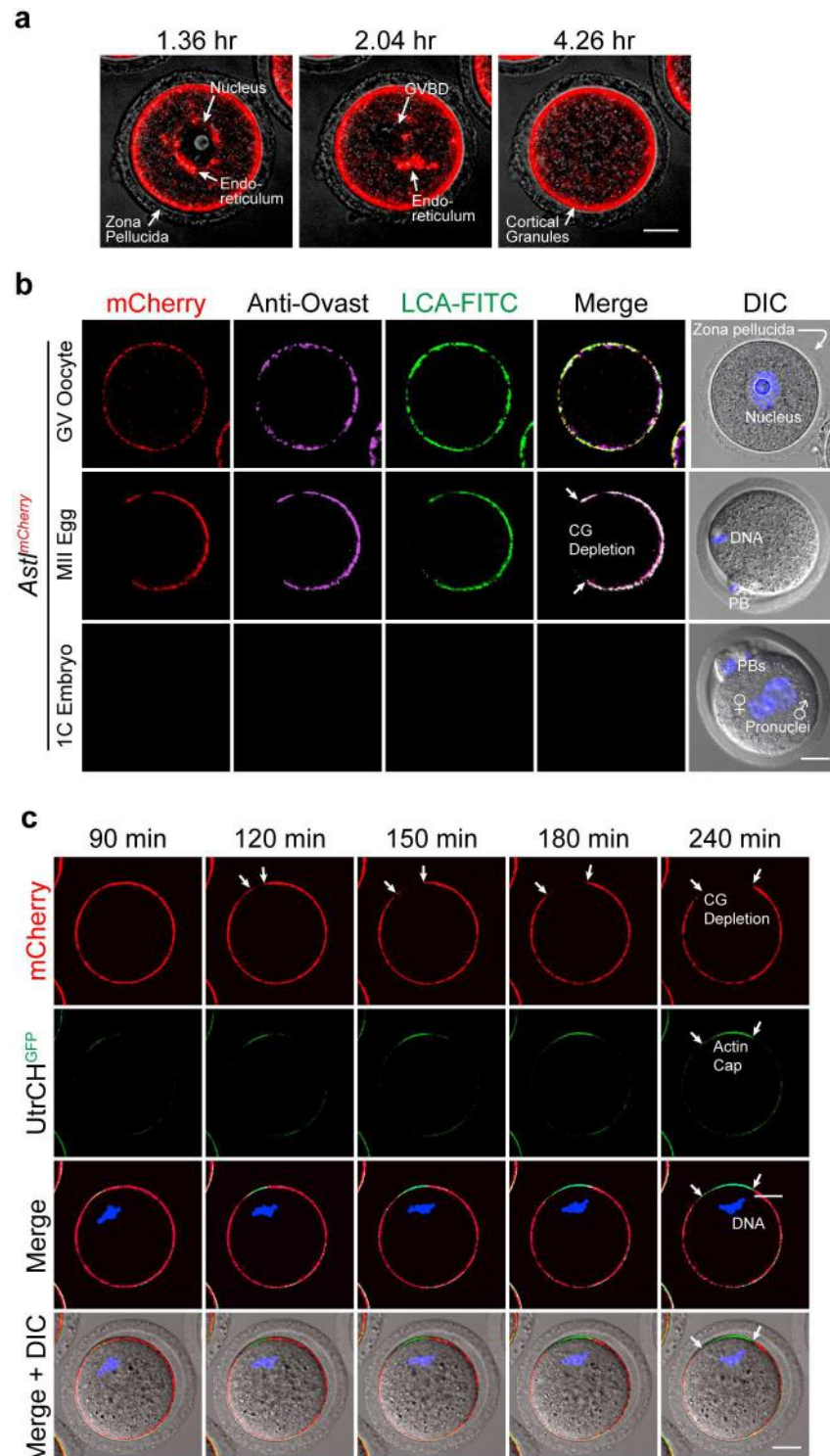


Fig 2. Localization of *Astl^{mCherry}* to cortical granules in transgenic mice. (a) Oocytes (70–75 μ m) were isolated from *Astl^{mCherry}* transgenic mice and imaged in an environmental chamber (37°C, 5% CO₂) by confocal microscopy during germinal vesicle (nucleus) breakdown (GVBD). (b) GV-intact oocytes (upper), ovulated metaphase II (MII) eggs (middle) and one cell (1C) embryos (lower) from *Astl^{mCherry}* transgenic mice were permeabilized, stained with antibody to ovastacin and with LCA-FITC to localize cortical granules and imaged with confocal and DIC microscopy. CG, cortical granule; PB, polar body. Scale bar, 20 μ m. (c) GV-intact oocytes from *Astl^{mCherry}* transgenic mice were injected with cRNA encoding UtrCH^{GFP} (calponin

homology domain of utrophin) to localize the actin cap associated with formation of the cortical granule free region during meiotic maturation. Live-images were obtained over time (4 hr) using confocal and DIC microscopy. Scale bars, 20 μ m.

doi:10.1371/journal.pgen.1006580.g002

in fixed samples in which ovastacin^{mCherry} partially co-localized with markers for the endoplasmic reticulum (GP73) and the Golgi apparatus (calregulin) in 70–75 μ m growing oocytes (S2a Fig) which confirmed its presence in the endomembrane system. The absence of co-localization with the endosome pathway marker (EEA1) indicates little diversion into degradation pathways. Thus, we conclude that ovastacin follows the normal progression from the endoplasmic reticulum to the Golgi apparatus and is then sequestered in peripheral cortical granules.

Ovastacin^{mCherry}, not present in wild-type GV-intact oocytes, co-localized with anti-ovastacin antibody staining and LCA consistent with the localization of endogenous ovastacin and ovastacin^{mCherry} in peripheral cortical granules (Fig 2b). During meiotic maturation, chromosomes move to the cortex at metaphase I where a cortical granule free domain (CGFD) develops (Fig 2b). The biological significance of CGFD is not understood, although it has been reported that sperm do not fuse with the egg plasma membrane in this region to protect the maternal genetic material [36]. However, whether cortical granules in this region are released or redistributed has not been fully resolved, although the latter has become the favored model [13].

To confirm that the presence of an actin cap correlated with the absence of cortical granules from the CGFD in the transgenic mice, cRNA encoding UtrCH-GFP, a green fluorescent protein tagged actin binding protein, was injected into oocytes from *Astl*^{mCherry} mice. Live imaging for 4 hr during meiotic maturation documented that the appearance of the actin cap and CGFD formation temporally coincided with complementary formation of the GFP (actin) and mCherry (ovastacin within cortical granules) signals (Fig 2c). To determine if formation of the CGFD was reversible, ovulated eggs from *Astl*^{mCherry} mice were incubated with CK-666 to stabilize the inactive form of the arp2/3 complex and depolymerize the actin cytoskeleton [37]. Within 3 hr, the cortical granules became uniformly distributed in the *Astl*^{mCherry} eggs and the metaphase plate migrates back towards the center of the cell (S2b Fig). Thus, we conclude that formation of the actin cap excludes cortical granules and results in a cortical granule free domain which has been reported to be physiologically induced by chromatin signaling [13].

Following fertilization and cortical granule exocytosis, ovastacin^{mCherry} was no longer detected in one-cell zygotes in fixed samples (Fig 2b). To detail this process, cortical granules were live-imaged with confocal microscopy during the 5 hr following fertilization. Sperm fused to eggs and cortical granules released ovastacin^{mCherry} 90–120 min after insemination. This process was complete by 150 min by which time the egg had extruded a second polar body (2nd PB) to complete meiosis II. The sperm nucleus then decondensed (180 min) leading to formation of male and female pronuclei within 5 hr of insemination which was indicative of successful fertilization (S2c Fig). These observations are consistent with ovastacin being directed into the endomembrane system via its signal peptide and being transported to cortical granules in the periphery of growing oocytes. Ovastacin is rapidly released from cortical granules following fertilization and formation of the 1 cell zygote. However, the molecular basis for localization of ovastacin in cortical granules was unclear.

Identification of a cortical granule localization motif

To search a motif for cortical granule localization, cRNA encoding full-length ovastacin (1–435 aa) fused at the C-terminus with mCherry was injected into the cytoplasm of growing oocytes and transiently expressed for 6 hr as a positive control (Fig 3a). Subsequently, cRNA

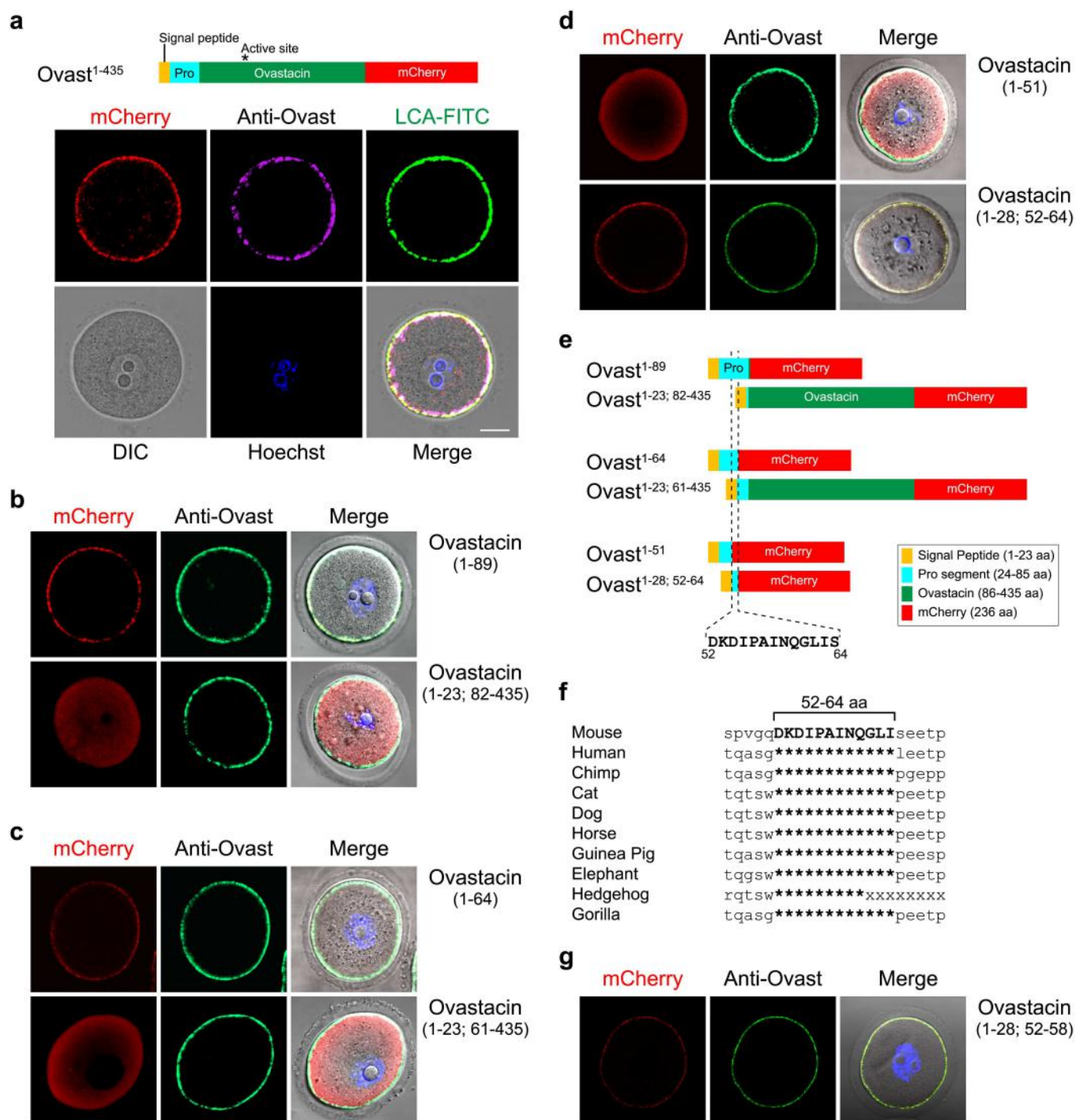


Fig 3. Ovastacin cortical granule localization motif. (a) Growing oocytes (60–65 μ m) were injected with cRNA encoding an ovastacin^{mCherry} fusion protein (top) with a signal peptide (1–23 aa), a pro segment (24–85 aa) and the mature ovastacin enzyme (86–435 aa) containing an active site (asterisk, ¹⁸²HELMHVLGF¹⁹²) fused to mCherry (236 aa). Six hr after injection, oocytes were fixed, permeabilized and stained with antibodies to ovastacin, LCA-FITC and Hoechst and imaged by confocal and DIC microscopy (bottom). Scale bar, 20 μ m. (b) Same as (a) after injection of cRNA encoding either ovastacin 1–89 aa or ovastacin 1–23; 82–435 aa indicated in (e). (c) Same as (a) after injection of cRNA encoding either ovastacin 1–64 aa or ovastacin 1–23; 61–435 aa indicated in (e). (d) Same as (a) after injection of cRNA encoding either ovastacin 1–51 aa or ovastacin 1–28; 52–64 aa indicated in (e). (e) Schematic representation of three pairs of complementary deletion constructs of ovastacin^{mCherry} fusion proteins injected into growing oocytes. Dotted lines indicate the minimal sequence (ovastacin^{Δ52–64}) for localization of the fusion protein to cortical granules. (f) Primary amino acid sequences of ovastacin from 10 mammals were aligned to mouse ovastacin^{Δ47–69}. The conservation of mouse ovastacin^{Δ52–64} cortical granule localization signal is indicated by asterisks. (g) Same as (a) after injection of cRNA encoding ovastacin 1–28; 52–58.

doi:10.1371/journal.pgen.1006580.g003

encoding deleted portions of ovastacin that retained the signal peptide, were injected into oocytes. Constructs encoding 1–89 aa, but not 82–435 aa (Fig 3b), localized to cortical granules as did constructs encoding 1–64 aa, but not 61–435 aa (Fig 3c). This initial delineation of a 41 aa motif (23–64 aa) was further refined by the observation that constructs with 52–64 aa, but not 1–51 aa, were sufficient for cortical granule localization (Fig 3d). Thus, ⁵²DKDIPAINQ-GLIS⁶⁴ is necessary and sufficient for the *in vitro* localization of a reporter protein to cortical granules (Fig 3e). Although well conserved among mammalian ovastacins (Fig 3f), the 13 amino acid motif was not identified in other proteins after a BLAST search of mouse databases.

Deletion mutation of the cortical granule localizing motif of endogenous *Astl*

The 13 aa cortical granule localizing motif is encoded by exons 2 and 3 of the endogenous *Astl* gene. To avoid disruption of RNA splicing, we elected to delete the first 7 aa (⁵²DKDIPAI⁵⁸) encoded entirely by exon 2 with a protospacer adjacent motif (PAM) sequence targeted by CRISPR/Cas9 (Fig 4a). To confirm the validity of this approach, cRNA encoding the signal peptide and ovastacin^{52–58} fused to mCherry were injected into oocytes. The localization of mCherry confirmed the sufficiency of the 7 aa to direct proteins to peripheral cortical granules (Fig 3g). To delete DNA encoding ⁵²DKDIPAI⁵⁸ at the endogenous *Astl* locus, Cas9 cRNA, sgRNA and HDR (homology directed repair) oligonucleotides (S3a and S3b Fig) were injected into zygotes, cultured to blastocysts, and transferred to uteri of pseudopregnant foster mothers. Of 7 pups screened by PCR (S3c Fig), two had bi-allelic mutations that were confirmed by DNA sequence (S3d and S3e Fig). In each line, the CRISPR/Cas9 mutation had been modified by homology directed repair to produce the desired deletion on one of the two endogenous alleles. Each line was crossed to wild-type mice to remove the non-desired mutant allele (either a single base pair insertion or deletion) and bred to homozygosity. Each expressed *Astl*^Δ alleles that encoded ovastacin lacking 52–58 aa (Fig 4a, ovastacin^{Δ52–58}).

Using a monospecific antibody to the C-terminal region of the metalloendoprotease [27], ovastacin (accumulated during oocyte growth) was detected in cortical granules defined by staining with the LCA lectin in the periphery of wild-type GV oocytes (Fig 4b). In contrast, ovastacin was detected as punctate loci throughout the endomembrane system of oocytes and eggs (upper two rows of panels) from *Astl*^{Δ/Δ} female mice (Fig 4c) which could reflect either an inability to correctly traffic to cortical granules for storage or retrograde transport after reaching cortical granules. These results confirmed the *in vitro* transient assays in growing oocytes in which expression of mutant mCherry-tagged proteins was below the detection level of the antibody (Fig 3) and defined the 7 aa motif (ovastacin^{Δ52–58}) as important for the correct intracellular trafficking of ovastacin. Following fertilization, cortical granule exocytosis was documented by the loss of LCA staining, but ovastacin remained diffusely present throughout the endomembrane system of zygotes and 2-cell embryos (Fig 4c, lower two rows of panels).

In oocytes and eggs from *Astl*^{+/Δ} mice, ovastacin was present both in the endomembrane system and at the periphery, where it partially co-localized with LCA in cortical granules (Fig 4d). To determine if the *Astl*^Δ allele was co-dominant, the *Astl*^{+/Δ} mice were crossed with *Astl*^{mCherry} transgenic mice to produce *Astl*^{+/Δ}; *Astl*^{mCherry} transgenic mice. In these mice, ovastacin^{mCherry} lacks the deletion mutation and provides a proxy for the wild-type allele. Ovastacin^{mCherry} was detected in cortical granules located in the subcortex of oocytes and eggs (Fig 4e). Taken together, these observations define the ovastacin^{Δ52–58} protein as co-dominant with the wild-type protein and the absence of the cortical granule localization motif results in persistence of the mutant protein in the endomembrane system.

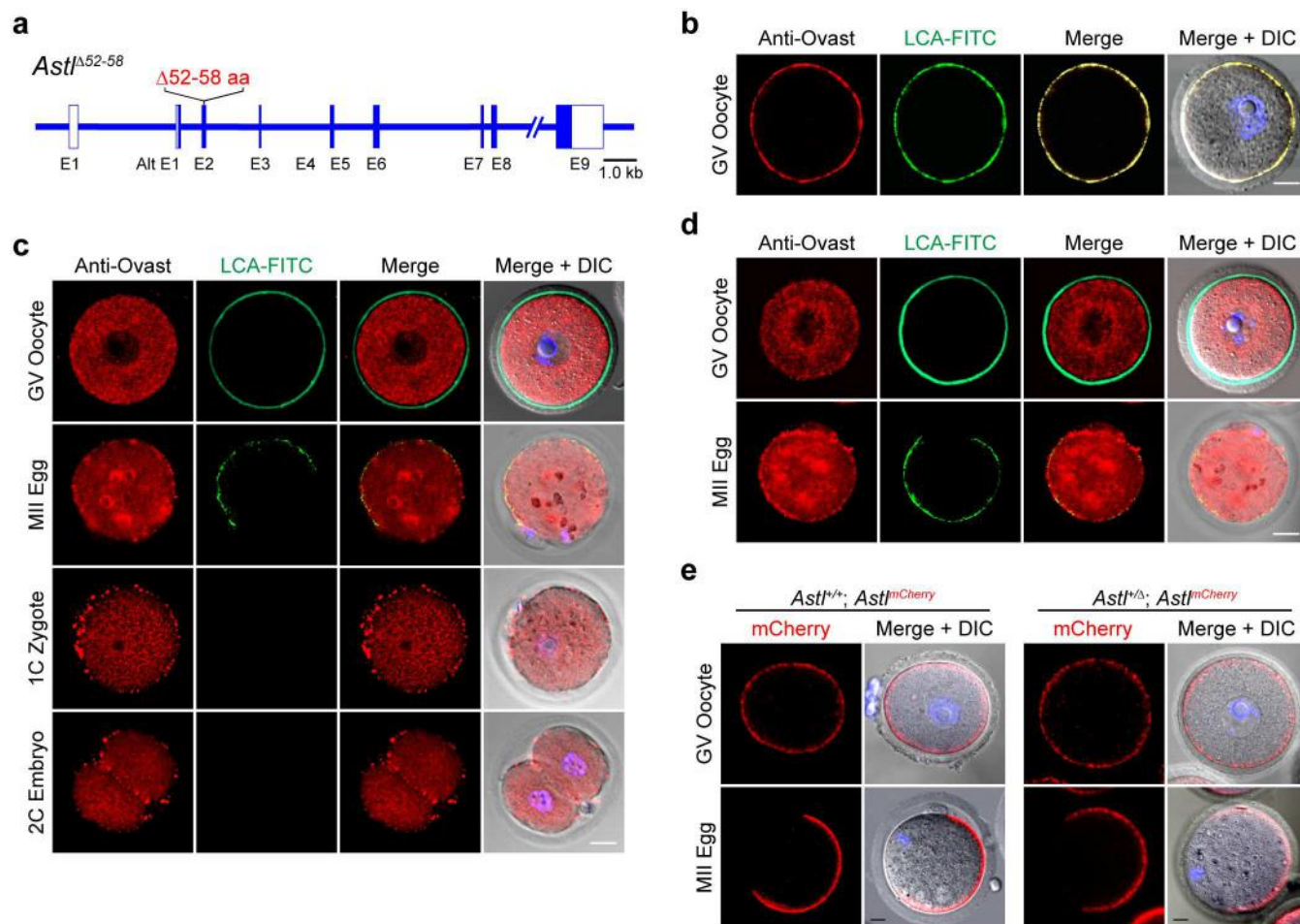


Fig 4. Ovastacin is not present in cortical granules after partial deletion of the localization motif. (a) Schematic representation of the CRISPR/Cas9 deletion mutation in *Astl* exon 2 that encodes ovastacin^{Δ52-58}. (b) Wild-type GV-intact oocytes were fixed, permeabilized and stained with antibodies to ovastacin, LCA-FITC and imaged by confocal and DIC microscopy. (c) Same as (b) with GV-intact oocytes, ovulated MII eggs, 1-cell zygotes and 2-cell embryos from *Astl*^{Δ/Δ} mice. (d) Same as (b) with GV-intact oocytes and ovulated MII eggs from *Astl*^{+/Δ} mice. (e) GV-intact oocytes and ovulated MII eggs from *Astl*^{+/+}; *Astl*^{mCherry} and *Astl*^{+/Δ}; *Astl*^{mCherry} mice were fixed, permeabilized and imaged by confocal and DIC microscopy. Scale bars, 20 μm.

doi:10.1371/journal.pgen.1006580.g004

Premature cleavage of ZP2 in *Astl*^{Δ/Δ} mice decreases female fertility

Zonae pellucidae isolated from eggs ovulated by wild-type, *Astl*^{+/Δ} and *Astl*^{Δ/Δ} female mice as well as from 2-cell embryos after mating wild-type mice were analyzed by immunoblot. As expected, ZP2 was uncleaved in wild-type eggs and completely cleaved in wild-type 2-cell embryos (Fig 5a). The partial cleavage of ZP2 observed in *Astl*^{+/Δ} eggs became more pronounced in *Astl*^{Δ/Δ} eggs and is similar to the 'hardening' reaction observed during *in vitro* fertilization in the absence of serum proteins [38].

Normally, sperm bind to the zona matrix surrounding eggs, but not 2-cell embryos. Compared to wild-type eggs, many fewer sperm bound *in vitro* to *Astl*^{+/Δ} eggs (18.9 ± 1.7 vs. 47.2 ± 3.0) and virtually no sperm (3.9 ± 0.7) bound to the zona pellucida surrounding *Astl*^{Δ/Δ} eggs (Fig 5b and 5c). *In vivo* fertilization of wild-type, *Astl*^{+/Δ} and *Astl*^{Δ/Δ} mice reflected these *in vitro* observations. After natural mating, eggs/embryos were recovered from the oviduct of female mice: $87.7 \pm 2.3\%$ of wild-type, $22.5 \pm 4.0\%$ of *Astl*^{+/Δ}, but only $0.8 \pm 0.8\%$ of *Astl*^{Δ/Δ} eggs were fertilized (S1 Table).

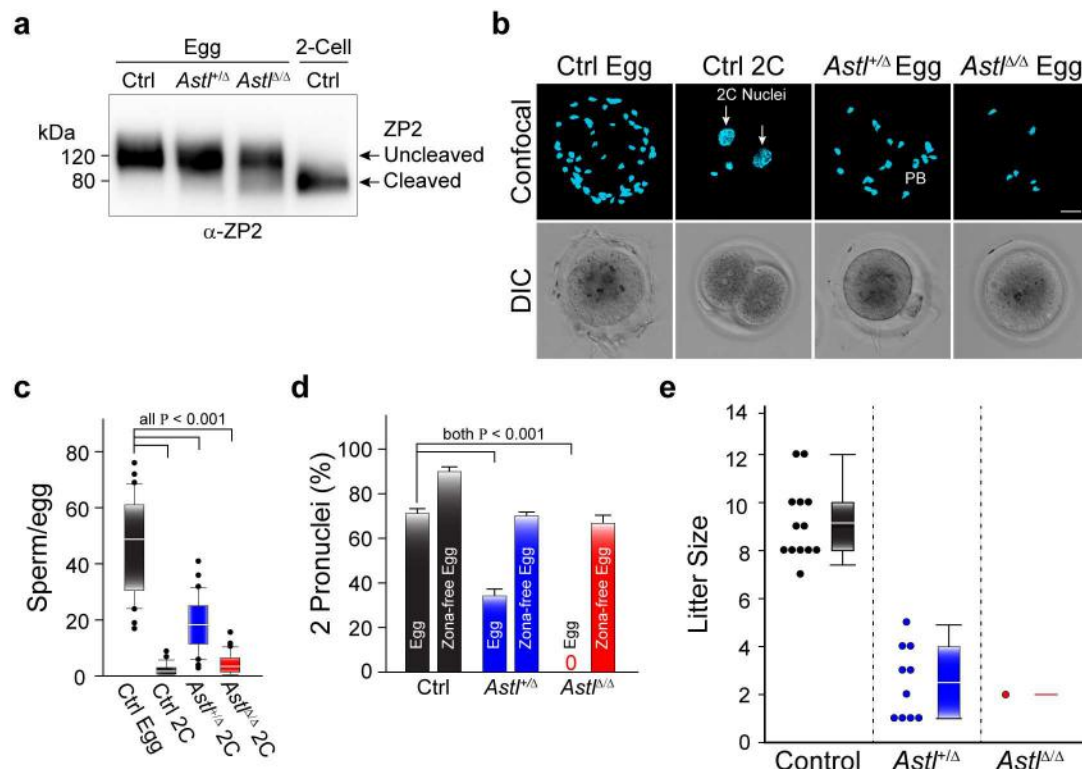


Fig 5. Premature cleavage of ZP2 affects fertility of *Astl* mutant mice. (a) Immunoblot of zonae pellucidae from wild-type (Ctrl), *Astl*^{+/Δ} and *Astl*^{Δ/Δ} ovulated eggs as well as wild-type 2C embryos (Ctrl) stained with a monoclonal antibody (M2c.2) that binds to the C-terminus of ZP2 and detected intact (upper arrow) and cleaved (lower arrow) protein. Molecular mass (kD) on left. (b) Sperm binding to wild-type eggs, 2C embryos, *Astl*^{+/Δ} and *Astl*^{Δ/Δ} eggs. Confocal projections (upper) and DIC (lower) images were obtained after fixation and staining nuclei with Hoechst. Arrows, nuclei; PB, polar body. Scale bar, 20 μm. (c) Average (± s.e.m) number of sperm bound to wild-type eggs (Ctrl), 2C embryos (Ctrl), *Astl*^{+/Δ} and *Astl*^{Δ/Δ} eggs imaged in (b). N = 30 in each case. (d) *In vitro* fertilization with wild-type (left), *Astl*^{+/Δ} (center) and *Astl*^{Δ/Δ} (right) eggs with and without zonae pellucidae. Fertilization was determined by the presence of 2 pronuclei 12 hr after insemination. (e) Dot density (left) and associated box plots (right) of litters from wild-type (Control), *Astl*^{+/Δ} and *Astl*^{Δ/Δ} females co-caged with fertile male mice. The box includes the mean (horizontal line) and data between the 25th and 75th percentile. Error bars indicate the 90th and 10th percentiles and outliers are indicated by dots. Statistical differences in c and d were determined by 2-tailed Student's T-test, P < 0.001.

doi:10.1371/journal.pgen.1006580.g005

To confirm that the block to fertilization was based on partially cleaved ZP2, fertility was assessed in the presence and absence of zonae pellucidae. After *in vitro* insemination with capacitated sperm, zona-intact *Astl*^{+/Δ} eggs had ~50% reduction in fertility compared to wild-type eggs and no *Astl*^{Δ/Δ} eggs were fertilized in these experiments. However, after removal of the zona pellucida matrix, the fertilization rates of zona-free *Astl*^{+/Δ} and *Astl*^{Δ/Δ} eggs were comparable (Fig 5d). Thus, we concluded that the partially cleaved ZP2 in the zona pellucida adversely affected fertilization.

The homozygous *Astl*^Δ allele had a profound effect on the fecundity of female mice. *In vivo* fertility of ovastacin^{Δ52–58} was assessed by co-caging wild-type, *Astl*^{+/Δ} and *Astl*^{Δ/Δ} females with male mice proven to be fertile. The number of litters from *Astl*^{+/Δ} was decreased compared to wild-type female mice (9 vs. 13) and the number of pups/litter produced by *Astl*^{+/Δ} was significantly lower than wild-type female mice (2.5 ± 0.8 vs. 9.2 ± 2.5). A single litter of 2 pups was obtained from eight *Astl*^{Δ/Δ} female mice (Fig 5e and S1 Table). Taken together, we conclude that ovastacin^{Δ52–58} does not properly traffic to cortical granules leading to premature cleavage of ZP2 which prevents sperm binding to the zona pellucida and decreases female fertility.

Conclusions

ZP2 is a major component of the zona pellucida to which sperm bind prior to penetrating the zona matrix and fusing with the egg. Following fertilization and cortical granule exocytosis, ZP2 is cleaved by ovastacin after which sperm do not bind to the zona pellucida. *Zp2^{Mut}* and *Astl^{Null}* mice documented that sperm binding to the surface of the zona pellucida is dependent on the cleavage status of ZP2, independent of fertilization and cortical granule exocytosis [27, 34]. In each of these mutant lines, ZP2 is uncleaved in the zona pellucida surrounding ovulated eggs which can be fertilized *in vitro* and *in vivo*. After fertilization and cortical granule exocytosis, ZP2 remains uncleaved and sperm can bind *de novo* to the zona matrix surrounding zygotes derived from *Zp2^{Mut}* and *Astl^{Null}* female mice. Although at risk, the additional post-fertilization block to sperm fusing with the egg plasma membrane [1, 2] and the relatively few sperm (<10 sperm/egg) that reach the egg in the ampulla of the oviduct [39, 40] help protect *Zp2^{Mut}* and *Astl^{Null}* females from polyspermy.

The observed partial cleavage of ZP2 in the *Astl^{A/A}* is puzzling and could reflect a continuous release of low concentrations of constitutively secreted ovastacin during oocyte growth rather than the abrupt release of higher concentrations of the enzyme thought to accompany cortical granule exocytosis at fertilization. This formulation is consistent with earlier observations in which incubation of ovulated eggs in the absence of serum proteins caused a ‘hardening’ reaction that prevented sperm binding to the zona pellucida and fertilization [41]. The molecular basis of this phenomenon has recently been ascribed to fetuin-B, a member of the cystatin superfamily of protease inhibitors that are secreted by the liver and circulate as serum proteins. Fetuin was reported to inhibit premature cleavage of ZP2 [38] and this activity has been attributed more precisely to fetuin-B which is present at low levels in follicular fluid [42]. It has been proposed that a minimal amount of fetuin-B is sufficient to inhibit the small amount of secreted ovastacin that escapes sequestration in cortical granules and prevent premature cleavage of ZP2. However, the ovastacin released from cortical granule exocytosis would overwhelm this fragile defense and cleave ZP2 to prevent post-fertilization sperm binding [43]. Similar to *Astl^{A/A}* mice, ZP2 is only partially cleaved in the zona matrix surrounding ovulated eggs from *Fetub^{Null}* mice and yet female mice are sub-fertile.

Thus, the timing of ZP2 cleavage by ovastacin is a critical determinant of whether or not sperm bind and fertilize eggs encased in the surrounding zona pellucida. Premature ZP2 cleavage (*Astl^{A/A}* or *Fetub^{Null}*) prevents sperm binding and fertility, whereas delayed or absent ZP2 cleavage runs the risk of post-fertilization polyspermy. Eggs from *Astl^{Null}* females do not accumulate ovastacin in their cortical granules and are unable to cleave ZP2 following fertilization and cortical granule exocytosis. The ability of *Astl^{mCherry}* to rescue this phenotype and restore fertility confirms the role of ovastacin in the post-fertilization cleavage of ZP2 and provides a marker for future investigations into the biology of cortical granules. The cortical granule localization motif defined *in vitro* and confirmed *in vivo* by deletion of a 7 amino acids in the endogenous gene locus is highly conserved among mammals. Identification of binding partners to ovastacin should provide further insight into the molecular basis for the translocation of ovastacin to these unique subcellular organelles of female germ cells.

Materials and Methods

Establishment of *Astl^{mCherry}* transgenic mice

All mice were handled in compliance with the guidelines of the Animal Care and Use Committee of the National Institutes of Health under the Division of Intramural Research, National

Institute of Diabetes and Digestive and Kidney Diseases approved animal study protocols. A summary of the transgenic mice used in these investigations is provided in [S2 Table](#).

To construct the transgene, bacterial artificial chromosome (BAC) DNA (Life Technologies) that included mouse *Astl* (BMQ56H22) was transformed into SW102 bacterial cells containing the λ prophage recombineering system [44]. A PCR fragment (1331 bp) containing the galK operon flanked by 50 bp homologous to the *Astl* gene that would insert the galK gene at the stop codon in the 3' region of the gene was amplified using Long Amp Taq Polymerase (New England Biolabs, Ipswich, MA). After digestion with DpnI and overnight gel purification (0.7% agarose, 15 V, 16 hr), the PCR fragment was electroporated into SW102 cells containing the BAC, and recombinants were selected by growth on minimal media with galactose. Using a clone from this first step, the galK cassette was replaced by recombineering with a second PCR fragment (880 bp) encoding mCherry with 50 bp homology arms. Clones were selected on minimal media with 2-deoxy-galactose and confirmed by DNA sequence. Finally, a NotI fragment containing the *Astl*^{mCherry} transgene was retrieved from the BAC with p1253, and the fidelity of coding regions was confirmed by DNA sequence.

After gel purification, the *Astl*^{mCherry} transgene was injected into the male pronucleus of >200 one-cell zygotes which were transferred to pseudopregnant female mice. Offspring were genotyped ([S1b Fig](#)) using tail DNA and *Astl* exon 9 oligonucleotides ([S3 Table](#)) that distinguished between the normal allele (268 bp) and the *Astl*^{mCherry} transgene (967 bp). From 30 pups, 6 founders were identified that passed the transgene through the germline. Three lines were maintained and the analysis of FVB/N-Tg(*Astl*-mCherry)1Dean is described herein. Tissue-specific expression of *Astl*^{mCherry} was determined by RT-PCR using total RNA from various tissues to make cDNA with SuperScript[®] III First-Strand Synthesis System (Life Technologies). PCR analysis of cDNA was performed using primers ([S3 Table](#)) designed to span an exon-intron boundary.

Establishment of *Astl*^{Δ/Δ} mice by CRISPR/Cas9

pMLM3613 (Addgene, Cambridge, MA #42251) expressing Cas9 was linearized by PmeI (New England Biolabs), purified with a PCR clean-up kit (Clontech Laboratories, Mountain View, CA) and *in vitro* transcribed with mMESSAGE mMACHINE T7 ULTRA (Life Technologies-Ambion, Carlsbad, CA). Double-stranded synthetic DNA targeting exon 2 of *Astl* (5'-GGACATCCCCGCAATTAACCAAGG-3') was cloned into the pair of BsaI sites of pDR274 (Addgene, #42250) expressing sgRNA. After linearization by digestion with DraI, the plasmid was purified with the PCR clean-up kit and *in vitro* transcribed using MEGAshortscript T7 (Life Technologies-Ambion). After transcription, the Cas9 cRNA and the sgRNA were purified with MEGAclear kit (Life Technologies-Ambion) according to the manufacturer's instruction and eluted in RNase-free water.

For zygote injection, B6D2_{F1} (C57BL/6 x DBA2) female mice were hormonally stimulated to ovulate (see below) and mated with B6D2_{F1} males. One-cell embryos were collected and injected with Cas9 cRNA (50 ng/μl), sgRNA (20 ng/μl) and donor oligo (20 ng/μl). The injected embryos were cultured in KSOM (Zenith Biotech, Guilford, CT) until the blastocyst stage and transferred into pseudopregnant CD1 female mice. The sequence of injected oligonucleotide was: 5'-TCTGGAGTCTGCAGTACCAGTGTTCAGAAAGGCTTCACTCCTGAGGGAAGCCCGGTATTTTCAGAACCAAGGTGAGAACACGGGGCCACACTCCAAAGCATGTCTGAATGTGGACATGCGGAAAAGA-3'. The genotype of the *Astl*^Δ allele was initially determined by DNA sequence of tail DNA and subsequently by PCR using an oligonucleotide primer that bridged the deleted sequence ([S3 Table](#)).

Oocyte, egg and embryo collection and culture

GV-intact oocytes from 4–6-wk-old female mice were collected by puncturing ovarian follicles in M2 medium (Sigma-Aldrich, St. Louis, MO) at 48 hr post-injection of 5 IU of equine gonadotropin hormone (eCG). Ovulated eggs and embryos from 4–6-wk-old female mice were collected before and after mating, respectively, in M2 medium after injection of 5 IU of eCG followed by 5 IU of human chorionic gonadotropin (hCG) 46–48 hr later. Embryos were subsequently cultured in KSOM (Zenith Biotech) at 37°C in 5% CO₂ to obtain 1- and 2-cell embryos. To inhibit actin polymerization, the medium was supplemented with 100 μM CK-666 (Sigma-Aldrich), a cell permeable inhibitor of arp2/3. For individual experiments, 20–30 cells were used from 3 different animals and representative images were included in figures.

Antibodies

A rabbit polyclonal antibody that binds a C-terminal peptide of ovastacin^{395–408} and monoclonal antibody M2c.2 that binds to the C-terminal region of ZP2 have been characterized previously [32][45]. The following antibodies and lectins were obtained commercially: LCA-FITC (Sigma-Aldrich); antibodies to GP73, calregulin and EEA1, Alex Fluor 488 goat anti-rabbit IgG (H+L) (Life Technologies-Invitrogen, Carlsbad, CA); Alexa Fluor 555 donkey anti-rabbit IgG (H+L) (Life Technologies-Invitrogen); DyLight 649 goat anti-rabbit IgG (H+L) (Life Technologies-Invitrogen); and goat anti-rat IgG-HRP (Santa Cruz).

Plasmid construction, cRNA *in vitro* transcription and microinjection

pCS2+/UtrCH-EGFP (Addgene, #26737) was linearized with NsiI and *in vitro* transcribed using SP6 mMESSAGE mMACHINE (Life Technologies-Ambion, AM1340). cRNA was purified by MEGAclear (Life Technologies-Ambion). Full-length and truncated ovastacin open reading frames were inserted into the pmCherry-N1 vector (Clontech Laboratories). Capped cRNAs were synthesized from PCR templates using T7 mMessage mMachine (Life Technologies-Ambion), and purified with MEGAclear (Life Technologies-Ambion). Microinjection was performed in M2 medium (Zenith Biotech) using a TransferMan NK2 micro-manipulator (Eppendorf, Hauppauge, NY). Typically, 10–12 pl (4% of the oocyte volume) of 0.5–1.0 μg/μl cRNA was injected into oocytes. For each cRNA construct, 20–30 GV-intact oocytes from 3 mice were injected, incubated in M2 media (37°C, 5% CO₂) for 6 hr prior to fixation and imaging by confocal microscopy. Variations in the intensity of the mCherry signal were noted among oocytes injected with the same construct and those with the strongest signals were selected for fixation and imaging by confocal microscopy using similar settings.

Immunofluorescence and confocal microscopy

GV-intact oocytes, ovulated eggs or embryos (20–30) were fixed in 4% paraformaldehyde (PFA) for 30 min, permeabilized in 0.5% Triton X-100 for 20 min, and blocked in SuperBlock (Piercenet, Thermo-Fisher Scientific, Rockford, IL) for 1 hr at room temperature. Samples were incubated with primary antibody (1:100) for 1 hr at room temperature or 4°C overnight. After three washes in 0.3% PVP/PBS containing 0.1% Tween 20 and 0.01% Triton X-100 for 5 min each, oocytes or embryos were incubated with secondary antibody (1:200) for 1 hr at room temperature. For LCA staining, eggs or embryos were stained with LCA-FITC (1:100) for 1 hr at room temperature. After three washes in 0.3% PVP/PBS containing 0.1% Tween 20 and 0.01% Triton X-100 for 5 min each, samples were mounted in PBS containing Hoechst 33342 (1 μg/ml). Confocal laser-scanning images were obtained using similar settings within

experiments on an LSM 510 confocal microscope (Carl Zeiss AG, Jena, Germany), with a 63 x 1/2 W objective and exported as full-resolution TIF files and processed in Photoshop (Adobe Systems, San Jose, CA) to adjust brightness and contrast.

Time-lapse imaging

Time-lapse imaging was obtained with the LSM 510 confocal microscope equipped with a Plan Apochromat 40x, 1.2 NA water immersion objective. mCherry was excited with a 561-nm laser line and detected with a 575–615-nm band pass. Ovulated eggs (10–20 from 3 animals) were collected, followed by removal of zonae pellucidae (see below), and placed in HTF medium supplemented with 5 ng/ml Hoechst 33342 (Life Technologies-Molecular Probes, Eugene, OR) on a gridded cover glass bottom dish (MatTek, Ashland, MA Cat. No. P35G-1.5-7-C-grid). The dish was placed in a humidified chamber (5% CO₂, 37°C) attached to the microscope and inseminated with 1×10^4 ml⁻¹ capacitated sperm.

Immunoblot analysis

GV-intact oocytes, ovulated eggs and two-cell embryos (10–15) were lysed in 4x LDS (lithium dodecyl sulfate) sample buffer with 10x reducing reagent (Life Technologies-Invitrogen), separated on 12% Bis-Tris precast gels, transferred to nitrocellulose membranes (Life Technologies-Invitrogen), blocked in 5% nonfat milk in TBS (Tris buffered saline, pH 7.4) with 0.1% Tween 20 (TBST) for 1 hr at room temperature, and then probed with 1:500–1:1,000 dilution of primary antibodies at 4°C overnight. On the following day, blots were incubated with a 1:10,000 dilution of secondary antibodies conjugated to HRP (horse radish peroxidase). Chemiluminescence was performed with ECL Plus (Piercenet) and signals were acquired by a Luminescent Image Analyzer LAS-3000 (Fujifilm, Valhalla, NY) or with BioMax XAR film (Kodak, Rochester, NY).

Sperm binding assay

Caudal epididymal sperm were isolated from wild-type ICR mice and placed under oil (EMD Millipore, Billerica, MA) in human tubal fluid (HTF) medium (Zenith Biotech) previously equilibrated with 90% N₂, 5% O₂, 5% CO₂ and capacitated by an additional 1 hr of incubation at 37°C. Sperm binding to ovulated eggs or two-cell embryos isolated from wild-type, *Astl*^{Null}, *Astl*^{Rescue}, *Astl*^{+/-Δ} and *Astl*^{Δ/Δ} mice was observed using capacitated sperm and wild-type 2-cell embryos as a negative wash control. Samples were fixed in 4% PFA for 30 min, stained with Hoechst 33342. Bound sperm were quantified from z projections acquired by confocal microscopy [46], and results reflect the mean ± s.e.m. from at least three independently obtained samples, each containing 6–12 mouse eggs/embryos. Statistical differences were determined by the 2-tailed Student's T-test.

In vitro fertilization

The zona pellucida of eggs was removed after 5 min incubation in 100 μl of acid Tyrode's solution (Sigma) and then washed 3 times in fresh M2 medium. Cauda epididymides were lanced in a dish of HTF to release sperm that were capacitated for 1 hr (37°C with 90% N₂, 5% O₂, 5% CO₂) and added to zona-intact or zona-free eggs (30 from 3 different animals) at a concentration of 4×10^5 ml⁻¹ sperm in 100 μl HTF for 5 hr at 37°C, 5% CO₂. The presence of two pronuclei was scored as successful fertilization. Statistical differences were determined by the 2-tailed Student's T-test.

Supporting Information

S1 Fig. *Astl*^{mCherry} transgenic mice. (a) Annotated representation of the *Astl*^{mCherry} transgene (upper) and the *Astl*^{Null} allele (lower) with the endogenous *Astl* allele. (b) PCR genotyping of tail DNA isolated from wild-type (Ctrl), *Astl*^{Null} (Null), *Astl*^{mCherry}, and *Astl*^{mCherry}; *Astl*^{Null} (Rescue) mice using primer pairs (1), (2) and (3) in (a). Molecular mass (kB) on left. (c) Total RNA was extracted from brain (Br), heart (H), kidney (K), liver (Li), lung (Lu), spleen (S), uterus (U), ovary (O) and testis (T), and analyzed by RT-PCR with primers (S3 Table) to detect normal and *Astl*^{mCherry} transcripts. GAPDH was used to as a load control and to ensure integrity of RNA. C, water control. Molecular mass (kB) on left.

S2 Fig. Localization of ovastacin in growing oocytes, ovulated eggs and zygotes from *Astl*^{mCherry} mice. (a) Growing *Astl*^{mCherry} oocytes (50–70 µm) were fixed and stained with antibodies specific to the endoplasmic reticulum (GP73), the Golgi apparatus (calregulin) and endosomes (EEA1) prior to imaging by confocal and DIC microscopy. Arrows, co-localization of marker and ovastacin. Scale bar, 20 µm. (b) Reversal of cortical granule free domain (CGFD) by inhibition of actin nucleation and cap formation. Ovulated eggs from *Astl*^{mCherry} mice were incubated for 3 hr with (lower panels) or without (upper panels) CK666 to inhibit Arp2/3. Eggs were stained with Hoechst prior to confocal and DIC microscopy. Scale bar, 20 µm. (c) Time-lapse images of cortical granule exocytosis after insemination of zona-free *Astl*^{mCherry} eggs (0 min) with capacitated sperm until formation of pronuclei in 1C zygotes (300 min). Eggs/embryos were imaged by confocal and DIC microscopy at the designated times after fixation and staining with Hoechst. PB, polar body. Scale bar, 20 µm.

S3 Fig. Deletion mutation of *Astl* using CRISPR/Cas9. (a) Schematic representation of Cas9 targeted with single-stranded guide RNA (ssRNA) to exon 2 of *Astl* 5' of the PAM (protospacer adjacent motif) to cut the double-stranded DNA with the RuvC and HNH sites. (b) Schematic representation of double-stranded donor DNA (126 bp) with a 21 bp (encodes ovastacin⁵²⁻⁵⁸) deletion used for homology directed DNA repair of the Cas9 induced DNA cleavage in exon 2 of *Astl*. (c) Genotype of tail DNA from 7 pups (AS1-7) derived from 1C zygotes injected with single-stranded guide RNA (20 ng/µl), RNA encoding Cas9 (50 ng/µl) and HDR oligonucleotide (20 ng/µl). The lower band in AS3 (d, left) and AS6 (e, left) were sequenced to confirm the 21 bp deletion. The middle band contained a single cytosine deletion in AS3 (d, right) and a single adenosine insertion in AS6 (e, right). The upper bands in AS3 and AS6 represent a heteroduplex of the two alleles migrating at a slower mobility. A c/t polymorphism is present in intron 2 of *Astl*.

S1 Table. Fertility of *Astl* mutant female mice.
(DOCX)

S2 Table. Mouse alleles and proteins.
(DOCX)

S3 Table. Primers.
(DOCX)

Author Contributions

Conceptualization: BX SB JD.

Funding acquisition: JD.

Investigation: BX YZ SB.

Methodology: BX SB JD.

Resources: SB ABS.

Supervision: JD.

Visualization: BX YZ JD.

Writing – original draft: BX JD.

Writing – review & editing: BX YZ SB JD.

References

1. Sato K. Polyspermy-preventing mechanisms in mouse eggs fertilized in vitro. *J Exp Zool.* 1979; 210:353–9. doi: [10.1002/jez.1402100219](https://doi.org/10.1002/jez.1402100219) PMID: [541603](https://pubmed.ncbi.nlm.nih.gov/541603/)
2. Stewart-Savage J, Bavister BD. A cell surface block to polyspermy occurs in golden hamster eggs. *Dev Biol.* 1988; 128:150–7. PMID: [2454853](https://pubmed.ncbi.nlm.nih.gov/2454853/)
3. Horvath PM, Kellom T, Caulfield J, Boldt J. Mechanistic studies of the plasma membrane block to polyspermy in mouse eggs. *Mol Reprod Dev.* 1993; 34:65–72. doi: [10.1002/mrd.1080340111](https://doi.org/10.1002/mrd.1080340111) PMID: [8418819](https://pubmed.ncbi.nlm.nih.gov/8418819/)
4. Maleszewski M, Kimura Y, Yanagimachi R. Sperm membrane incorporation into oolemma contributes to the oolemma block to sperm penetration: evidence based on intracytoplasmic sperm injection experiments in the mouse. *Mol Reprod Dev.* 1996; 44(2):256–9. doi: [10.1002/\(SICI\)1098-2795\(199606\)44:2<256::AID-MRD16>3.0.CO;2-0](https://doi.org/10.1002/(SICI)1098-2795(199606)44:2<256::AID-MRD16>3.0.CO;2-0) PMID: [9115725](https://pubmed.ncbi.nlm.nih.gov/9115725/)
5. Ducibella T, Huneau D, Angelichio E, Xu Z, Schultz RM, Kopf GS, et al. Egg-to-embryo transition is driven by differential responses to Ca(2+) oscillation number. *Dev Biol.* 2002; 250(2):280–91. PMID: [12376103](https://pubmed.ncbi.nlm.nih.gov/12376103/)
6. Inoue M, Wolf DP. Sperm binding characteristics of the murine zona pellucida. *Biol Reprod.* 1975; 13(3):340–6. PMID: [1218199](https://pubmed.ncbi.nlm.nih.gov/1218199/)
7. Austin CR. Cortical granules in hamster eggs. *Exp Cell Res.* 1956; 10(2):533–40. PMID: [13317917](https://pubmed.ncbi.nlm.nih.gov/13317917/)
8. Ducibella T, Duffy P, Buetow J. Quantification and localization of cortical granules during oogenesis in the mouse. *Biol Reprod.* 1994; 50(3):467–73. PMID: [8167217](https://pubmed.ncbi.nlm.nih.gov/8167217/)
9. Connors SA, Kanatsu-Shinohara M, Schultz RM, Kopf GS. Involvement of the cytoskeleton in the movement of cortical granules during oocyte maturation, and cortical granule anchoring in mouse eggs. *Dev Biol.* 1998; 200(1):103–15. doi: [10.1006/dbio.1998.8945](https://doi.org/10.1006/dbio.1998.8945) PMID: [9698460](https://pubmed.ncbi.nlm.nih.gov/9698460/)
10. Ducibella T, Anderson E, Albertini DF, Aalberg J, Rangarajan S. Quantitative studies of changes in cortical granule number and distribution in the mouse oocyte during meiotic maturation. *Dev Biol.* 1988; 130:184–97. PMID: [3141231](https://pubmed.ncbi.nlm.nih.gov/3141231/)
11. Ducibella T, Rangarajan S, Anderson E. The development of mouse oocyte cortical reaction competence is accompanied by major changes in cortical vesicles and not cortical granule depth. *Dev Biol.* 1988; 130:789–92. PMID: [3197932](https://pubmed.ncbi.nlm.nih.gov/3197932/)
12. Ducibella T, Duffy P, Reindollar R, Su B. Changes in the distribution of mouse oocyte cortical granules and ability to undergo the cortical reaction during gonadotropin-stimulated meiotic maturation and aging in vivo. *Biol Reprod.* 1990; 43(5):870–6. PMID: [2291919](https://pubmed.ncbi.nlm.nih.gov/2291919/)
13. Deng M, Kishikawa H, Yanagimachi R, Kopf GS, Schultz RM, Williams CJ. Chromatin-mediated cortical granule redistribution is responsible for the formation of the cortical granule-free domain in mouse eggs. *Dev Biol.* 2003; 257(1):166–76. PMID: [12710965](https://pubmed.ncbi.nlm.nih.gov/12710965/)
14. Ducibella T, Buetow J. Competence to undergo normal, fertilization-induced cortical activation develops after metaphase I of meiosis in mouse oocytes. *Dev Biol.* 1994; 165(1):95–104. doi: [10.1006/dbio.1994.1237](https://doi.org/10.1006/dbio.1994.1237) PMID: [8088454](https://pubmed.ncbi.nlm.nih.gov/8088454/)
15. Shiraishi K, Okada A, Shirakawa H, Nakanishi S, Mikoshiba K, Miyazaki S. Developmental changes in the distribution of the endoplasmic reticulum and inositol 1,4,5-trisphosphate receptors and the spatial pattern of Ca²⁺ release during maturation of hamster oocytes. *Dev Biol.* 1995; 170(2):594–606. doi: [10.1006/dbio.1995.1239](https://doi.org/10.1006/dbio.1995.1239) PMID: [7649386](https://pubmed.ncbi.nlm.nih.gov/7649386/)

16. Ikebuchi Y, Masumoto N, Matsuoka T, Yokoi T, Tahara M, Tasaka K, et al. SNAP-25 is essential for cortical granule exocytosis in mouse eggs. *Am J Physiol*. 1998; 274(6 Pt 1):C1496–C500. PMID: [9696691](#)
17. Masumoto N, Sasaki T, Tahara M, Mammoto A, Ikebuchi Y, Tasaka K, et al. Involvement of Rabphilin-3A in cortical granule exocytosis in mouse eggs. *J Cell Biol*. 1996; 135(6 Pt 2):1741–7. PMID: [8991087](#)
18. Gross VS, Wessel G, Florman HM, Ducibella T. A monoclonal antibody that recognizes mammalian cortical granules and a 32-kilodalton protein in mouse eggs. *Biol Reprod*. 2000; 63(2):575–81. PMID: [10906067](#)
19. Peng Q, Yang H, Xue S, Shi L, Yu Q, Kuang Y. Secretome profile of mouse oocytes after activation using mass spectrum. *J Assist Reprod Genet*. 2012; 29(8):765–71. doi: [10.1007/s10815-012-9789-8](#) PMID: [22573034](#)
20. Hoodbhoy T, Talbot P. Characterization, fate, and function of hamster cortical granule components. *Mol Reprod Dev*. 2001; 58(2):223–35. doi: [10.1002/1098-2795\(200102\)58:2<223::AID-MRD12>3.0.CO;2-9](#) PMID: [11139235](#)
21. Gwatkin RB, Williams DT, Hartmann JF, Kniazuk M. The zona reaction of hamster and mouse eggs: production in vitro by a trypsin-like protease from cortical granules. *J Reprod Fertil*. 1973; 32:259–65. PMID: [4734596](#)
22. Wolf DP, Hamada M. Induction of zonal and egg plasma membrane blocks to sperm penetration in mouse eggs with cortical granule exudate. *Biol Reprod*. 1977; 17:350–4. PMID: [901888](#)
23. Moller CC, Wassarman PM. Characterization of a proteinase that cleaves zona pellucida glycoprotein ZP2 following activation of mouse eggs. *Dev Biol*. 1989; 132:103–12. PMID: [2492959](#)
24. Schmell ED, Gulyas BJ. Ovoperoxidase activity in ionophore treated mouse eggs. II. Evidence for the enzyme's role in hardening the zona pellucida. *Gamete Res*. 1980; 3:279–80.
25. Miller DJ, Gong X, Decker G, Shur BD. Egg cortical granule N-acetylglucosaminidase is required for the mouse zona block to polyspermy. *J Cell Biol*. 1993; 123:1431–40. PMID: [8253842](#)
26. Pierce KE, Siebert MC, Kopf GS, Schultz RM, Calarco PG. Characterization and localization of a mouse egg cortical granule antigen prior to and following fertilization or egg activation. *Dev Biol*. 1990; 141(2):381–92. PMID: [1698670](#)
27. Burkart AD, Xiong B, Baibakov B, Jimenez-Movilla M, Dean J. Ovastacin, a cortical granule protease, cleaves ZP2 in the zona pellucida to prevent polyspermy. *J Cell Biol*. 2012; 197:37–44. doi: [10.1083/jcb.201112094](#) PMID: [22472438](#)
28. Bleil JD, Beall CF, Wassarman PM. Mammalian sperm-egg interaction: Fertilization of mouse eggs triggers modification of the major zona pellucida glycoprotein, ZP2. *Dev Biol*. 1981; 86:189–97. PMID: [6793422](#)
29. Bleil JD, Wassarman PM. Structure and function of the zona pellucida: Identification and characterization of the proteins of the mouse oocyte's zona pellucida. *Dev Biol*. 1980; 76:185–202. PMID: [7380091](#)
30. Bauskin AR, Franken DR, Eberspaecher U, Donner P. Characterization of human zona pellucida glycoproteins. *Mol Hum Reprod*. 1999; 5(6):534–40. PMID: [10341000](#)
31. Baibakov B, Boggs NA, Yauger B, Baibakov G, Dean J. Human sperm bind to the N-terminal domain of ZP2 in humanized zonae pellucidae in transgenic mice. *J Cell Biol*. 2012; 197:897–905. doi: [10.1083/jcb.201203062](#) PMID: [22734000](#)
32. Avella MA, Baibakov B, Dean J. A single domain of the ZP2 zona pellucida protein mediates gamete recognition in mice and humans. *J Cell Biol*. 2014; 205(6):801–9. doi: [10.1083/jcb.201404025](#) PMID: [24934154](#)
33. Guevara T, Yiallourou I, Kappelhoff R, Bissdorf S, Stocker W, Gomis-Ruth FX. Proenzyme structure and activation of astacin metalloproteinase. *J Biol Chem*. 2010; 285(18):13958–65. doi: [10.1074/jbc.M109.097436](#) PMID: [20202938](#)
34. Gahlay G, Gauthier L, Baibakov B, Epifano O, Dean J. Gamete recognition in mice depends on the cleavage status of an egg's zona pellucida protein. *Science*. 2010; 329:216–9. doi: [10.1126/science.1188178](#) PMID: [20616279](#)
35. Quesada V, Sanchez LM, Alvarez J, Lopez-Otin C. Identification and characterization of human and mouse ovastacin: a novel metalloproteinase similar to hatching enzymes from arthropods, birds, amphibians, and fish. *J Biol Chem*. 2004; 279(25):26627–34. doi: [10.1074/jbc.M401588200](#) PMID: [15087446](#)
36. Nicosia S, Wolf DP, Inoue M. Cortical granule distribution and cell surface characteristics in mouse eggs. *Dev Biol*. 1977; 57:56–74. PMID: [863112](#)
37. Nolen BJ, Tomasevic N, Russell A, Pierce DW, Jia Z, McCormick CD, et al. Characterization of two classes of small molecule inhibitors of Arp2/3 complex. *Nature*. 2009; 460(7258):1031–4. doi: [10.1038/nature08231](#) PMID: [19648907](#)

38. Schroeder AC, Schultz RM, Kopf GS, Taylor FR, Becker RB, Eppig JJ. Fetuin inhibits zona pellucida hardening and conversion of ZP2 to ZP2f during spontaneous mouse oocyte maturation in vitro in the absence of serum. *Biol Reprod.* 1990; 43(5):891–7. PMID: [1705446](#)
39. Cummins JM, Yanagimachi R. Sperm-egg ratios and the site of the acrosome reaction during in vivo fertilization in the hamster. *Gamete Res.* 1982; 5:239–56.
40. Muro Y, Hasuwa H, Isotani A, Miyata H, Yamagata K, Ikawa M, et al. Behavior of Mouse Spermatozoa in the Female Reproductive Tract from Soon after Mating to the Beginning of Fertilization. *Biol Reprod.* 2016; 94(4):80. doi: [10.1095/biolreprod.115.135368](#) PMID: [26962112](#)
41. De Felici M, Siracusa G. Spontaneous hardening of the zona pellucida of mouse oocytes during *in vitro* culture. *Gamete Res.* 1982; 6:107–13.
42. Olivier E, Soury E, Ruminy P, Husson A, Parmentier F, Daveau M, et al. Fetuin-B, a second member of the fetuin family in mammals. *Biochem J.* 2000; 350 Pt 2:589–97.
43. Dietzel E, Wessling J, Floehr J, Schafer C, Ensslen S, Denecke B, et al. Fetuin-B, a liver-derived plasma protein is essential for fertilization. *Dev Cell.* 2013; 25(1):106–12. doi: [10.1016/j.devcel.2013.03.001](#) PMID: [23562279](#)
44. Liu P, Jenkins NA, Copeland NG. A highly efficient recombineering-based method for generating conditional knockout mutations. *Genome Res.* 2003; 13(3):476–84. doi: [10.1101/gr.749203](#) PMID: [12618378](#)
45. Rankin TL, Coleman JS, Epifano O, Hoodbhoy T, Turner SG, Castle PE, et al. Fertility and taxon-specific sperm binding persist after replacement of mouse 'sperm receptors' with human homologues. *Dev Cell.* 2003; 5:33–43. PMID: [12852850](#)
46. Rankin T, Talbot P, Lee E, Dean J. Abnormal zonae pellucidae in mice lacking ZP1 result in early embryonic loss. *Development.* 1999; 126:3847–55. PMID: [10433913](#)

Melatonin improves the fertilization ability of post-ovulatory aged mouse oocytes by stabilizing ovastacin and Juno to promote sperm binding and fusion

Xiaoxin Dai, Yajuan Lu, Mianqun Zhang, Yilong Miao, Changyin Zhou, Zhaokang Cui, and Bo Xiong*

College of Animal Science and Technology, Nanjing Agricultural University, Nanjing 210095, China

*Correspondence address: College of Animal Science and Technology, Nanjing Agricultural University, Nanjing, China.
Tel: +86-25-84399605; E-mail: xiongbo@njau.edu.cn

Submitted on October 26, 2016; resubmitted on December 18, 2016; accepted on January 1, 2017

STUDY QUESTION: What are the underlying mechanisms of the decline in the fertilization ability of post-ovulatory aged oocytes?

SUMMARY ANSWER: Melatonin improves the fertilization ability of post-ovulatory aged oocytes by reducing aging-induced reactive oxygen species (ROS) levels and inhibiting apoptosis and by maintaining the levels and localization of the fertilization proteins, ovastacin and Juno.

WHAT IS KNOWN ALREADY: Following ovulation, the quality of mammalian metaphase II oocytes irreversibly deteriorates over time with a concomitant loss of fertilization ability. Melatonin has been found to prevent post-ovulatory oocyte aging and extend the window for optimal fertilization in mice.

STUDY DESIGN, SIZE, DURATION: Mouse oocytes were randomly assigned to three groups and aged *in vitro* for 0, 6, 12 and 24 h, respectively. Increasing concentrations of melatonin (10^{-9} M, 10^{-7} M, 10^{-5} M and 10^{-3} M) were added to the 24 h aging group.

PARTICIPANTS/MATERIALS, SETTING, METHODS: Sperm binding assays, *in-vitro* fertilization, immunofluorescent staining and western blotting were performed to investigate key regulators and events during fertilization of post-ovulatory aged mouse oocytes.

MAIN RESULTS AND THE ROLE OF CHANCE: We found that the actin cap which promotes a cortical granule (CG) free domain is disrupted with a re-distribution of CGs in the subcortex of aged oocytes. Ovastacin, a CG metalloendoprotease, is mis-located and prematurely exocytosed in aged oocytes with subsequent cleavage of the zona pellucida protein ZP2. This disrupts the sperm recognition domain and dramatically reduces the number of sperm binding to the zona pellucida. The abundance of Juno, the sperm receptor on the oocyte membrane, also is reduced in aged oocytes. Exposure of aged oocytes to melatonin significantly elevates *in-vitro* fertilization rates potentially by rescuing the above age-associated defects of fertilization, and reducing ROS and inhibiting apoptosis.

LARGE SCALE DATA: N/A

LIMITATIONS, REASONS FOR CAUTION: We explored the mechanisms of the decline in fertilization ability decline in aged mouse oocytes, *in vitro* but not *in vivo*.

WIDER IMPLICATIONS OF THE FINDINGS: Our findings may contribute to the development a more efficient method, involving melatonin, for improving IVF success rates.

STUDY FUNDING/COMPETING INTEREST(S): This study was supported by the National Natural Science Foundation (31571545) and the Natural Science Foundation of Jiangsu Province (BK20150677). The authors have no conflict of interest to disclose.

Key words: post-ovulatory aging / zp2 cleavage / ovastacin / junos / melatonin

Introduction

Ovulated mouse oocytes are surrounded by an extracellular zona pellucida composed of ZP1, ZP2 and ZP3. For successful fertilization, a single capacitated sperm binds to the N-terminal domain of ZP2, penetrates the zona matrix and binds to the oocyte via interactions between Izumo1 on the sperm head and Juno on the oocyte membrane. Fusion of the oocyte with a second sperm results in polyspermy and this is protected against by postfertilization modifications of both the zona matrix and the oocyte plasma membrane. Dysregulation of these protective measures results in loss of reproductive fitness.

The postfertilization modification of the zona pellucida is mediated by cortical granule (CG) exocytosis. CGs are subcellular organelles unique to oocytes that originate from the Golgi apparatus at the onset of follicular growth and migrate to the cortex to form a continuous layer under the oolemma (Zamboni, 1970; Ducibella et al., 1994; Hoodbhoy and Talbot, 1994; Liu et al., 2005). In mammals, CG distribution is polarized because of exclusion from an actin cap which forms a CG-free domain (CGFD) overlying the second meiotic spindle (Szollosi, 1967; Nicosia et al., 1977; Longo and Chen, 1985; Okada et al., 1986). After fertilization, the CGs fuse with the oocyte plasma membrane and exocytose their contents into the extracellular space. A mammalian component of CGs is ovastacin, an oocyte-specific metalloendoprotease that cleaves ZP2 (¹⁶⁶LA¹DE¹⁶⁹) after fertilization (Quesada et al., 2004; Burkart et al., 2012). Genetic mutation of the ZP2 cleavage site or ablation of ovastacin leaves ZP2 unmodified which supports sperm binding to the zona pellucida despite fertilization and CG exocytosis (Gahlay et al., 2010; Burkart et al., 2012).

After successful navigation of the zona pellucida, only acrosome-reacted sperm are present in the perivitelline space and available for fusion with the oocyte. Izumo1 on the surface of sperm head interacts with Juno (formerly Folr4) in the oocyte membrane to promote gamete fusion (Inoue et al., 2005; Bianchi et al., 2014; Grayson, 2015). Juno is a glycoposphatidylinositol-anchored protein that is uniquely present in oocytes and rapidly disappears following fertilization (Bianchi et al., 2014). Genetic ablation of either Izumo1 or Juno prevents gamete fusion and leads to gender-specific infertility (Inoue et al., 2005; Bianchi et al., 2014).

In mammals, timely fertilization of oocytes following ovulation is crucial for successful reproduction (Lord et al., 2015). However, many mammalian species restrict sexual activity to distinct estrous periods and ovulation and fertilization may not be synchronized (Tarin et al., 2002). With increasing time following ovulation, oocytes deteriorate *in vivo* and *in vitro* in a process known as post-ovulatory aging (Tarin et al., 1999; Lord and Aitken, 2013; Zhang et al., 2016). Numerous studies have shown that post-ovulatory aging of mammalian oocytes *in vitro* is inherently linked with oxidative stress (Lord and Aitken, 2013; Lord et al., 2013), a result of the imbalance between the production and consumption of reactive oxygen species (ROS) (Tamura et al., 2008; Galano et al., 2011).

ROS can damage the cell membrane and induce the apoptosis, which thereby harms the fertilization potential of oocytes by perturbing fertilization-related regulators and events (Zhao et al., 2016). Melatonin (*N*-acetyl-5-methoxytrypt amine) is a major pineal secretory product (Gao et al., 2012) that mediates circadian rhythms and regulates seasonal reproductive activity (Lincoln et al., 2006). Melatonin is especially effective as an antioxidant because it exhibits a wide variety of means to reduce oxidative stress (Garcia et al., 2014; Manchester et al., 2015; Reiter et al., 2016), and its metabolites are potent free radical

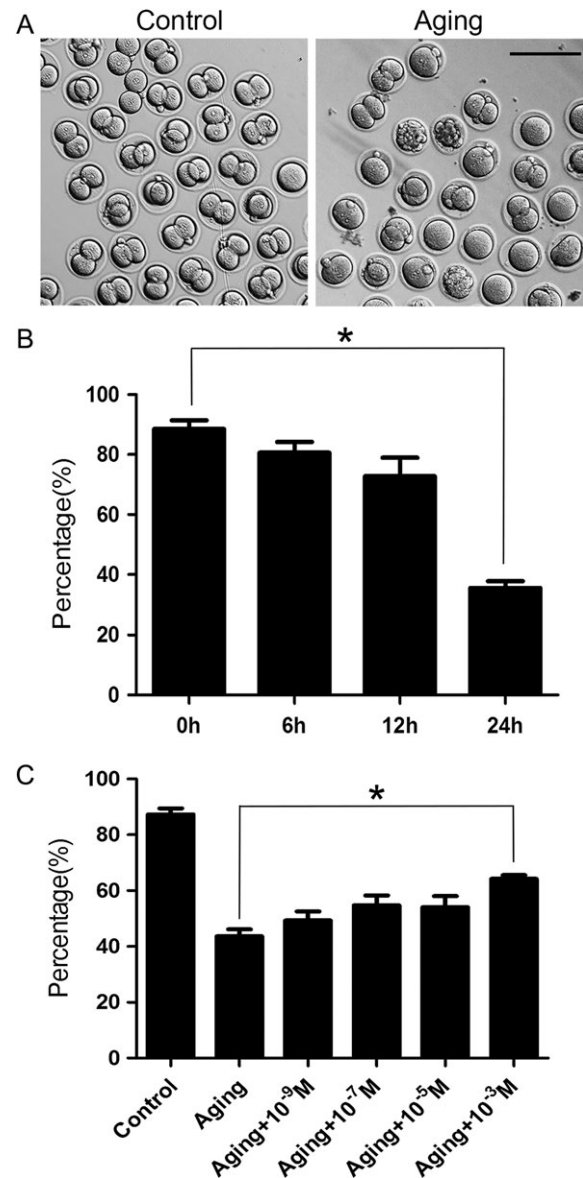


Figure 1 Effect of melatonin on *in-vitro* fertilization of post-ovulatory aged oocytes. (A) Representative images of fertilized oocytes in control and aged groups. Scale bar, 200 μ m. (B) *In-vitro* fertilization rates of oocytes aged *in-vitro* for 0, 6, 12 and 24 h, respectively. (C) *In-vitro* fertilization rates of aged oocytes exposed to different concentrations of melatonin. Data in (B) and (C) are presented as mean percentage (mean \pm SEM) of at least three independent experiments. Asterisk denotes statistical difference at a $P < 0.05$.

scavengers and antioxidants (Chen et al., 2006; Manda et al., 2007; Bonnefont-Rousselot et al., 2011; Galano et al., 2011; Zhang and Zhang, 2014). Recent studies have shown that supplementation of melatonin during oocyte culture increases the rate of fertilization and promotes early embryonic development in mice (Ishizuka et al., 2000; Wang et al., 2013). However, the underlying mechanisms regarding how melatonin improves the quality and fertilization potential of the post-ovulatory aged oocytes are still not fully defined.

We now report that post-ovulatory aging compromises the fertilization ability of mouse oocytes by inducing precocious exocytosis of ovastacin that causes premature cleavage of the sperm binding domain of ZP2 and loss of sperm binding to the zona pellucida. Post-ovulatory aging also disrupts the abundance of Juno, the sperm receptor on the oocyte membrane, which affects gamete fusion. These post-ovulatory aging defects appear in line with the generation of ROS and can be ameliorated by media supplementation with melatonin.

Materials and Methods

Animals and feeding

All mice were handled in accordance with the Animal Research Institute Committee guidelines of Nanjing Agricultural University, China. The female 4-week-old ICR (Institute of Cancer Research) mice were kept under controlled conditions with a constant temperature (20–23°C) and a 12-h light/dark cycle, and had free access to food and water throughout the period of the study.

In-vitro fertilization

Cauda epididymides were lanced in a dish of human tubal fluid (HTF) medium (EMD Millipore, Billerica, MA, USA) to release sperm that were

capacitated for 1 h (37°C, 5% CO₂) and added to ovulated oocytes at a concentration of 4×10^5 /ml sperm in 100 µl HTF for 5 h at 37°C, 5% CO₂. The presence of two pronuclei was scored as successful fertilization.

Sperm binding assay

Caudal epididymal sperm were isolated from 12-week-old ICR male mice and placed under oil (Sigma-Aldrich, MO, USA) in HTF medium previously equilibrated with 5% CO₂ and capacitated by an additional 1 h of incubation at 37°C. Sperm binding to control, aged and melatonin-treated aged oocytes or two-cell embryos was observed using capacitated sperm and control two-cell embryos as a negative wash control. Samples were fixed in 4% PFA for 30 min and stained with Hoechst 33342. Bound sperm were quantified from z projections acquired by confocal microscopy, and the results reflect the mean \pm SEM from at least three independently obtained samples, each containing 10–12 mouse oocytes or embryos.

Immunofluorescence and confocal microscopy

Mouse oocytes were fixed in 4% paraformaldehyde in PBS (pH 7.4) for 30 min and permeabilized in 0.5% Triton-X-100 for 20 min at room temperature. Then, oocytes were blocked with 1% BSA (bovine serum albumin)-supplemented PBS for 1 h and incubated at 4°C overnight or at room

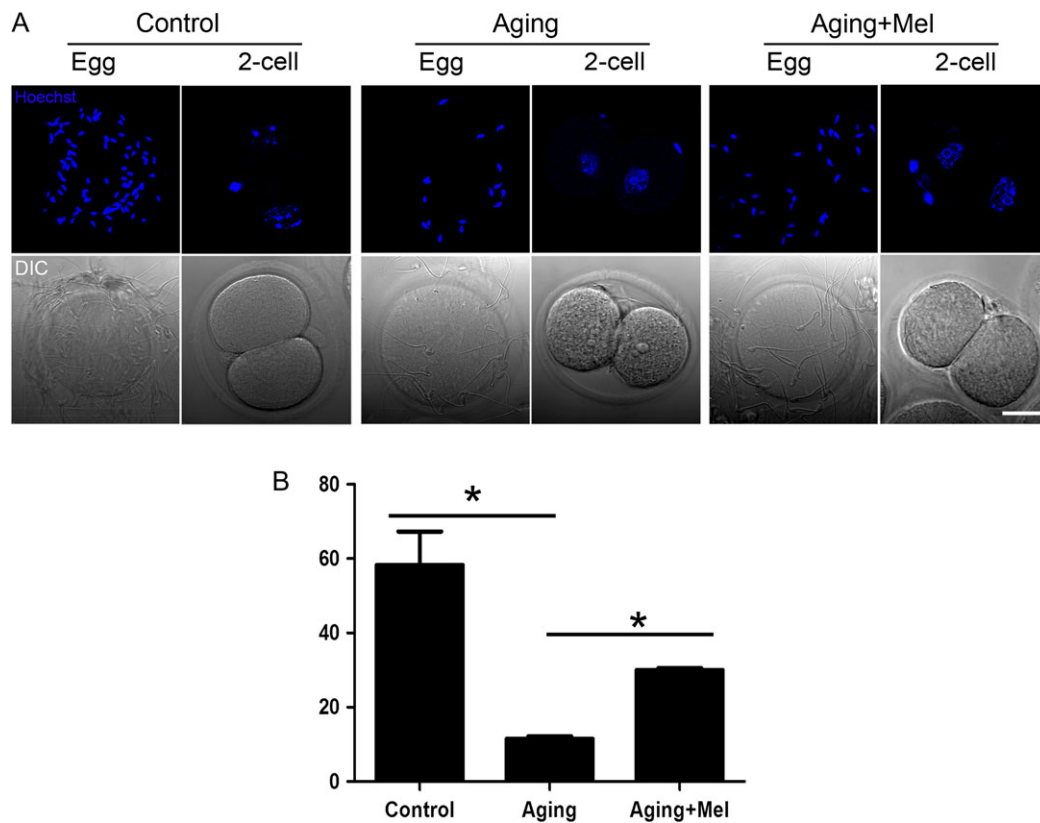


Figure 2 Effect of melatonin on sperm binding to the zona pellucida of post-ovulatory aged oocytes. **(A)** Oocytes and two-cell embryos from control and aged groups were incubated with capacitated sperm for 1 h. After washing with a wide-bore pipette, which removes all but two to six sperm on normal two-cell embryos (negative control), oocytes and embryos with sperm were fixed and stained with Hoechst 33342. Scale bar, 20 µm. **(B)** The number of sperm binding to the surface of zona pellucida surrounding oocytes from control, aged and melatonin-supplemented groups. Data are presented as mean percentage (mean \pm SEM) of at least three independent experiments. Asterisk denotes statistical difference at a $P < 0.05$.

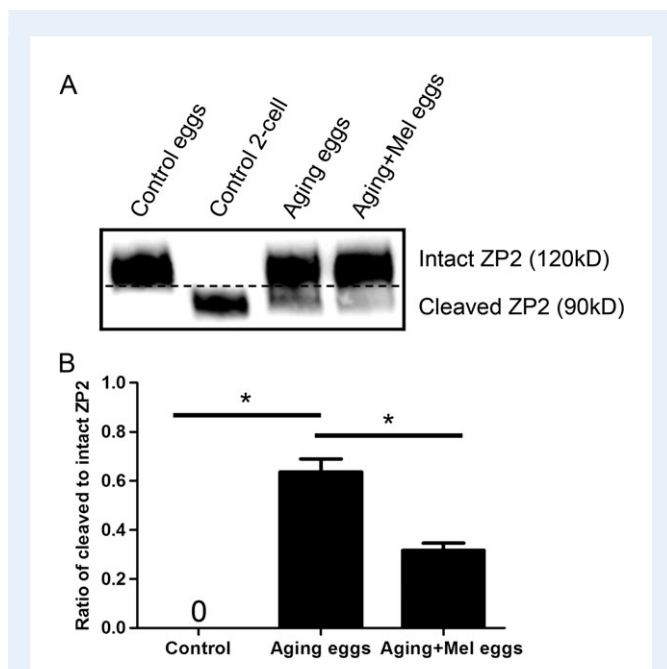


Figure 3 Effect of melatonin on ZP2 cleavage level in post-ovulatory aged oocytes. **(A)** Western blot of ZP2 cleavage status in oocytes and two-cell embryos using M2c.2 antibody that recognizes the C-terminus of cleaved ZP2. The size of intact ZP2 is 120 kD; the size of the cleaved C-terminal fragment of ZP2 is 90 kD. **(B)** The ratio of cleaved ZP2 to intact ZP2 in control, aged and melatonin-supplemented oocytes. Data are presented as mean percentage (mean ± SEM) of at least three independent experiments. Asterisk denotes statistical difference at a $P < 0.05$ level of significance.

temperature for 4 h with rat monoclonal anti-mouse Folr4-FITC antibody (1:100, BioLegend, CA, USA) or rabbit polyclonal anti-mouse ovastacin antibody (1:100, obtained from Dr Jurrien Dean). After washing four times (5 min each) in PBS containing 1% Tween 20 and 0.01% Triton-X 100, oocytes were incubated with an appropriate secondary antibody for 1 h at room temperature. Alexa Fluor 488 donkey anti-rabbit IgG (H+L) was obtained from Invitrogen (Carlsbad, CA, USA). After washing three times, oocytes were counterstained with Hoechst 33342 (10 µg/ml) for 10 min. Finally, oocytes were mounted on glass slides and viewed under a confocal laser scanning microscope (Carl Zeiss LSM 700 META).

Western blot analysis

For ZP2 cleavage experiments, 12 mouse oocytes or two-cell embryos were lysed in 4× LDS sample buffer with 10× reducing reagent (Life Technologies) and heated at 95°C for 5 min. For Juno and ovastacin detection, 400 mouse oocytes were lysed in 4× LDS sample buffer and heated at 95°C for 5 min. Proteins were separated on 12% Bis-Tris precast gels, transferred to PVDF membranes, blocked in 5% nonfat milk in TBS (Tris buffered saline, pH 7.4) with 0.1% Tween 20 (TBST) for 1 h at room temperature, and then probed with 1:500 dilution of M2c.2 antibody (obtained from Dr Jurrien Dean), rat monoclonal anti-mouse Folr4 antibody (1:1000, BioLegend, CA, USA) or rabbit polyclonal anti-mouse ovastacin antibody (1:1000) at 4°C overnight. After washing three times in TBST (10 min each), blots were incubated for 1 h with a 1:5000 dilution of Horse Radish Peroxidase conjugated goat anti-rat or goat anti-rabbit IgG secondary antibodies (Santa Cruz, TX, USA). Chemiluminescence was performed with ECL Plus (Piercenet) and signals were acquired by Tanon-3900.

Determination of ROS generation

To determine the levels of intracellular ROS production, cumulus-denuded mouse oocytes were incubated with the oxidation-sensitive fluorescent probe [dichlorofluorescein (DCFH)] for 30 min at 37°C in DPBS (Dulbecco's Phosphate Buffered Saline) that contained 10 µM DCFH diacetate (DCFHDA) (Beyotime Institute of Biotechnology, China). Oocytes were then washed three times in DPBS containing 0.1% BSA and placed on glass slides. The fluorescent intensity in each oocyte was measured by Zeiss LSM 700 META confocal system with the same scanning settings.

Annexin-V staining

As per the manufacturer's instruction (Beyotime Institute of Biotechnology, Hangzhou, China), mouse oocytes were stained with the Annexin-V staining kit. After washing twice in PBS, the viable oocytes were stained for 30 min in the dark with 90 µl of binding buffer containing 10 µl of Annexin-V-FITC. Fluorescent signals were measured by the confocal microscope with the same scanning settings (Zeiss LSM 700 META).

Statistical analysis

The data from at least three repeated experiments were expressed as mean ± SEM and analyzed by one-way ANOVA, followed by LSD's *post hoc* test, which was provided by SPSS16.0 statistical software. The level of significance was accepted as $P < 0.05$.

Results

Melatonin improves the fertilization potential of post-ovulatory aged mouse oocytes

To examine whether post-ovulatory aging impairs fertilization, we compared *in-vitro* fertilization rates of mouse oocytes aged *in vitro* for 0, 6, 12 and 24 h. Most control oocytes could be fertilized and could develop to two-cell embryos, while aged oocytes had varying degrees of reduced fertilization ability (Fig. 1A, B). Oocytes aged for 24 h had significantly lower fertilization rate compared to controls ($88.6 \pm 2.9\%$, $n = 110$ vs. $35.6 \pm 2.2\%$, $n = 83$) and this time point was chosen for subsequent investigations (Fig. 1B). To determine the effect of melatonin on the fertilization of aged oocytes, we cultured oocytes for 24 h with increasing concentrations of melatonin (10^{-9} M, 10^{-7} M, 10^{-5} M and 10^{-3} M) and then performed *in-vitro* fertilization. As expected, the rate of fertilization increased in the melatonin-treated aged oocytes and supplementation with 10^{-3} M melatonin significantly increased the fertilization rate compared to control aged oocytes to $64.2 \pm 1.3\%$ ($n = 92$) from $43.7 \pm 2.5\%$ ($n = 87$) (Fig. 1C). Due to limited solubility, 10^{-3} M was the maximum concentration that we tested and this was used for subsequent investigations. Collectively, these results indicate that melatonin can improve the fertilization ability of aged mouse oocytes.

Melatonin elevates the sperm binding ability of post-ovulatory aged oocytes

To determine the number of sperm binding to the extracellular zona pellucida, gamete nuclei were stained with Hoechst and imaged by confocal microscopy. The zona pellucida surrounding control, unfertilized oocytes robustly supported sperm binding and the postfertilization cleavage of ZP2 prevented sperm binding to the zona matrix surrounding two-cell embryos. However, in aged oocytes, the number of sperm binding to the

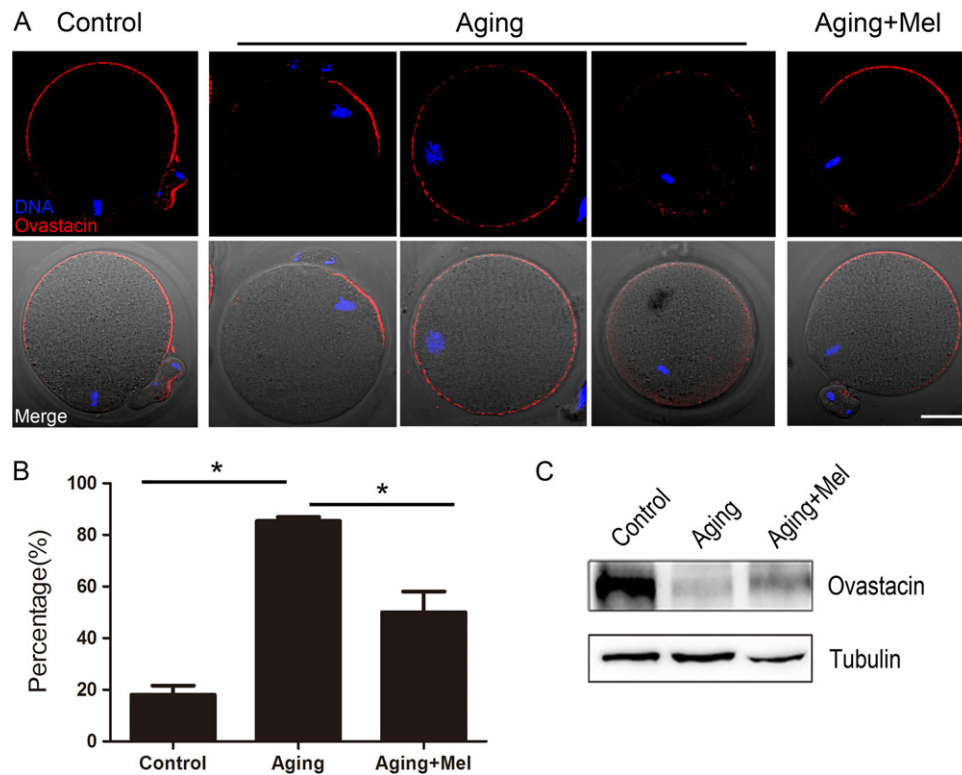


Figure 4 Effect of melatonin on the localization and protein level of ovastacin in post-ovulatory aged oocytes. **(A)** Representative images of ovastacin in control and aged oocytes. Ovastacin was immunostained with rabbit polyclonal anti-mouse ovastacin antibody and examined by confocal microscopy. Scale bar, 20 μ m. **(B)** Abnormal rates of ovastacin localization in control, aged and melatonin-supplemented oocytes. Data are presented as mean percentage (mean \pm SEM) of at least three independent experiments. Asterisk denotes statistical difference at a $P < 0.05$ level of significance. **(C)** Protein levels of ovastacin examined by western blot in control, aged and melatonin-supplemented oocytes.

zona pellucida was substantially reduced compared with the control oocytes (58.3 ± 9.0 , $n = 42$ vs. 11.5 ± 0.7 , $n = 35$) (Fig. 2A, B). In contrast, after treatment with melatonin, the number of sperm binding to unfertilized aged oocytes was significantly increased compared with untreated aged oocytes (11.5 ± 0.7 , $n = 35$ vs. 30.0 ± 0.6 , $n = 33$) (Fig. 2A, B). Taken together, these results indicate that melatonin can restore the ability of sperm to bind to aged oocytes.

Melatonin reduces ZP2 cleavage in post-ovulatory aged oocytes

Sperm binding to zona pellucida is determined by the cleavage status of N-terminus of ZP2, independent of fertilization and CG exocytosis (Gahlay et al., 2010). Using M2c.2 antibody which has been previously used to detect the cleavage of ZP2 by western blot (Gahlay et al., 2010; Burkart et al., 2012), we observed that ZP2 was intact (120 kD) in unfertilized oocytes and cleaved (90 kD) in two-cell embryos (Fig. 3A). Unexpectedly, partially cleaved ZP2 was observed in unfertilized oocytes in the aged group (Fig. 3A, B) suggesting that aged oocytes lose ZP2 sperm binding sites. These observations are consistent with the above sperm binding assay in which fewer sperm bound to the zona pellucida surrounding aged oocytes. Since melatonin can partially restore the sperm binding of aged oocytes, we investigated

the cleavage status of ZP2 in the zona pellucida in the presence of melatonin. As expected, although ZP2 was also partially cleaved in the melatonin-supplemented aged group, the cleavage level was lower compared to that in the aged oocytes (Fig. 3A, B).

Melatonin rescues the localization and abundance of ovastacin in post-ovulatory aged oocytes

To further investigate the inability of sperm to bind the zona pellucida of aged oocytes, we determined the localization and protein level of ovastacin, an oocyte, CG-specific metalloprotease responsible for the postfertilization cleavage of ZP2. Immunofluorescent analysis detected ovastacin in the subcortex of ovulated control oocytes with exclusion from the CGFD. In striking contrast, ovastacin was abnormally located in aged oocytes and these spatial anomalies could be rescued by treatment with melatonin (Fig. 4A). The frequency of abnormally located ovastacin in aged oocytes was significantly higher than that in controls ($85.4 \pm 1.5\%$, $n = 98$ vs. $18.1 \pm 3.6\%$, $n = 87$) and was markedly reduced by treatment with melatonin ($85.4 \pm 1.5\%$, $n = 98$ vs. $50.0 \pm 8.1\%$, $n = 90$) (Fig. 4B). In addition, the abundance of ovastacin protein was substantially decreased in aged oocytes (Fig. 4C), suggesting that a portion of ovastacin had been prematurely exocytosed which could account for the partial cleavage of

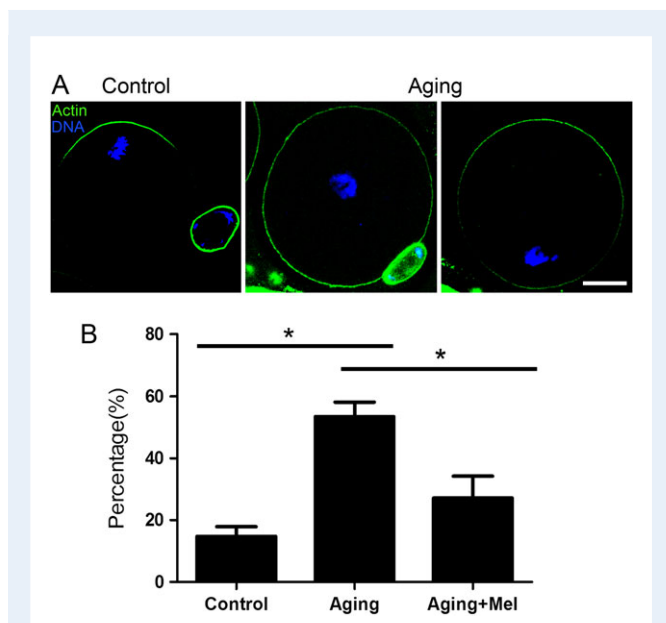


Figure 5 Effect of melatonin on the actin cap formation in post-ovulatory aged oocytes. **(A)** Representative images of actin caps in control and aged oocytes. Actin was immunostained with phalloidin-FITC and observed by the confocal microscopy. Scale bar, 20 μ m. **(B)** The rates of aberrant of actin cap formation in control, aged and melatonin-supplemented oocytes. Data are presented as mean percentage (mean \pm SEM) of at least three independent experiments. Asterisk denotes statistical difference at a $P < 0.05$ level of significance.

ZP2 in the extracellular zona matrix. However, treatment with melatonin partially restored the protein levels of ovastacin (Fig. 4C). Collectively, these data indicate that post-ovulatory aging of oocytes results in the mislocalization and premature exocytosis of ovastacin which leads to defects in sperm binding and failed fertilization.

Melatonin restores formation of the actin cap in post-ovulatory aged oocytes

During meiotic maturation, chromosomes move to the oocyte cortex and stimulate formation of a CGFD in which actin polymerizes to form an actin cap. The biological significance of the CGFD is not fully clear, but it is thought that sperm are less likely to fuse at this region to protect the maternal genetic material. Based on the above observation that ovastacin in the CGs is mislocalized in aged oocytes, we hypothesized that formation of the actin cap also would be impaired during aging process. In control oocytes, the actin caps formed normally in the CGFD region with few exceptions (Fig. 5A). However, in aged oocytes, the rate of aberrant actin cap formation was increased compared to control oocytes ($53.5 \pm 4.7\%$, $n = 69$ vs. $14.8 \pm 3.1\%$, $n = 73$), but could be reduced by treatment with melatonin ($27.2 \pm 7.1\%$, $n = 77$ vs. $53.5 \pm 4.7\%$, $n = 69$) (Fig. 5B).

Melatonin restores Juno in the membrane of post-ovulatory aged oocytes

After sperm bind and penetrate the zona pellucida, they fuse with the oocyte membrane via Juno's interaction with Izumo I, a sperm surface

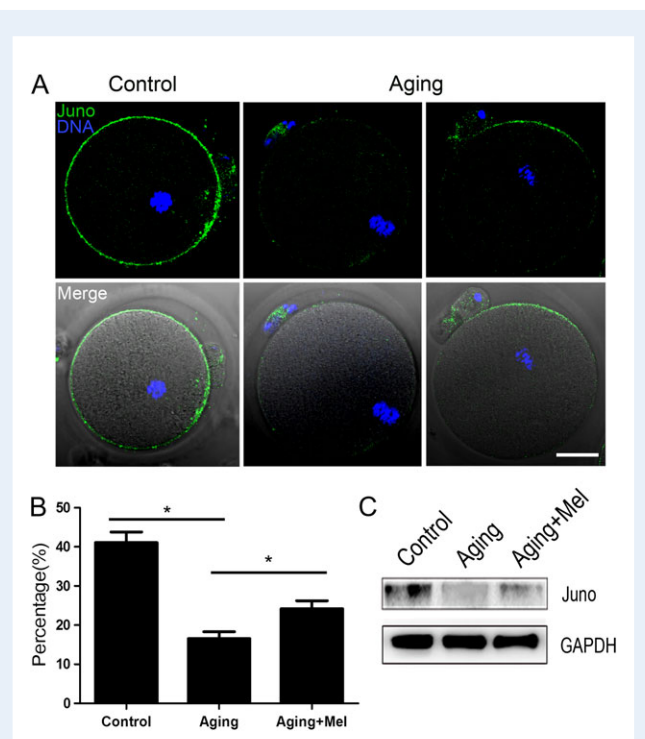


Figure 6 Effect of melatonin on the localization and protein level of Juno in post-ovulatory aged oocytes. **(A)** Representative images of Juno in control and aged oocytes. Juno was immunostained with rat monoclonal anti-mouse Folr4 antibody and examined by confocal microscopy. Scale bar, 20 μ m. **(B)** Abnormal rates of Juno localization in control, aged and melatonin-supplemented oocytes. Data are presented as mean percentage (mean \pm SEM) of at least three independent experiments. Asterisk denotes statistical difference at a $P < 0.05$ level of significance. **(C)** Protein levels of Juno examined by western blot in control, aged and melatonin-supplemented oocytes.

receptor. In control oocytes, Juno was evenly distributed on the oocyte membranes, but it was partly or entirely absent in aged oocytes (Fig. 6A). Based on immunofluorescent intensity, the abundance of Juno was significantly decreased in aged oocytes compared to control oocytes (16.6 ± 1.7 , $n = 78$ vs. 41.1 ± 2.7 , $n = 69$) (Fig. 6B). Incubation with melatonin during aging partially restored the Juno signal on the oocyte membrane (24.2 ± 2.0 , $n = 72$ vs. 16.6 ± 1.7 , $n = 78$) (Fig. 6B) which was confirmed by western blot (Fig. 6C). We conclude that the reduced abundance of Juno in the oocyte membrane is likely to play an important role in the decreased fertilization ability of aged mouse oocytes.

Melatonin decreases ROS and suppresses early apoptosis in post-ovulatory aged oocytes

We hypothesized that aging induces oxidative stress which accelerates apoptosis and leads to degradation of ovastacin and Juno which are critical regulators of fertilization. To investigate potential antioxidant effects of melatonin, we assessed ROS levels and apoptosis. In aged oocytes, the fluorescent intensity of ROS was increased compared to controls (153.6 ± 10.8 , $n = 45$ vs. 78.8 ± 5.1 , $n = 40$) and supplementation with melatonin during aging reduced ROS levels (153.6 ± 10.8 ,

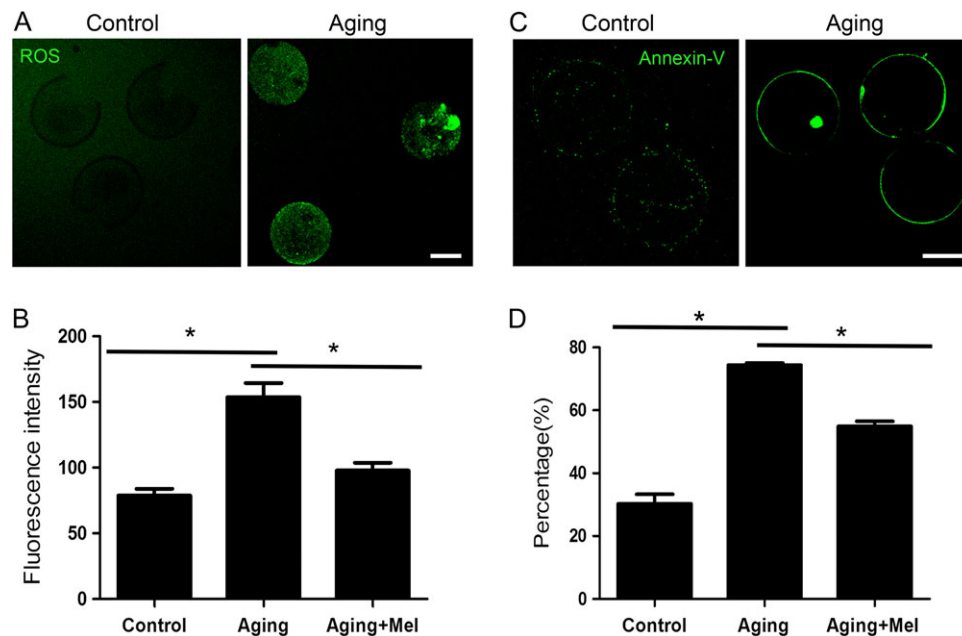


Figure 7 Effect of melatonin on reactive oxygen species (ROS) levels and early apoptosis in post-ovulatory aged oocytes. **(A)** Representative images of ROS levels in control and aged oocytes. The ROS signals were increased in aged oocytes compared to controls. Scale bar, 20 μ m. **(B)** Fluorescence intensities of ROS in control, aged and melatonin-supplemented oocytes were measured by confocal microscopy using identical settings and parameters. **(C)** Representative images of apoptosis in control and aged oocytes. Oocytes were immunostained with Annexin-V-FITC. Scale bar, 20 μ m. **(D)** The rate of early apoptosis was recorded in control, aged and melatonin-supplemented oocytes. Data in (B) and (D) are presented as mean percentage (mean \pm SEM) of at least three independent experiments. Asterisk denotes statistical difference at a $P < 0.05$ level of significance.

$n = 45$ vs. 97.8 ± 5.9 , $n = 50$) (Fig. 7A, B). We also investigated apoptosis by staining for Annexin-V to detect the translocation of phosphatidylserine from the inner to the outer leaflet of the cell membrane. The green fluorescent signal was detected faintly in control oocytes, but clearly observed on the membrane of aged oocytes (Fig. 7C). The proportion of apoptotic oocytes was dramatically higher in aged group than in controls ($74.3 \pm 0.7\%$, $n = 34$ vs. $30.3 \pm 3.0\%$, $n = 35$) but was rescued in melatonin-supplemented group ($74.3 \pm 0.7\%$, $n = 34$ vs. $54.9 \pm 1.6\%$, $n = 30$) (Fig. 7D).

Collectively, these results provide a body of evidence documenting that melatonin improves the fertilization potential of post-ovulatory aged oocytes by maintaining the localization and protein level of two critical fertilization participants, ovastacin and Juno, and by reducing aging-induced ROS levels and by inhibiting apoptosis (Fig. 8).

Discussion

The application of melatonin in human clinics to improve success rates of IVF traces a long historic road of scientific discovery. Melatonin, now known to be a robust antioxidant (Reiter et al., 2016), was first reported in human preovulatory follicular fluid almost 30 years ago (Brzezinski et al., 1987) and was subsequently shown to increase IVF rates and early embryo development in mice (Ishizuka et al., 2000) and to increase IVF rates in humans (Tamura et al., 2008). More recently, melatonin has been found to prevent post-ovulatory oocyte aging and extend the window for optimal fertilization in mice (Lord and Aitken,

2013). However, the underlying molecular basis for these observations has remained unknown.

Recent advances based on molecular cell biology and mouse genetics have proposed a model of gamete recognition in which capacitated sperm bind to the N-terminus of ZP2 in the extracellular zona pellucida, penetrate through the zona matrix and fuse to Juno in the oocyte membrane to effect fertilization (Gahlay et al., 2010; Baibakov et al., 2012; Avella et al., 2014; Bianchi et al., 2014). After fertilization, Juno is lost from the oocyte plasma membrane (Bianchi et al., 2014) and exocytosis of ovastacin from CGs modifies ZP2 so that sperm cannot bind to the zona pellucida (Burkart et al., 2012).

In our current results, we document that post-ovulatory aging dramatically reduced the number of sperm binding to the zona pellucida concomitant with mislocalized CGs. The subsequent partial cleavage of ZP2 most likely results from premature exocytosis of ovastacin and is the hallmark of the zona hardening reaction (Burkart et al., 2012), which effectively blocks sperm binding to the surface of the zona matrix. In addition, we observed a decrease in the abundance of Juno on the membrane of aged oocytes which would prevent interactions with Izumo1 on the sperm surface and decreased rates of fertilization.

Most importantly, we found that the defects caused by the post-ovulatory aging could be restored, at least partially, by supplementation with melatonin during the aging process *in vitro*. It has been shown by us and others that post-ovulatory aged oocytes suffer from oxidative stress with increased level of ROS which induces apoptosis. The deleterious

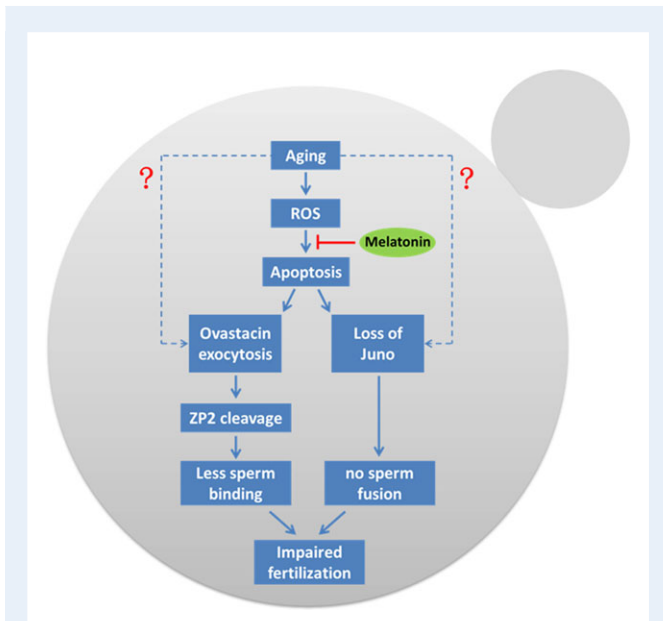


Figure 8 Working model of melatonin-mediated improvement of fertilization in post-ovulatory aged mouse oocytes. Post-ovulatory aging induces high level of ROS and early apoptosis which may damage two critical regulators of fertilization, ovastacin and Juno. Consequently, premature exocytosis of ovastacin causes the cleavage of ZP2 and decreased sperm binding ability to the zona pellucida. The concomitant loss of Juno on the oocyte membrane compromised gamete fusion, and combined, these two defects result in decrease fertilization rates of post-ovulatory aged oocytes. Melatonin restores the fertilization ability possibly by inhibiting the ROS and apoptosis and maintaining the functions of ovastacin and Juno. Dash lines denote that post-ovulatory aging might disrupt ovastacin and Juno via additional, yet to be described, mechanisms.

effect on the developmental potential of oocytes adversely affects fertilization rates (Simon *et al.*, 2000; Gao *et al.*, 2012; Zhao *et al.*, 2016).

Taken together, our findings provide a clinical implication in that supplementation with melatonin has the potential to prolong *in vitro* culture periods of retrieved oocytes for IVF cycle and elevate the IVF rate in human ART. Although re-insemination of aged unfertilized oocytes failing in IVF cycles could be achieved with ICSI via bypassing impaired sperm binding and fusion, the deteriorated oocyte quality would impede the subsequent development potential.

Acknowledgements

We thank Dr Jurrien Dean for providing antibodies and editorial review of the manuscript.

Authors' roles

X.D. and B.X. designed the research; X.D., Y.L., M.Z., Y.M., C.Z. and Z.C. performed the experiments; X.D. and B.X. analyzed the data; X.D. and B.X. wrote the manuscript.

Funding

This work was supported by the National Natural Science Foundation (31571545) and Natural Science Foundation of Jiangsu Province (BK20150677).

Conflict of interest

None declared.

References

- Avella MA, Baibakov B, Dean J. A single domain of the ZP2 zona pellucida protein mediates gamete recognition in mice and humans. *J Cell Biol* 2014;**205**:801–809.
- Baibakov B, Boggs NA, Yauger B, Baibakov G, Dean J. Human sperm bind to the N-terminal domain of ZP2 in humanized zonae pellucidae in transgenic mice. *J Cell Biol* 2012;**197**:897–905.
- Bianchi E, Doe B, Goulding D, Wright GJ. Juno is the egg Izumo receptor and is essential for mammalian fertilization. *Nature* 2014;**508**:483–487.
- Bonnefont-Rousselot D, Collin F, Jore D, Gardes-Albert M. Reaction mechanism of melatonin oxidation by reactive oxygen species in vitro. *J Pineal Res* 2011;**50**:328–335.
- Brzezinski A, Seibel MM, Lynch HJ, Deng MH, Wurtman RJ. Melatonin in human preovulatory follicular fluid. *J Clin Endocrinol Metab* 1987;**64**:865–867.
- Burkart AD, Xiong B, Baibakov B, Jimenez-Movilla M, Dean J. Ovastacin, a cortical granule protease, cleaves ZP2 in the zona pellucida to prevent polyspermy. *J Cell Biol* 2012;**197**:37–44.
- Chen HY, Chen TY, Lee MY, Chen ST, Hsu YS, Kuo YL, Chang GL, Wu TS, Lee EJ. Melatonin decreases neurovascular oxidative/nitrosative damage and protects against early increases in the blood-brain barrier permeability after transient focal cerebral ischemia in mice. *J Pineal Res* 2006;**41**:175–182.
- Ducibella T, Duffy P, Buetow J. Quantification and localization of cortical granules during oogenesis in the mouse. *Biol Reprod* 1994;**50**:467–473.
- Gahlay G, Gauthier L, Baibakov B, Epifano O, Dean J. Gamete recognition in mice depends on the cleavage status of an egg's zona pellucida protein. *Science* 2010;**329**:216–219.
- Galano A, Tan DX, Reiter RJ. Melatonin as a natural ally against oxidative stress: a physicochemical examination. *J Pineal Res* 2011;**51**:1–16.
- Gao C, Han HB, Tian XZ, Tan DX, Wang L, Zhou GB, Zhu SE, Liu GS. Melatonin promotes embryonic development and reduces reactive oxygen species in vitrified mouse 2-cell embryos. *J Pineal Res* 2012;**52**:305–311.
- Garcia JJ, Lopez-Pingarron L, Almeida-Souza P, Tres A, Escudero P, Garcia-Gil FA, Tan DX, Reiter RJ, Ramirez JM, Bernal-Perez M. Protective effects of melatonin in reducing oxidative stress and in preserving the fluidity of biological membranes: a review. *J Pineal Res* 2014;**56**:225–237.
- Grayson P. Izumo I and Juno: the evolutionary origins and coevolution of essential sperm-egg binding partners. *R Soc Open Sci* 2015;**2**:150296.
- Hoodbhoy T, Talbot P. Mammalian cortical granules: contents, fate, and function. *Mol Reprod Dev* 1994;**39**:439–448.
- Inoue N, Ikawa M, Isotani A, Okabe M. The immunoglobulin superfamily protein Izumo is required for sperm to fuse with eggs. *Nature* 2005;**434**:234–238.
- Ishizuka B, Kuribayashi Y, Murai K, Amemiya A, Itoh MT. The effect of melatonin on *in vitro* fertilization and embryo development in mice. *J Pineal Res* 2000;**28**:48–51.

- Lincoln GA, Clarke IJ, Hut RA, Hazlerigg DG. Characterizing a mammalian circannual pacemaker. *Science* 2006;**314**:1941–1944.
- Liu XY, Mal SF, Miao DQ, Liu DJ, Bao S, Tan JH. Cortical granules behave differently in mouse oocytes matured under different conditions. *Hum Reprod* 2005;**20**:3402–3413.
- Longo FJ, Chen DY. Development of cortical polarity in mouse eggs: involvement of the meiotic apparatus. *Dev Biol* 1985;**107**:382–394.
- Lord T, Aitken RJ. Oxidative stress and ageing of the post-ovulatory oocyte. *Reproduction* 2013;**146**:R217–227.
- Lord T, Martin JH, Aitken RJ. Accumulation of electrophilic aldehydes during postovulatory aging of mouse oocytes causes reduced fertility, oxidative stress, and apoptosis. *Biol Reprod* 2015;**92**:33.
- Lord T, Nixon B, Jones KT, Aitken RJ. Melatonin prevents postovulatory oocyte aging in the mouse and extends the window for optimal fertilization in vitro. *Biol Reprod* 2013;**88**:67.
- Manchester LC, Coto-Montes A, Boga JA, Andersen LP, Zhou Z, Galano A, Vriend J, Tan DX, Reiter RJ. Melatonin: an ancient molecule that makes oxygen metabolically tolerable. *J Pineal Res* 2015;**59**:403–419.
- Manda K, Ueno M, Anzai K. AFMK, a melatonin metabolite, attenuates X-ray-induced oxidative damage to DNA, proteins and lipids in mice. *J Pineal Res* 2007;**42**:386–393.
- Nicosia SV, Wolf DP, Inoue M. Cortical granule distribution and cell surface characteristics in mouse eggs. *Dev Biol* 1977;**57**:56–74.
- Okada A, Yanagimachi R, Yanagimachi H. Development of a cortical granule-free area of cortex and the perivitelline space in the hamster oocyte during maturation and following ovulation. *J Submicrosc Cytol* 1986;**18**:233–247.
- Quesada V, Sanchez LM, Alvarez J, Lopez-Otin C. Identification and characterization of human and mouse ovastacin: a novel metalloproteinase similar to hatching enzymes from arthropods, birds, amphibians, and fish. *J Biol Chem* 2004;**279**:26627–26634.
- Reiter RJ, Mayo JC, Tan DX, Sainz RM, Alatorre-Jimenez M, Qin L. Melatonin as an antioxidant: under promises but over delivers. *J Pineal Res* 2016;**61**:253–278.
- Simon HU, Haj-Yehia A, Levi-Schaffer F. Role of reactive oxygen species (ROS) in apoptosis induction. *Apoptosis* 2000;**5**:415–418.
- Szollasi D. Development of cortical granules and the cortical reaction in rat and hamster eggs. *Anat Rec* 1967;**159**:431–446.
- Tamura H, Takasaki A, Miwa I, Taniguchi K, Maekawa R, Asada H, Taketani T, Matsuoka A, Yamagata Y, Shimamura K et al. Oxidative stress impairs oocyte quality and melatonin protects oocytes from free radical damage and improves fertilization rate. *J Pineal Res* 2008;**44**:280–287.
- Tarin JJ, Perez-Albala S, Aguilar A, Minarro J, Hermenegildo C, Cano A. Long-term effects of postovulatory aging of mouse oocytes on offspring: a two-generational study. *Biol Reprod* 1999;**61**:1347–1355.
- Tarin JJ, Perez-Albala S, Perez-Hoyos S, Cano A. Postovulatory aging of oocytes decreases reproductive fitness and longevity of offspring. *Biol Reprod* 2002;**66**:495–499.
- Wang F, Tian X, Zhang L, Tan D, Reiter RJ, Liu G. Melatonin promotes the in vitro development of pronuclear embryos and increases the efficiency of blastocyst implantation in murine. *J Pineal Res* 2013;**55**:267–274.
- Zamboni L. Ultrastructure of mammalian oocytes and ova. *Biol Reprod* 1970;**2**(Suppl 2):44–63.
- Zhang HM, Zhang Y. Melatonin: a well-documented antioxidant with conditional pro-oxidant actions. *J Pineal Res* 2014;**57**:131–146.
- Zhang T, Zhou Y, Li L, Wang HH, Ma XS, Qian WP, Shen W, Schatten H, Sun QY. SIRT1, 2, 3 protect mouse oocytes from postovulatory aging. *Aging* 2016;**8**:685–696.
- Zhao XM, Hao HS, Du WH, Zhao SJ, Wang HY, Wang N, Wang D, Liu Y, Qin T, Zhu HB. Melatonin inhibits apoptosis and improves the developmental potential of vitrified bovine oocytes. *J Pineal Res* 2016;**60**:132–141.

REPORT

Smc1 β is required for activation of SAC during mouse oocyte meiosis

Yilong Miao, Changyin Zhou, Zhaokang Cui, Xiaoxin Dai, Mianqun Zhang, Yajuan Lu, and Bo Xiong

College of Animal Science and Technology, Nanjing Agricultural University, Nanjing, China

ABSTRACT

Smc1 β is a meiosis-specific cohesin subunit that is essential for sister chromatid cohesion and DNA recombination. Previous studies have shown that Smc1 β -deficient mice in both sexes are sterile. Ablation of Smc1 β during male meiosis leads to the blockage of spermatogenesis in pachytene stage, and ablation of Smc1 β during female meiosis generates a highly error-prone oocyte although it could develop to metaphase II stage. However, the underlying mechanisms regarding how Smc1 β maintains the correct meiotic progression in mouse oocytes have not been clearly defined. Here, we find that GFP-fused Smc1 β is expressed and localized to the chromosomes from GV to MII stages during mouse oocyte meiotic maturation. Knockdown of Smc1 β by microinjection of gene-specific morpholino causes the impaired spindle apparatus and chromosome alignment which are highly correlated with the defective kinetochore-microtubule attachments, consequently resulting in a prominently higher incidence of aneuploid eggs. In addition, the premature extrusion of polar bodies and escape of metaphase I arrest induced by low dose of nocodazole treatment in Smc1 β -depleted oocytes indicates that Smc1 β is essential for activation of spindle assembly checkpoint (SAC) activity. Collectively, we identify a novel function of Smc1 β as a SAC participant beyond its role in chromosome cohesion during mouse oocyte meiosis.

ARTICLE HISTORY

Received 21 November 2016
Revised 5 January 2017
Accepted 10 January 2017

KEYWORDS

aneuploid egg; chromosome alignment; kinetochore-microtubule attachment; Smc1 β ; spindle assembly; SAC

Introduction

Cohesin complex is well known as its roles in mediating chromosome cohesion and segregation in both mitosis and meiosis.¹ To ensure correct meiotic chromosome segregation, sister chromatid cohesion (SCC) needs to be maintained from its establishment in prophase I oocytes before birth until continuation of meiosis into metaphase II upon oocyte maturation in the adult.² At anaphase II cohesin is cleaved by separase between sister chromatids, allowing them segregated to generate haploid gametes.^{1–6} Aging human oocytes suffer a steep increase in chromosome mis-segregation and aneuploidy, which may be caused by loss of SCC through slow deterioration of cohesin.^{7–9} This hypothesis assumes that cohesin expression in embryonic oocytes is sufficient to provide adequate long-term SCC. With increasing age, mouse oocytes deficient in the meiosis-specific cohesin Smc1 β massively lose SCC and chiasmata.^{9,10} Specific inactivation of mouse *Smc1 β* gene at the primordial follicle stage shortly after birth when oocytes had just entered meiosis I dictyate arrest has normal chiasma positions and SCC in the adult, suggesting that Smc1 β cohesin needs only be expressed during prophase I before the primordial follicle stage to ensure SCC up to advanced age of mice.²⁸

Beyond its well-known role in SCC, Smc1 β also exerts other functions in various biologic events. Smc1 β determines meiotic chromatin loop organization and proper axes/loop structure of

axial elements (AEs) and synaptonemal complexes (SCs). In the absence of Smc1 β , AEs and SCs are greatly shortened to about half length of those in wild-type mice.^{11,12} In addition, Smc1 β serves a specific role at telomeres independent of its role in determining AE/SC length and loop extension. In Smc1 β ^{−/−} meocytes, one fifth of their telomeres fail to attach to the nuclear envelope.¹³ Telomeres in Smc1 β ^{−/−} spermatocytes and oocytes lose their structural integrity and suffer a range of abnormalities, suggesting that a telomere structure protected from DNA rearrangements depends on Smc1 β . Smc1 β -deficient mice in both sexes are sterile. Ablation of Smc1 β during male meiosis leads to the blockage of spermatogenesis in pachytene stage, and ablation of Smc1 β during female meiosis generates a highly error-prone oocyte although it could develop to metaphase II stage.¹¹ Loss of Smc1 β affects spermatocytes more dramatically than oocytes, for spermatocytes arrest in mid-pachytene with a failure to complete synapsis, Smc1 β -deficient spermatocytes die in midpachytene.¹¹ Despite accumulating previous research, the functional roles of Smc1 β during oocyte meiotic maturation remain elusive.

Here, we report that Smc1 β localizes at chromosomes during mouse oocyte meiosis and is required for normal spindle assembly, proper chromosome alignment and correct kinetochore-microtubule attachments. Notably, Smc1 β is involved in the activation of SAC function to maintain the euploidy during mouse oocyte maturation.

Results

Smc1 β localizes to the chromosomes during mouse oocyte meiosis

To examine the localization of Smc1 β during meiotic maturation in mouse oocytes, a construct fused with a fluorescent tag GFP to the C-terminus of Smc1 β was made and *in vitro* transcribed into cRNA. Following microinjection with cRNA, oocytes were arrested at GV stage for another 6 h to allow cRNA to be fully translated to protein, and then cultured to specific time points to observe Smc1 β -GFP under the confocal microscope. The result showed that Smc1 β exhibited a co-localization with chromosome staining by Hoechst from GV to MII stages (Fig. 1), indicating that Smc1 β is localized to chromosomes during oocyte meiosis.

Depletion of Smc1 β impairs spindle assembly and chromosome alignment during mouse oocyte meiosis

To clearly define the role of Smc1 β during meiotic maturation, a morpholino-based gene-silencing approach was applied to deplete Smc1 β . Fully-grown GV oocytes were microinjected with non-targeting or Smc1 β -targeting morpholinos and arrested in medium supplemented with milrinone for 20 h, allowing sufficient time to inhibit mRNA translation. As shown in Fig. 2A, the protein level of Smc1 β in Smc1 β -K_D oocytes was pronouncedly decreased compared with control oocytes, confirming the knockdown effect through morpholino injection. Then oocytes were immunostained with anti- α -tubulin-FITC antibody and counterstained with Hoechst to observe the spindle morphologies as well as the chromosome alignment. The staining result showed that a great mass of control oocytes displayed a typical barrel-shape spindle apparatus with a well-aligned chromosome on the equatorial plate (Fig. 2B). However, a diversity of disorganized spindle apparatuses with scattered chromosomes was present in Smc1 β -K_D oocytes (Fig. 2B). Quantitatively, almost 80% of oocytes displayed the aberrant spindle morphologies ($78.3\% \pm 2.1\%$, $n = 142$) and more than 80% of oocytes exhibited misaligned chromosomes ($81\% \pm 1.0\%$, $n = 140$) compared with approximately 20% of defects in controls ($20\% \pm 1.0\%$, $n = 121$; $17.5\% \pm 0.5\%$, $n = 127$; $p < 0.05$; Fig. 2C, D). Thus, our data reveal that Smc1 β participates in the regulation of spindle assembly and chromosome alignment during mouse oocyte meiotic maturation.

Depletion of Smc1 β compromises kinetochore-microtubule attachments during mouse oocyte meiosis

Impaired spindle formation and incorrect chromosome alignment predicts that the interaction between kinetochores and microtubules might be defective. To test this possibility, we assessed the stability of kinetochore-microtubule attachments by using cold treatment to depolymerize unstable microtubules upon depletion of Smc1 β . To this end, MI oocytes were briefly chilled to induce depolymerization of microtubules that are not attached to kinetochores, and then immunostained with CREST to detect kinetochores, with anti- α -tubulin-FITC

antibody to visualize the microtubules and counterstained with Hoechst to observe chromosomes. The staining result showed that kinetochores were fully attached by microtubules and chromosomes were well-aligned after cold treatment in most of control oocytes ($13.2\% \pm 1.4\%$, $n = 98$; Fig. 3A, B). By contrast, a prominently increased rate of kinetochores with very few cold-stable microtubules was observed in Smc1 β -K_D oocytes ($74.7\% \pm 2.3\%$, $n = 101$, $p < 0.05$; Fig. 3A, B). Collectively, this observation suggests that kinetochore-microtubule attachments are less stable after depletion of Smc1 β , which might lead to the failure of spindle assembly and chromosome alignment.

Smc1 β is required for prevention of aneuploidy in mouse oocytes

Since chromosome misalignment is highly correlated with the generation of aneuploidy, an abnormal number of chromosomes which might lead to miscarriage, embryonic lethality or genetic disorders in mouse eggs, we then performed the karyotyping analysis of MII eggs by chromosome spreading. As shown in Fig. 4A, the number of single chromosomes (univalents) in the normal eggs was 20, which is the prerequisite for genomic integrity in the mouse. However, a remarkably higher incidence of aneuploid eggs that had more or less 20 univalents was found in Smc1 β -K_D oocytes compared with controls ($13.9\% \pm 1.4\%$, $n = 59$ VS $83.8\% \pm 0.8\%$, $n = 61$, $p < 0.05$; Fig. 4B), indicating that oocytes are unable to correctly assemble the spindles and properly align the chromosomes to generate euploid eggs in the absence of Smc1 β .

Smc1 β is necessary for activation of SAC during oocyte meiosis

We next examined the effect of Smc1 β knockdown on the meiotic progression. After culture of GV oocytes to the specific time points, the rates of GVBD and polar body extrusion were counted in the control and Smc1 β -K_D oocytes, respectively. The result showed that loss of Smc1 β did not affect either germinal vesicle breakdown or extrusion of first polar body ($72.2\% \pm 3.4\%$, $n = 143$ VS $75.6\% \pm 1.5\%$, $n = 178$; $69.8\% \pm 1.7\%$, $n = 130$ VS $67.2\% \pm 2.2\%$, $n = 166$; Fig. 5A, B), 2 critical developmental events during oocyte maturation. However, at the time point of 7 h post-GVBD, a higher percentage of PBE was observed in Smc1 β -K_D oocytes than that in controls ($13.6\% \pm 1.1\%$, $n = 137$ VS $32.5\% \pm 0.9\%$, $n = 170$, $p < 0.05$; Fig. 5C), suggesting that polar bodies were precociously extruded in the absence of Smc1 β .

The premature PBE indicates that SAC activity is compromised in Smc1 β -K_D oocytes. To further verify this possibility, we tested whether oocytes depleted of Smc1 β would override the MI arrest induced by low dose of nocodazole treatment, indicative of SAC inactivation. For this purpose, GV oocytes were cultured to 4 h post-GVBD and then transferred to the medium supplemented with $0.04 \mu\text{g/ml}$ of nocodazole for 6 h to observe the polar body extrusion. The result showed that only about 8% of control oocytes could abrogate MI arrest and extrude the first polar body in the presence of low dose of nocodazole. Whereas Smc1 β -K_D oocytes showed a prominent increase in the overriding

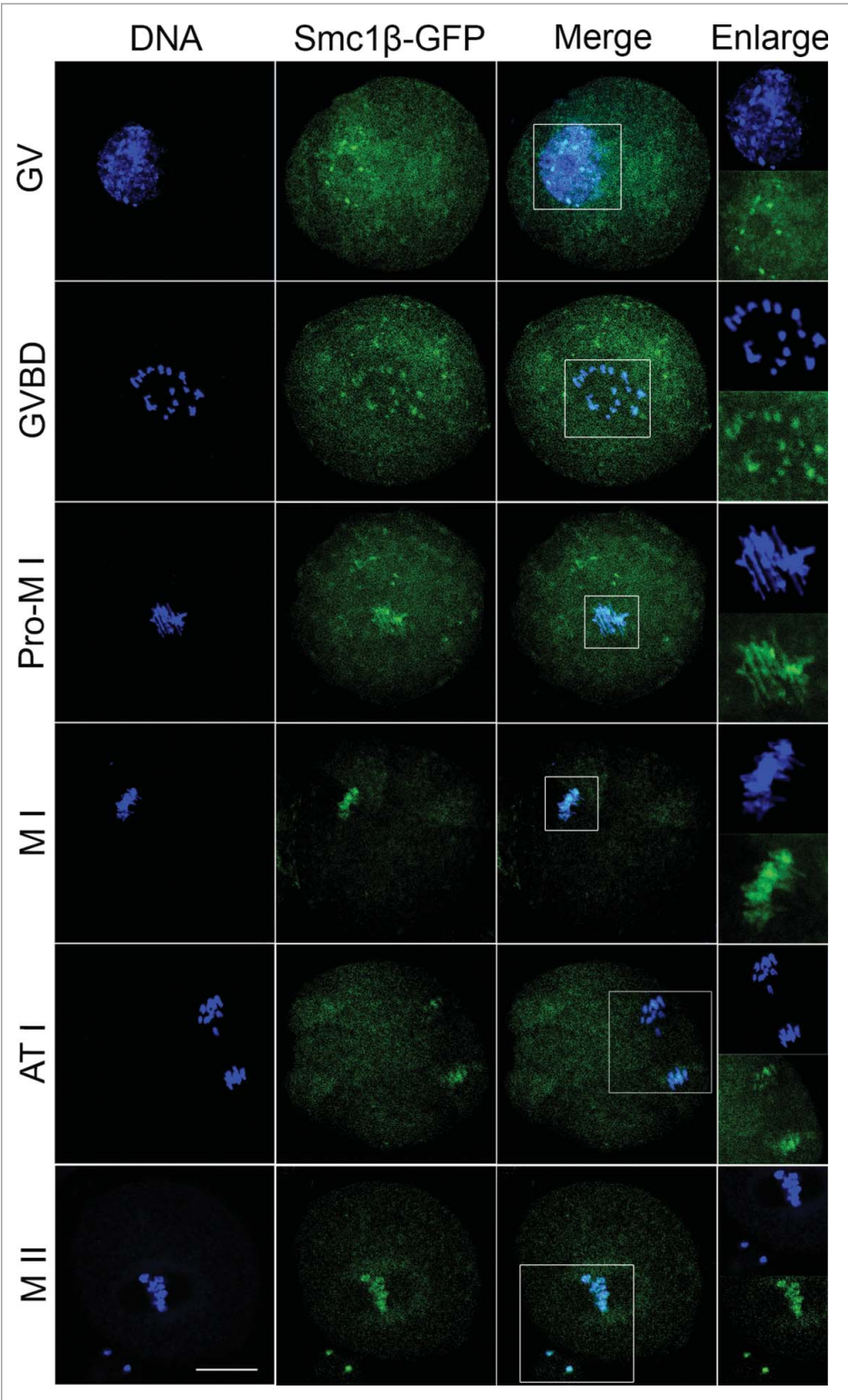


Figure 1. Subcellular localization of Smc1 β during mouse oocyte meiotic maturation. Mouse oocytes were microinjected with Smc1 β -GFP cRNA at GV stage, and then cultured to GVBD, Pro-M I, M I, AT I and M II stages, respectively, followed by nuclear staining with Hoechst (blue). GV, oocytes at germinal vesicle stage; GVBD, oocytes at germinal vesicle breakdown stage; Pro-M I, oocytes at first prometaphase stage; M I, oocytes at first metaphase stage; AT I, oocytes at first anaphase/telophase stage; M II, oocytes at second metaphase stage. Scale bar, 20 μ m.

rate and around 30% of oocytes finally reached the M II stage ($10.5\% \pm 0.6\%$, $n = 161$ VS $30.5\% \pm 2.6\%$, $n = 187$, $p < 0.05$; Fig. 5D). Therefore, the above observations reveal that Smc1 β is required for SAC activation and might regulate SAC proteins during meiosis.

Discussion

The cohesin complex and its accessory factors contribute in many ways to genomic organization and stability. Proteins in this network have been shown to execute functions in chromosome

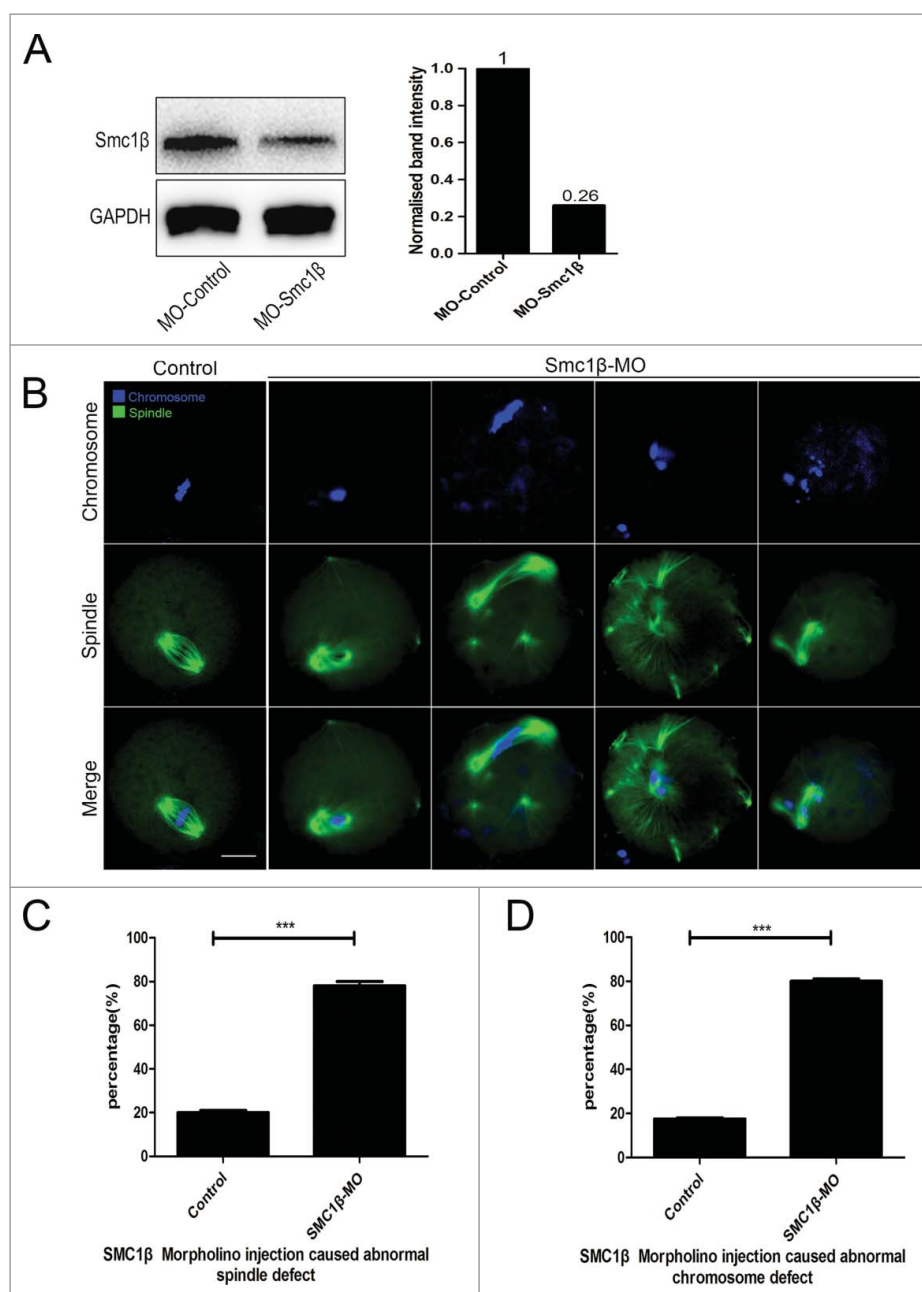


Figure 2. Knockdown of Smc1 β causes spindle/chromosome abnormalities in mouse oocytes. (A) Protein levels of Smc1 β in control and Smc1 β -MO (morpholino injected) oocytes. The blots were probed with anti-Smc1 β antibody and anti-GAPDH antibody, respectively. (B) Representative images of spindle morphologies and chromosome alignment in control and Smc1 β -MO oocytes. Oocytes were immunostained with anti- α -tubulin-FITC antibody to visualize spindles and counterstained with Hoechst to visualize chromosomes. Scale bar, 20 μ m. (C) The proportion of abnormal spindles was recorded in control and Smc1 β -MO oocytes. Data were presented as mean percentage (mean \pm SEM) of at least 3 independent experiments. Asterisk denotes statistical difference at a $p < 0.05$ level of significance. (D) The proportion of misaligned chromosomes was recorded in control and Smc1 β -MO oocytes. Data were presented as mean percentage (mean \pm SEM) of at least 3 independent experiments. Asterisk denotes statistical difference at a $p < 0.05$ level of significance.

segregation, gene regulation, DSB repair and chromosome morphology.¹ In meiosis, the generation of mammalian gametes comprises 2 subsequent cell divisions (meiosis I and II) during their development to reduce the ploidy.^{9,10} Any errors in these processes generating aneuploidy would lead to the miscarriage, age-related infertility, and high incidence of genetic disorders such as Down syndrome in humans.¹⁴⁻¹⁷

Meiotic cohesin complexes are composed of 4 essential subunits, including a meiosis-specific Smc1 subunit (Smc1 β), 2 additional α -kleisins (Rad21L and Rec8) and another stromal antigen protein (Stag3).^{18,19} Previous studies have investigated

the functions of Smc1 β in determining the axis-loop structure of synaptonemal complexes, in providing sister chromatid cohesion in metaphase I and thereafter, in protecting telomere structure, and in synapsis.¹³ However, little is known about the roles of Smc1 β during the development window of oocyte meiotic maturation.

Prevention of generating aneuploid cells is very important for the health of offspring during meiotic divisions and aneuploid embryos usually perish in utero, and even when they survive to term, they suffer from severe congenital birth defects.²⁰ Loss of sister chromatid cohesion during meiosis has been

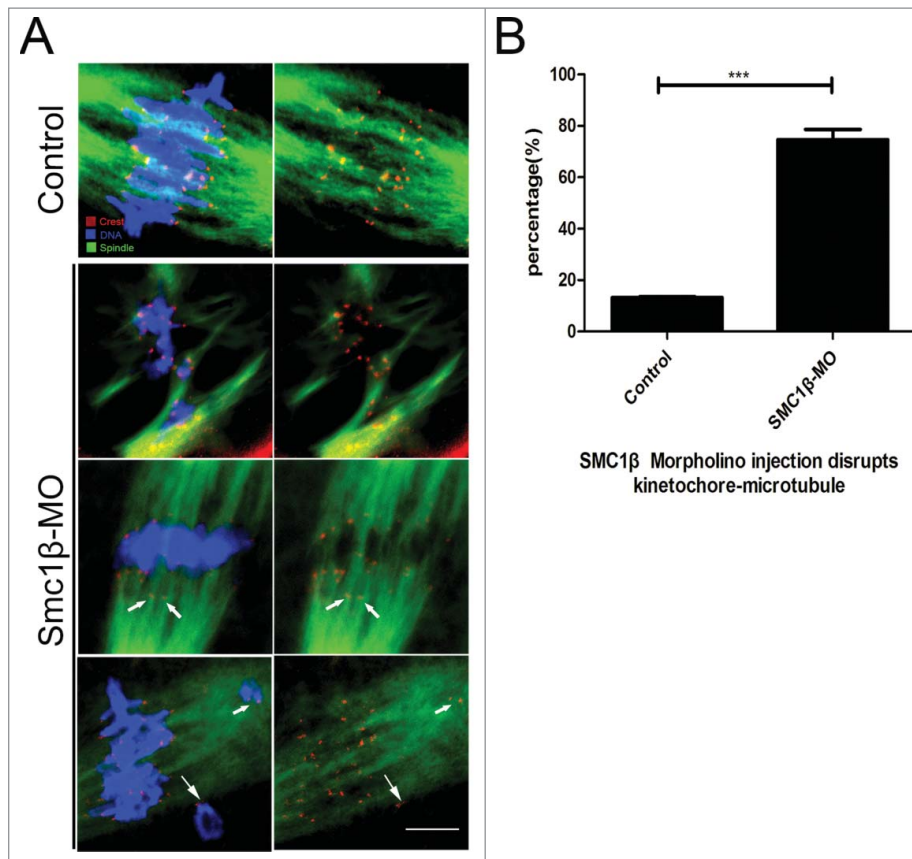


Figure 3. Knockdown of *Smc1β* leads to the disrupted kinetochore-microtubule attachment in mouse oocytes. (A) Representative images of kinetochore-microtubule attachments in control and *Smc1β*-MO oocytes. Oocytes were immunostained with anti- α -tubulin-FITC antibody to visualize spindles, with CREST to visualize kinetochores, and counterstained with Hoechst to visualize chromosomes. Scale bar, 5 μ m. (B) The proportion of defective kinetochore-microtubule attachments was recorded in control and *Smc1β*-MO oocytes. Data were presented as mean percentage (mean \pm SEM) of at least 3 independent experiments. Asterisk denotes statistical difference at a $p < 0.05$ level of significance.

postulated as a key factor in age-related non-disjunction in human oocytes.²¹⁻²⁵ Notably, a recent research has shown that the integrity of the spindle checkpoint response depends on the centromeric cohesin in mammalian oocytes.²⁶

In this study, we found that *Smc1β* accumulated on the chromosomes during mouse oocyte meiotic maturation. This localization pattern is consistent with the typical chromatin distribution of cohesin subunits in mitosis. Also, it is in line with *Smc1β* localization on chromosome axes in early meiosis.^{11,27,28} To clearly define its role during meiotic maturation, loss-of-function experiments were performed by gene-targeting morpholino microinjection in GV oocytes. In mammalian females, cohesin complex has been loaded and locked on chromosomes in fetal oocytes, and would not undergo turnover after birth during arrest at the prolonged dictyate stage.^{29,30} Thus, during the window of oocyte meiotic maturation, cohesin complex no longer needs *Smc1β*, suggesting that another pool of *Smc1β* might play a particular role in this process. As expected, our data showed that spindle assembly was disrupted in *Smc1β*-KD oocytes. Accompanied by this defect, scattered and lagging chromosomes were also observed in the absence of *Smc1β*.

The observation of spindle/chromosome abnormalities further prompted us to examine the kinetochore-microtubule attachment following knockdown of *Smc1β*. The kinetochore contains approximately 100 different proteins that

clustered in several different complexes on centromeric DNA, including inner kinetochore proteins, outer kinetochore proteins, as well as regulatory proteins.³¹⁻³³ Through these multiprotein structures, kinetochore attaches chromosomes to spindle microtubules and maintain the attachment to growing or disassembling microtubule to drive chromosomes segregation.³⁴⁻³⁶ Therefore, if errors of kinetochore-microtubule attachment could not be corrected until anaphase, they would cause chromosome misalignment and missegregation.^{37,38} We thus propose that *Smc1β* is involved in the maintenance of the attachment between kinetochores and microtubules during mouse oocyte meiosis. Consistent with our expectation, the quantitative data showed that an apparently increased rate of kinetochores was unattached by microtubules upon cool treatment which is able to depolymerize unattached microtubules. As a result, loss of *Smc1β* generated an elevated incidence of aneuploid eggs which are highly correlated with miscarriage, birth defects and genetic disorders.

Finally, we tested the effect of *Smc1β* on the meiotic progression. Knockdown of *Smc1β* did not affect GVBD and PBE, 2 key events occurring during meiotic maturation. However, it did cause the precocious PBE at anaphase phase, indicating that SAC activity is compromised in depletion of *Smc1β*. Another line of evidence to prove that SAC function is impaired in *Smc1β*-depleted oocytes is that

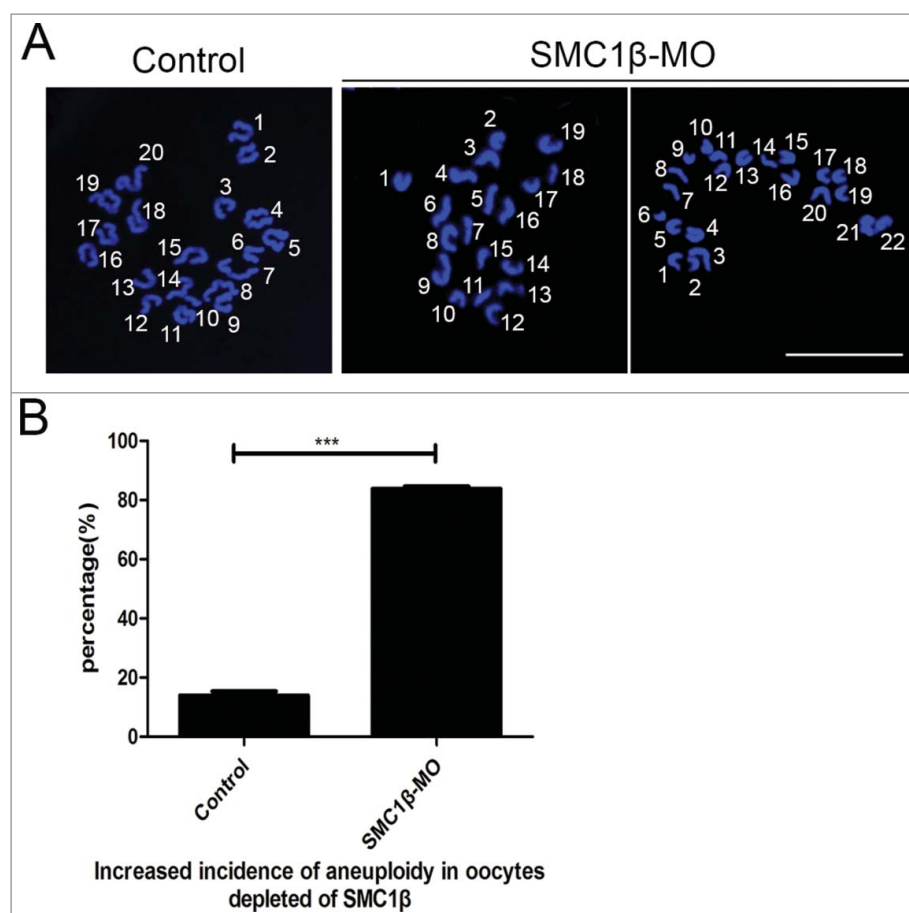


Figure 4. Knockdown of *Smc1β* results in the generation of aneuploidy in mouse eggs. (A) Representative images of euploid and aneuploid MII eggs. Chromosome spread was performed to calculate the number of chromosomes. Chromosomes were counterstained with PtdIns. Scale bar, 5 μ m. (B) The proportion of aneuploid eggs was recorded in control and *Smc1β*-MO oocytes. Data were presented as mean percentage (mean \pm SEM) of at least 3 independent experiments. Asterisk denotes statistical difference at a $p < 0.05$ level of significance.

oocytes were able to override the MI arrest induced by nocodazole in the absence of *Smc1β*. These observations are coincident with the recent proposed concept that the spindle checkpoint response depends on centromeric cohesin in mammalian oocytes.²⁶

In summary, our study presents several lines of evidence revealing that *Smc1β* is a SAC regulator that maintains normal spindle assembly, proper chromosome alignment and correct kinetochore-microtubule attachment to prevent generation of aneuploid eggs, discovering a new molecular determinant controlling oocyte development.

Materials and methods

Antibodies

Rabbit polyclonal anti-*Smc1β* antibody was purchased from Abcam (Cambridge, MA, USA; Cat#: EP2879Y); mouse monoclonal anti- α -tubulin-fluorescein isothiocyanate (FITC) antibody was purchased from Sigma (St. Louis, MO, USA; Cat#: F2168); human anti-centromere antibody was purchased from Antibodies Inc. (Davis, CA, USA; Cat#: 15-234); Alexa Fluor 555 conjugated goat anti-Human IgG ($H^{+}L$) was purchased from ThermoFisher (Waltham, MA, USA; Cat#: A-21433).

Oocyte collection and culture

All experiments were approved by the Animal Care and Use Committee of Nanjing Agricultural University, China and were performed in accordance with institutional guidelines. Female ICR mice (4–6 weeks) were killed by cervical dislocation after intraperitoneal injections of 5 IU pregnant mare serum gonadotropin (PMSG) for 46 h. Fully-grown oocytes arrested at prophase of meiosis I were collected from ovaries in M2 medium (Sigma, St. Louis, MO, USA). Only those immature oocytes displaying a germinal vesicle (GV) were cultured further in M16 medium (Sigma, St. Louis, MO, USA) under liquid paraffin oil at 37°C in an atmosphere of 5% CO₂ incubator for *in vitro* maturation. At different time points after culture, oocytes were collected for subsequent analysis.

cRNA construct and *in vitro* transcription

For *in vitro* transcription, full-length *Smc1β* cDNA was subcloned into pcDNA3-EGFP vector. Capped cRNA was synthesized from linearized plasmid using T7 mMessage mMachine kit (ThermoFisher, Waltham, MA, USA), and purified with MEGAclean kit (ThermoFisher, Waltham, MA, USA). Typically, 10–12 μ l (4% of the oocyte volume) of 0.5–1.0 μ g/ μ l cRNA was injected into oocytes. The oocytes were then arrested at the GV stage in M16 medium containing 2.5 μ M milrinone.

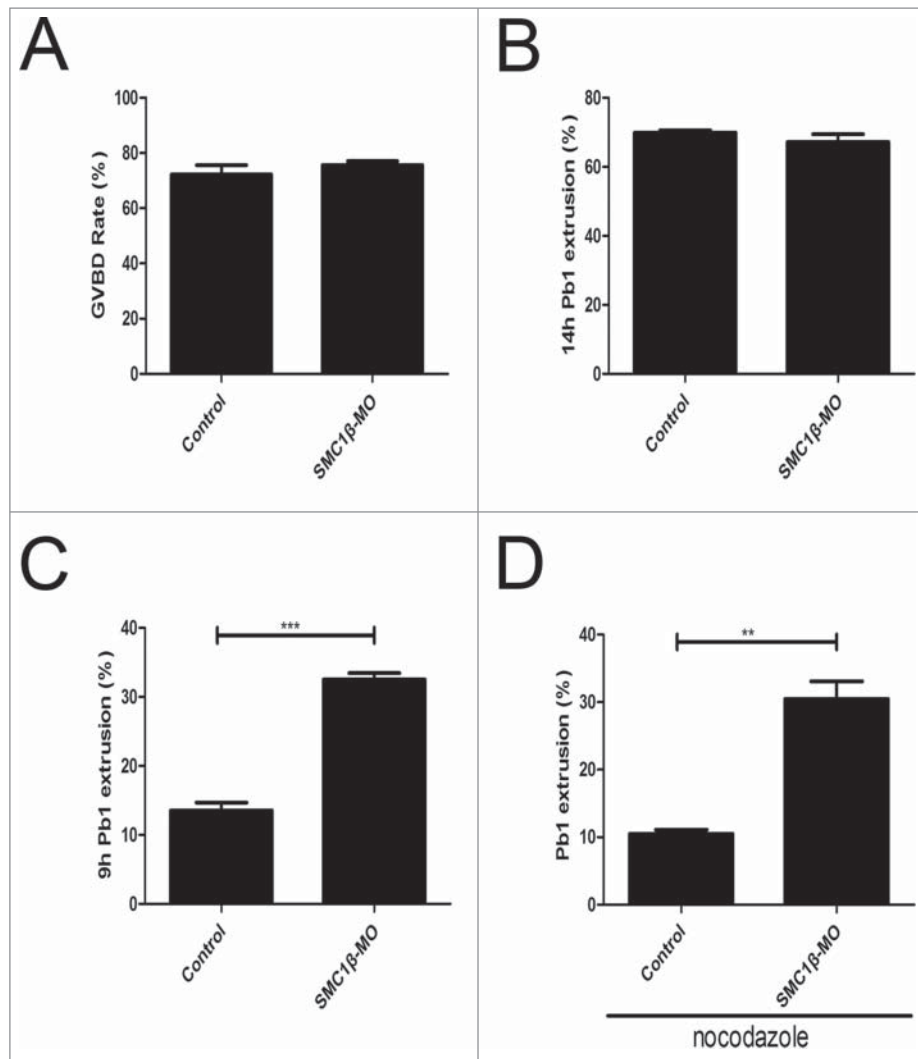


Figure 5. Effects of *Smc1β* Knockdown on the meiotic progression and SAC activity in mouse oocytes. (A) The proportion of germinal vesicle breakdown was recorded in control and *Smc1β*-MO oocytes. (B) The proportion of polar body extrusion was recorded in control and *Smc1β*-MO oocytes at the time point of 12 h post-GVBD. (C) The proportion of precocious polar body extrusion was recorded in control and *Smc1β*-MO oocytes at the time point of 7 h post-GVBD. (D) The proportion of overriding MI arrest was recorded in control and *Smc1β*-MO oocytes by low dose of nocodazole treatment. Data were presented as mean percentage (mean \pm SEM) of at least 3 independent experiments. Asterisk denotes statistical difference at a $p < 0.05$ level of significance.

for 6 h, allowing enough time for translation, and then released into milrinone-free M16 medium for further study.

Morpholino knockdown

Smc1β-targeting morpholino (5'-GAGCAGCAGCTCAAGGT GCCCAT-3') was obtained from Gene Tools LLC (Philomath, OR, USA), and then diluted to 1 μ M as working concentration. For knockdown experiment, about 5–10 μ l of morpholino was microinjected into the cytoplasm of fully grown GV oocytes using a Narishige microinjector (Tokyo, Japan). A non-targeting morpholino was injected as a control. To facilitate the morpholino-mediated inhibition of mRNA translation, oocytes were arrested at GV stage in M16 medium containing 2.5 μ M milrinone for 20 h, and then cultured in milrinone-free M16 medium for subsequent experiments.

Immunofluorescence and confocal microscopy

Oocytes were fixed in 4% paraformaldehyde in PBS (pH 7.4) for 30 minutes and permeabilized in 0.5% Triton-X-100 for

20 min at room temperature. Then, oocytes were blocked with 1% BSA-supplemented PBS for 1 h and incubated with anti- α -tubulin-FITC (1:200) or anti-centromere (1:200) antibodies at 4°C overnight. After washing 4 times (5 min each) in PBS containing 1% Tween 20 and 0.01% Triton-X 100, oocytes were incubated with an appropriate secondary antibody for 1 h at room temperature. After washing 3 times, oocytes were counterstained with PI (Propidium Iodide) or Hoechst 33342 (10 μ g/ml) for 10 min. Finally, oocytes were mounted on glass slides and observed under a confocal laser scanning microscope (Carl Zeiss 700).

Western blotting

A pool of 300 oocytes was lysed in 4 \times LDS sample buffer (ThermoFisher, Waltham, MA, USA) containing protease inhibitor, and then separated on 10% Bis-Tris precast gels and transferred onto PVDF membranes. The blots were blocked in TBST (Tris-buffered saline containing 0.1% Tween 20) containing 5% low fat dry milk for 1 h at room temperature and then

incubated with anti-Smc1 β antibody (1:1000) overnight at 4°C. After 3 times of washes in TBST, the blots were incubated with 1:10,000 dilution of HRP (Horse Radish Peroxidase) conjugated secondary antibodies for 1 h at room temperature. Chemiluminescence was detected with ECL Plus Western Blotting Detection System (GE, Piscataway, NJ, USA) and protein bands were visualized by Tanon-3900. The blots were then stripped and reblotted with anti- β -actin antibody (1:5000) for loading control.

Chromosome spread

Oocytes were exposed to Tyrode's buffer (pH 2.5) for about 30 s at 37°C to remove zona pellucidae. After recovery in M2 medium for 10 min, oocytes were fixed in a drop of 1% paraformaldehyde with 0.15% Triton X-100 on a glass slide. After air drying, chromosomes were counterstained with PtdIns and examined under a laser scanning confocal microscope.

Statistical analysis

The data were expressed as mean \pm SEM and analyzed by one-way ANOVA, followed by LSD's post hoc test, which was provided by SPSS16.0 statistical software. The level of significance was accepted as $p < 0.05$.

Author contributions

Y.M. and B.X. designed the research; Y.M., C.Z., Z.C., X.D., M.Z. and Y.L. performed the experiments; Y.M. and B.X. analyzed the data; Y.M. and B.X. wrote the manuscript.

Disclosure of potential conflicts of interest

No potential conflicts of interest were disclosed.

Funding

This work was supported by the National Natural Science Foundation (31571545) and Natural Science Foundation of Jiangsu Province (BK20150677).

References

- Xiong B, Gerton JL. Regulators of the cohesin network. *Annu Rev Biochem* 2010; 79(1):131-53; PMID:20331362; <http://dx.doi.org/10.1146/annurev-biochem-061708-092640>
- Michaelis C, Ciosk R, Nasmyth K. Cohesins: chromosomal proteins that prevent premature separation of sister chromatids. *Cell* 1997; 91:35-6; PMID:9335333; [http://dx.doi.org/10.1016/S0092-8674\(01\)80007-6](http://dx.doi.org/10.1016/S0092-8674(01)80007-6)
- Nasmyth K. Disseminating the genome: joining, resolving, and separating sister chromatids during mitosis and meiosis. *Annu Rev Genet* 2001; 35:673-45; PMID:11700297; <http://dx.doi.org/10.1146/annurev-genet.35.102401.091334>
- Guacci V, Koshland D, Strunnikov A. A direct link between sister chromatid cohesion and chromosome condensation revealed through the analysis of MCD1 in *S. cerevisiae*. *Cell* 1997; 91:47-8; PMID:9335334; [http://dx.doi.org/10.1016/S0092-8674\(01\)80008-8](http://dx.doi.org/10.1016/S0092-8674(01)80008-8)
- Losada A, Hirano M, Hirano T. Identification of *Xenopus* SMC protein complexes required for sister chromatid cohesion. *Gene Dev* 1998; 12:1986-97; PMID:9649503; <http://dx.doi.org/10.1101/gad.12.13.1986>
- Buonomo SBC, Clyne RK, Fuchs J, Loidl J, Uhlmann F, Nasmyth K. Disjunction of homologous chromosomes in meiosis I depends on proteolytic cleavage of the meiotic cohesin REC8 by separin. *Cell* 2000; 103:387-98; PMID:11081626; [http://dx.doi.org/10.1016/S0092-8674\(00\)00131-8](http://dx.doi.org/10.1016/S0092-8674(00)00131-8)
- Herbert M, Kalleas D, Cooney D, Lamb M, Lister L. Meiosis and maternal aging: insights from aneuploid oocytes and trisomy births. *CSH Perspect Biol* 2015; 7:a017970
- Jones KT, Lane SI. Molecular causes of aneuploidy in mammalian eggs. *Development* 2013; 140:3719-3730; PMID:23981655; <http://dx.doi.org/10.1242/dev.090589>
- Eppig JJ. Coordination of nuclear and cytoplasmic oocyte maturation in eutherian mammals. *Reprod Fert Develop* 1996; 8:485-89; <http://dx.doi.org/10.1071/RD9960485>
- Uchiyama S, Fukui K. Condensin in Chromatid Cohesion and Segregation. *Cytogenet Genome Res* 2015; 147:212-16; PMID:26998746; <http://dx.doi.org/10.1159/000444868>
- Revenkova E, Eijpe M, Heyting C. Cohesin SMC1 beta is required for meiotic chromosome dynamics, sister chromatid cohesion and DNA recombination. *Nat Cell Biol* 2004; 6(6):555-62; PMID:15146193; <http://dx.doi.org/10.1038/ncb1135>
- Biswas U, Wetzker C, Lange J. Meiotic cohesin SMC1 β provides prophase I centromeric cohesion and is required for multiple synapsis-associated functions. *Plos Genet* 2013; 9(12):e1003985; PMID:24385917; <http://dx.doi.org/10.1371/journal.pgen.1003985>
- Adelfalk C, Janschek J, Revenkova E. Cohesin SMC1 β protects telomeres in meiocytes. *J Cell Biol* 2009; 187(2):185-99; PMID:19841137; <http://dx.doi.org/10.1083/jcb.200808016>
- MacLennan M, Crichton JH, Playfoot CJ, Adams IR. Oocyte development, meiosis and aneuploidy. *Semin Cell Dev Biol* 2015; 45:68-6; PMID:26454098; <http://dx.doi.org/10.1016/j.semcdb.2015.10.005>
- Baudot A, de la Torre V, Valencia A. Mutated genes, pathways and processes in tumours. *EMBO Rep* 2010; 11:805-810; PMID:20847737; <http://dx.doi.org/10.1038/embor.2010.133>
- Yin S, Sun XF, Schatten H, Sun QY. Molecular insights into mechanisms regulating faithful chromosome separation in female meiosis. *Cell Cycle* 2008; 7:2997-05; PMID:18802407; <http://dx.doi.org/10.4161/cc.7.19.6809>
- Jordan P. Initiation of homologous chromosome pairing during meiosis. *Biochem Soc T* 2006; 34:545-49; <http://dx.doi.org/10.1042/BST0340545>
- Gruber S. Evidence that loading of cohesin onto chromosomes involves opening of its SMC hinge. *Cell* 2006; 127:523-37; PMID:17081975; <http://dx.doi.org/10.1016/j.cell.2006.08.048>
- Gutiérrez-Caballero C, Herrán Y, Sánchez-Martín M. Identification and molecular characterization of the mammalian α -kleisin RAD21L. *Cell Cycle* 2011; 10(9):1477-87; PMID:21527826; <http://dx.doi.org/10.4161/cc.10.9.15515>
- Hassold T, Hunt P. To err (meiotically) is human: the genesis of human aneuploidy. *Nat Rev Genet* 2001; 2:280-91; PMID:11283700; <http://dx.doi.org/10.1038/35066065>
- Wolstenholme J, Angell RR. Maternal age and trisomy—a unifying mechanism of formation. *Chromosoma* 2000; 109:435-38; PMID:11151672; <http://dx.doi.org/10.1007/s004120000088>
- Eichenlaub-Ritter U, Vogt E, Yin H, Gosden R. Spindles, mitochondria and redox potential in ageing oocytes. *Reprod Biomed Online* 2004; 8:45-8; PMID:14759287; [http://dx.doi.org/10.1016/S1472-6483\(10\)60497-X](http://dx.doi.org/10.1016/S1472-6483(10)60497-X)
- Hodges CA, Revenkova E, Jessberger R, Hassold TJ, Hunt PA. SMC1 β -deficient female mice provide evidence that cohesins are a missing link in age-related non-disjunction. *Nat Genet* 2005; 37:1351-55; PMID:16258540; <http://dx.doi.org/10.1038/ng1672>
- Subramanian VV, Bickel SE. Aging predisposes oocytes to meiotic non-disjunction when the cohesin subunit SMC1 is reduced. *Plos Genet* 2008; 4:e1000263; PMID:19008956; <http://dx.doi.org/10.1371/journal.pgen.1000263>
- Vogt E, Kirsch-Volders M, Parry J. Spindle formation, chromosome segregation and the spindle checkpoint in mammalian oocytes and susceptibility to meiotic error. *Mutat Res-Gen Tox En* 2008; 651(1):14-9; <http://dx.doi.org/10.1016/j.mrgentox.2007.10.015>

- [26] Tachibana-Konwalski K, Godwin J, Borsos M. Spindle assembly checkpoint of oocytes depends on a Kinetochore structure determined by Cohesin in Meiosis I. *Curr Biol* 2013; 23(24):2534-9; PMID:24291092; <http://dx.doi.org/10.1016/j.cub.2013.10.052>
- [27] Eijpe M, Offenbergh H, Jessberger R, Revenkova E, Heyting C. Meiotic cohesin REC8 marks the axial elements of rat synaptonemal complexes before cohesins SMC1beta and SMC3. *J Cell Biol* 2003; 160:657-670; PMID:12615909; <http://dx.doi.org/10.1083/jcb.200212080>
- [28] Revenkova E, Herrmann K, Adelfalk C, Jessberger R. Oocyte cohesin expression restricted to predictate stages provides full fertility and prevents aneuploidy. *Curr Biol* 2010; 20:1529-33; PMID:20817531; <http://dx.doi.org/10.1016/j.cub.2010.08.024>
- [29] Hirano T. Chromosome cohesion, condensation and separation. *Annu Rev Biochem* 2000; 69:115-44; PMID:10966455; <http://dx.doi.org/10.1146/annurev.biochem.69.1.115>
- [30] Tachibana K, Godwin J, van der Weyden L, Champion L, Kudo NR, Adams DJ, Nasmyth K. Rec8-containing cohesin maintains bivalents without turnover during the growing phase of mouse oocytes. *Gene Dev* 2010; 24: 2505-16; PMID:20971813; <http://dx.doi.org/10.1101/gad.605910>
- [31] Miell MD, Straight AF. In vitro kinetochore assembly. *Methods Mol Biol*. 2016; 1413:111-33; PMID:27193846.
- [32] Wynne DJ, Funabiki H. Kinetochore function is controlled by a phospho-dependent coexpansion of inner and outer components. *J Cell Biol* 2015; 210:899-16; PMID:26347137; <http://dx.doi.org/10.1083/jcb.201506020>
- [33] Nijenhuis W, Vallardi G, Teixeira A, Kops G J, Sauri A T. Negative feedback at kinetochores underlies a responsive spindle checkpoint signal. *Nat Cell Biol* 2014; 16:1257-64; PMID:25402682; <http://dx.doi.org/10.1038/ncb3065>
- [34] Moon HM. LIS1 controls mitosis and mitotic spindle organization via the LIS1-NDEL1-dynein complex. *Hum Mol Genet* 2014; 23:449-66; PMID:24030547; <http://dx.doi.org/10.1093/hmg/ddt436>
- [35] Walczak CE, Heald R. Mechanisms of mitotic spindle assembly and function. *Int Rev Cytol* 2008; 265:111-158; PMID:18275887
- [36] Rieder CL, Salmon ED. The vertebrate cell kinetochore and its roles during mitosis. *Trends Cell Biol* 1998; 8:310-18; PMID:9704407; [http://dx.doi.org/10.1016/S0962-8924\(98\)01299-9](http://dx.doi.org/10.1016/S0962-8924(98)01299-9)
- [37] Kleyman M, Kabeche L, Compton DA. STAG2 promotes error correction in mitosis by regulating kinetochore-microtubule attachments. *J Cell Sci* 2014; 127:4225-33; PMID:25074805; <http://dx.doi.org/10.1242/jcs.151613>
- [38] Shomper M, Lappa C, FitzHarris G. Kinetochore microtubule establishment is defective in oocytes from aged mice. *Cell Cycle* 2014; 13:1171-79; PMID:24553117; <http://dx.doi.org/10.4161/cc.28046>



Cullin9 protects mouse eggs from aneuploidy by controlling microtubule dynamics via Survivin



Xiaoxin Dai, Mianqun Zhang, Yajuan Lu, Yilong Miao, Changyin Zhou, Bo Xiong*

College of Animal Science and Technology, Nanjing Agricultural University, Nanjing 210095, China

ARTICLE INFO

Article history:

Received 13 July 2016

Received in revised form 20 September 2016

Accepted 22 September 2016

Available online 24 September 2016

Keywords:

Cullin9

Spindle assembly

Chromosome alignment

Aneuploid eggs

Microtubule dynamics

Survivin

Mouse oocytes

ABSTRACT

The *Cullin9* gene encodes a putative E3 ligase that serves a wide variety of biological functions in mitosis, whereas its roles in meiosis have not yet clearly defined. Here, we report that Cullin9 accumulates on the spindle apparatus and colocalizes with the microtubule fibers during mouse oocyte meiotic maturation. Depletion of Cullin9 by morpholino microinjection results in a remarkably higher rate of disorganized spindles and misaligned chromosomes in oocytes, which is coupled with the impaired kinetochore-microtubule attachments. Resultantly, the incidence of aneuploid eggs significantly increases in Cullin9-depleted oocytes. Moreover, we show that Cullin9 controls Survivin's protein level during meiotic maturation, and thus regulates microtubule stability in oocytes. Thus, our study assigns a new meiotic function to Cullin9 and reveals that it prevents mouse eggs from aneuploidy by regulating microtubule dynamics via Survivin.

© 2016 Elsevier B.V. All rights reserved.

1. Introduction

Accurate chromosome segregation ensures proper distribution of genetic material during mitosis and meiosis [1]. In mammals, an oocyte undergoes two rounds of asymmetric division called meiosis I and meiosis II to generate a haploid gamete. During meiosis I, homologous chromosomes are pulled apart by microtubules emanating from opposite spindle poles that attach to kinetochores, a large protein-based structure that are assembled onto the centromere of each chromosome. Subsequently, during meiosis II, the sister chromatids are separated through proper kinetochore-microtubule attachments [2]. Any errors in this consecutive process will lead to aneuploid eggs which in turn lead to miscarriages, birth defects and genetic disorders [3–5].

In both mitosis and meiosis, microtubules, as the essential cytoskeletal polymers, are composed of α -tubulin and β -tubulin dimers that exhibit a highly dynamic state, making alternate between periods of rapid growth and shrinkage [2,6–8]. Defects in microtubule dynamics impair diverse cellular processes such as maintenance of cell structure, protein trafficking, intracellular transport of vesicles and organelles, chromosome segregation, and cell division. The speedy reorganization of dynamic microtubule fibers is responsible for establishing a highly elegant bipolar apparatus called the spindle which functions to

accurately and precisely segregate the replicated chromosomes into two daughter cells during cell division [9]. Moreover, a surveillance mechanism, spindle assembly checkpoint (SAC), exists to inhibit the anaphase-promoting complex (APC) until all kinetochores are correctly bound to microtubules and chromosomes align on the metaphase plate [10,11], ensuring the euploidy and genome integrity in the cells.

Cullin9 (formerly PARC) is a member of evolutionarily conserved Cullin family proteins that function as scaffold proteins in the assembly of E3 ubiquitin ligases by binding to the small RING finger protein ROC1 (RBX1) [6,12]. Cullin9 contains multiple functional domains and has been shown to act as a tumor suppressor. Cullin9 knockout cells showed an remarkable increase in aneuploidy in hepatocytes and thymocytes [13], and genetic ablation of Cullin9 in mice promoted spontaneous tumor development via p53-dependent apoptosis [6,12]. In addition, a recent report has demonstrated that Cullin9 is a key regulator in the maintenance of microtubule dynamics and genome integrity by ubiquitinating and degrading Survivin (BIRC5) [7].

Survivin belongs to the inhibitor of apoptosis protein (IAP) family and is also a component of the chromosomal passenger complex (CPC) functioning in bipolar spindle formation, kinetochore-microtubule attachments, and cytokinesis to maintain the genome stability [14]. Reduction or loss of Survivin markedly increases the occurrence of abnormal centrosomes [15], aberrant spindle assembly [16], inactivation of spindle assembly checkpoints [17], and cytokinesis failure [15] in mammalian cells. In meiosis, both depletion and overexpression of Survivin leads to the defects in kinetochore-microtubule attachments and chromosome alignment [18].

* Corresponding author at: College of Animal Science and Technology, Nanjing Agricultural University, Nanjing, China.

E-mail address: xiongbo@njau.edu.cn (B. Xiong).

Although Cullin9 plays important roles in multiple critical biological processes in mitosis, its functions in oocyte meiosis have not yet been explored. In the present study, we provide the data showing that Cullin9 localizes on the microtubule fibers to control the microtubule stability, and thereby regulates spindle assembly and chromosome alignment to prevent aneuploidy during mouse oocyte meiotic maturation. Also, Survivin might act as a downstream effector of Cullin9 to mediate these events.

2. Materials and methods

2.1. Antibodies

Rabbit polyclonal *anti*-PARC/H7-AP1(Cullin9) antibody was purchased from Bethyl Laboratories (Montgomery, TX, USA; Cat#: A300-098A-T); mouse monoclonal *anti*-Survivin antibody was purchased from Cell Signaling Technology (Beverly, MA, USA; Cat#: 2808p); mouse monoclonal *anti*- α -tubulin-fluorescein isothiocyanate (FITC) antibody and mouse monoclonal *anti*-acetyl-tubulin (Lys-40) antibody were purchased from Sigma (St. Louis, MO, USA; Cat#: F2168 and T7451); human anti-centromere antibody was purchased from Antibodies Incorporated (Davis, CA, USA; Cat#: 15–234); FITC-conjugated goat *anti*-rabbit IgG (H + L), TRITC-conjugated goat anti-rabbit IgG (H + L) and TRITC-conjugated goat anti-mouse IgG (H + L) were purchased from Zhongshan Golden Bridge Biotechnology Co., LTD (Beijing, China).

2.2. Oocyte collection and culture

Animal care and use were conducted in accordance with the Animal Research Committee guidelines of Nanjing Agricultural University, China.

Female mice (4–6 weeks) were sacrificed by cervical dislocation. Oocytes were harvested from ovaries, and only those oocytes displaying a germinal vesicle (GV) were cultured further in M16 medium covered with liquid paraffin oil at 37 °C in an atmosphere of 5% CO₂ in air. At different time points after culture, oocytes were collected for subsequent analysis.

2.3. Morpholino knockdown and cRNA construct

For knockdown experiments, GV oocytes were microinjected with 5–10 μ l of non-targeting or Cullin9-targeting morpholinos (Gene tools, Philomath, OR, USA) in M2 medium containing 2.5 μ M milrinone. Cullin9 morpholino sequence: 5'-ACGCCGTCCCTACCATCTGATC-3' (Gene Tools, Philomath, OR, USA). The working concentration of morpholinos was 1 mM. To facilitate the inhibition of mRNA translation by morpholinos, microinjected oocytes were arrested at GV stage in M16 medium containing 2.5 μ M milrinone for 20 h, followed by washing 4 times in milrinone-free M2 medium, and then transferred to milrinone-free M16 medium to resume the meiosis for further experiments.

For overexpression experiments, full-length of Cullin9 cDNAs were inserted into the pcDNA3.1 vector (Addgene, Cambridge, MA, USA). Capped cRNAs were synthesized from linearized plasmid using T7 mMessage mMachine kit (ThermoFisher, Waltham, MA, USA), and purified with RNA purification kit (Tiangen Biotech, Beijing, China). Typically, 10–12 μ l (4% of the oocyte volume) of 1 μ g/ μ l cRNA was injected into oocytes.

2.4. Immunofluorescent analysis and confocal microscopy

Oocytes were fixed in 4% paraformaldehyde in PBS (pH 7.4) for 30 min and permeabilized in 0.5% Triton-X-100 for 20 min at room temperature. Then, oocytes were blocked with 1% BSA-supplemented PBS for 1 h and incubated overnight at 4 °C or for 4 h at room temperature with *anti*-Cullin9 (1:50), *anti*-acetyl-tubulin (Lys-40) (1:100), *anti*- α -

tubulin-FITC (1:300), or *anti*-centromere (1:200) antibodies. After washing four times (5 min each) in PBS containing 1% Tween 20 and 0.01% Triton- \times 100, oocytes were incubated with an appropriate secondary antibody for 1 h at room temperature. After washing four times, oocytes were counterstained with PI (Propidium Iodide) or Hoechst 33342 (10 μ g/ml) for 10 min. Finally, oocytes were mounted on glass slides and observed under a confocal laser scanning microscope (Carl Zeiss 700).

For measurement of immunofluorescent intensity, the signals from both control and experimental oocytes were acquired by performing the same immunostaining procedure and setting up the same parameters of confocal microscope. Data were analyzed by Image J software.

2.5. Chromosome spread

MII eggs were treated with 1% sodium citrate for 20 min, individually transferred to a glass slide, and then fixed with several drops of 3 parts methanol to 1 part acetic acid. After air drying, chromosomes were counterstained with PI and examined under a laser scanning confocal microscope.

2.6. Nocodazole treatment of oocytes

For nocodazole treatment, 10 mM nocodazole in DMSO stock was diluted in M2 medium to give a final concentration of 10 μ M. Oocytes at MI stage were transferred to the medium containing nocodazole for 10 min, followed by washing 3 times in nocodazole-free medium, and then used for immunofluorescent analysis. In controls, oocytes were cultured in M2 medium containing the same concentration of DMSO for 10 min and then washed 3 times in nocodazole-free medium, followed by immunofluorescent analysis.

2.7. Western blotting

A pool of 250 oocytes was lysed in 4 \times LDS sample buffer (ThermoFisher, Waltham, MA, USA) containing protease inhibitor and heated at 95 °C for 5 min. Proteins were separated on 10% Bis-Tris precast gels and transferred to PVDF membranes. The blots were blocked in TBST (TBS containing 0.1% Tween 20) containing 5% nonfat milk for 1 h at room temperature, followed by incubation overnight at 4 °C with the rabbit *anti*-Cullin9 antibody (1:1000), mouse *anti*-Survivin antibody (1:1000), or mouse *anti*-tubulin antibody (1:1000). After washing 3 times in TBST, the blots were incubated with a 1:10,000 dilution of HRP (Horse Radish Peroxidase) conjugated secondary antibodies for 1 h at room temperature. Chemiluminescence was detected with ECL Plus (Pierce, Rockford, IL, USA) and signals were acquired by Tanon-3900.

2.8. Statistical analysis

The data were given as mean \pm SEM and analyzed by one-way ANOVA followed by Duncan's multiple comparisons test. A value of $p < 0.05$ was considered as significance.

3. Results

3.1. Cullin9 localizes on the spindle fibers during mouse oocyte meiotic maturation

We firstly examined the subcellular localization of Cullin9 at different developmental stages of mouse oocytes by immunofluorescent staining. As shown in Fig. 1A, Cullin9 was mainly concentrated in the germinal vesicle in GV oocytes. After GVBD, Cullin9 distributed around the chromosomes at prometaphase I stage and then exhibited spindle-like localization at metaphase I and metaphase II stages. At anaphase I/telophase I stage it accumulated to the midzone of the

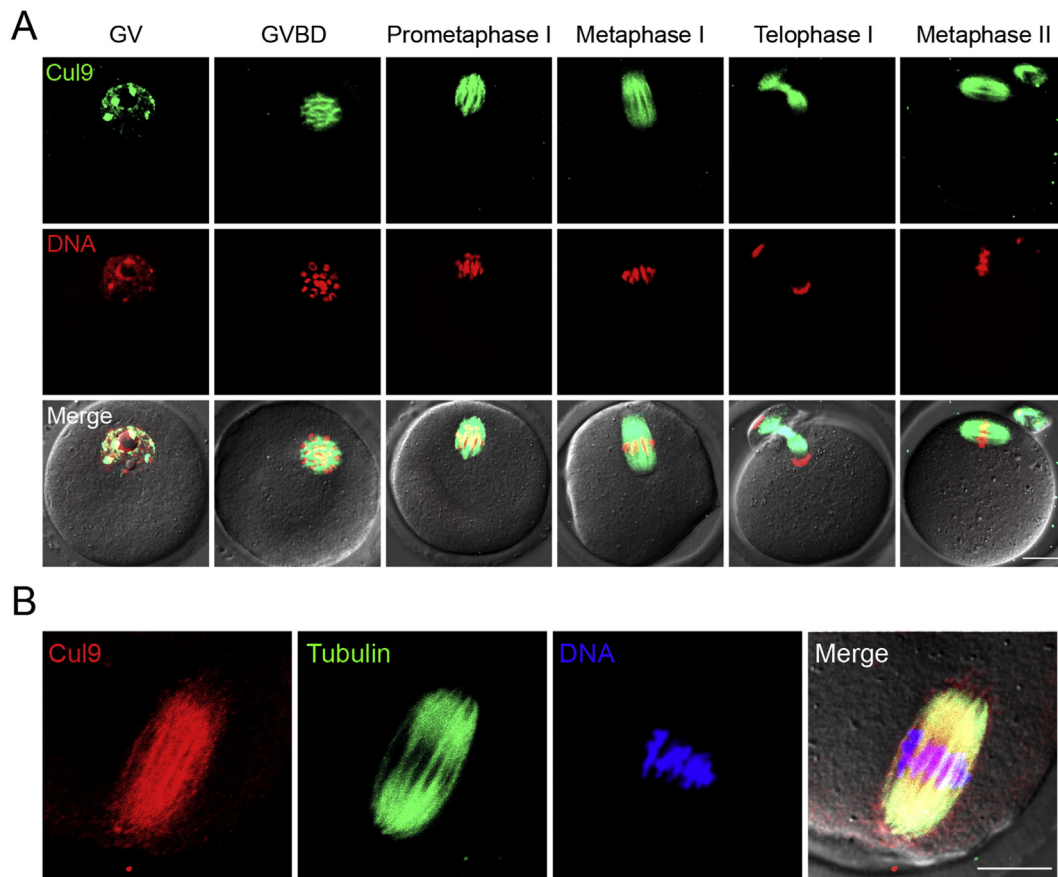


Fig. 1. Subcellular localization of Cullin9 during mouse oocyte meiotic maturation. (A) Mouse oocytes at various developmental stages were immunostained with *anti*-Cullin9 antibody and counterstained with PI for chromosomes. GV, oocytes at germinal vesicle stage; GVBD, oocytes at germinal vesicle breakdown stage. Scale bar, 20 μ m. (B) Double staining of Cullin9 and microtubules in metaphase I oocytes. Red, Cullin9; Green, α -tubulin; Blue, chromosomes. Scale bar, 20 μ m.

spindle. These spindle-like localization patterns of Cullin9 prompted us to further determine its relationship with spindles, we thus co-stained Cullin9 with microtubule component α -tubulin in metaphase I oocytes. Double staining result showed that the signals of Cullin9 and α -tubulin were completely overlapped (Fig. 1B), confirming the localization of Cullin9 on spindle fibers.

3.2. Cullin9 is required for normal spindle assembly and proper chromosome alignment in oocytes

The spindle localization of Cullin9 predicts its possible function in spindle organization and chromosome alignment. We then employed the microinjection of gene-targeting morpholino (Cullin9 MO) to carry out the loss-of-function experiment. After microinjection, oocytes were arrested at the GV stage for 20 h to allow enough time to deplete the endogenous Cullin9, and then oocytes were cultured to the metaphase I stage to analyze the spindle morphology and chromosome alignment. Immunofluorescent staining results showed that most of control oocytes exhibited a normal barrel-shape spindle with a well-aligned chromosome on the equatorial plate (Fig. 2A). By contrast, various types of abnormal spindle morphologies including elongated, multipolar and nonpolar spindles with misaligned chromosomes were observed in Cullin9-depleted oocytes (Fig. 2A). In control oocytes, the rates of aberrant spindles and misaligned chromosomes were $17.94\% \pm 1.91\%$ and $19.24\% \pm 2.56\%$ ($n = 109$), respectively, whereas increased to $47.13\% \pm 3.42\%$ and $51.99\% \pm 0.75\%$ ($n = 118$), respectively, in Cullin9-depleted oocytes ($p < 0.05$; Fig. 2B, C).

3.3. Cullin9 is required for correct kinetochore-microtubule attachments in oocytes

The disrupted spindle assembly and chromosome alignment are always related to the impaired interaction between kinetochores and microtubules. To assess the stability of kinetochore-microtubule attachments, we employed cold treatment to depolymerize the unstable microtubules that are not attached to kinetochores. Metaphase I oocytes were briefly chilled to induce depolymerization of unstable microtubules, and then immunolabeled with CREST to detect kinetochores, with *anti*-tubulin-FITC antibody to visualize the spindles and counterstained with Hoechst for chromosomes. Immunofluorescent analysis showed that in most of control oocytes kinetochores at the well-aligned chromosome remained fully attached by the spindle fibers after cold treatment, and the rate of defective kinetochore-microtubule attachments was quite low ($10.42\% \pm 2.09\%$, $n = 45$; Fig. 3A, B). However, in Cullin9-depleted oocytes, a significantly increased proportion of scattered kinetochores with very few cold-stable microtubules was observed ($27.25\% \pm 0.93\%$, $n = 37$; Fig. 3A, B). Therefore, these data suggest that Cullin9 contributes to the stable formation of kinetochore-microtubule attachments during oocyte meiosis.

3.4. Cullin9 is required for maintenance of euploidy in oocytes

We next tested whether chromosome misalignment in Cullin9-depleted oocytes would produce aneuploid eggs. We then analyzed the karyotype of MII eggs by chromosome spreading. As shown in

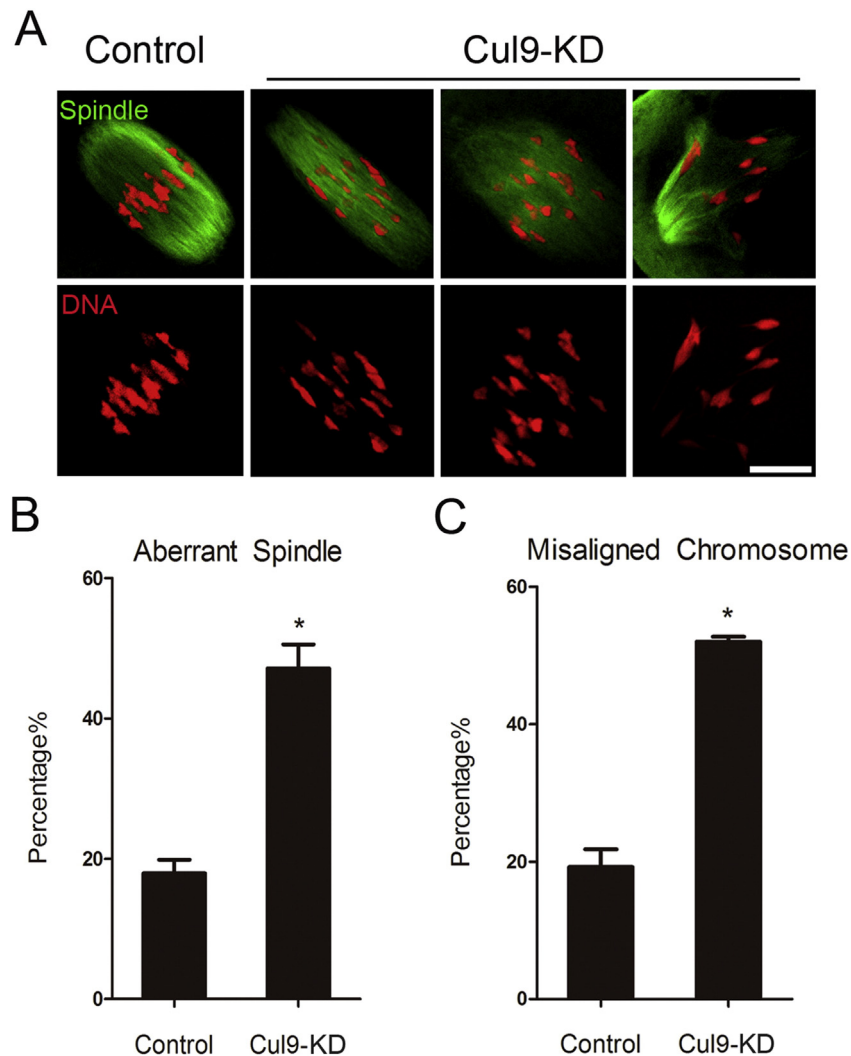


Fig. 2. Depletion of Cullin9 impairs Spindle assembly and chromosome alignment in mouse oocytes. (A) Representative images of spindle morphologies and chromosome alignment in control and Cullin9-KD (Cullin9-MO injected) oocytes. Green, tubulin; Red, DNA. Scale bar, 10 μ m. (B) The rate of aberrant spindles in control and Cullin9-KD oocytes was recorded. Data were presented as mean percentage (mean \pm SEM) of at least three independent experiments. Asterisk denotes significant difference ($p < 0.05$). (C) The rate of misaligned chromosomes in control and Cullin9-KD oocytes was recorded. Data were presented as mean percentage (mean \pm SEM) of at least three independent experiments. Asterisk denotes significant difference ($p < 0.05$).

Fig. 4A, a large majority of control oocytes had 20 univalents to maintain the euploidy. In striking contrast, the incidence of aneuploid eggs that had more or less 20 univalents in Cullin9-depleted oocytes ($42.78\% \pm 3.08\%$, $n = 42$) was much higher than that in controls ($14.39\% \pm 3.08\%$, $n = 35$, $p < 0.05$), suggesting that Cullin9 is required to prevent aneuploidy in oocytes (Fig. 4B). To rule out the possibility that the occurrence of aneuploidy was caused by the off-target effects of morpholinos, we injected *Cullin9* cRNA in Cullin9-depleted oocytes to observe the rescue phenotype. As expected, the karyotyping result showed that the rate of aneuploidy in rescue oocytes ($16.24\% \pm 1.95\%$, $n = 29$) was reduced to the normal level comparable to controls (Fig. 4B).

3.5. Cullin9 maintains acetylation level of α -tubulin and microtubule stability via Survivin in oocytes

Because Cullin9 is an E3 ligase that promotes the ubiquitylation and degradation of Survivin in somatic cells, we attempted to determine whether this is conserved in oocyte meiosis. We then examined the protein level of Survivin in Cullin9-depleted oocytes by Western blotting. The result showed that depletion of Cullin9 in oocytes substantially increased the protein level of Survivin (Fig. 5A). To rule out the possibility

that the above observation was not caused by the off-target effect of morpholinos, we microinjected Cullin9 cRNA which was transcribed in vitro to the Cullin9-depleted oocytes. The result that exogenous Cullin9 was able to reduce the increased protein level of Survivin indicates that Survivin is indeed the downstream effector of Cullin9 (Fig. 5B). In addition, knockdown of Survivin in Cullin9-depleted oocytes could restore the Survivin's protein level comparable to controls (Fig. 5B), suggesting that Cullin9 could at least suppress Survivin's protein level, although we did not have direct evidence showing that Cullin9 is able to ubiquitinate and degrade Survivin in mouse oocytes.

Survivin has been reported to regulate microtubule dynamics in both mitosis and meiosis, we thus reasoned that Cullin9 would be also involved in this event in oocytes. We first examined the state of acetylated α -tubulin, a post-translationally modified tubulin found in stabilized microtubules, using anti-acetylated α -tubulin antibody. The Cullin9-depleted oocytes showed a significant increase in the fluorescence intensity of acetylated tubulin compared to control oocytes (87.67 ± 3.93 , $n = 46$ VS 71.69 ± 4.69 , $n = 54$, $p < 0.05$; Fig. 6A, B), suggesting that the microtubule is over-stabilized in the absence of Cullin9. Whereas knockdown of Survivin in Cullin9-depleted oocytes restored the acetylation level of α -tubulin comparable to controls (68.45 ± 3.99 , $n = 45$; Fig. 6A, B), indicating that Survivin is the

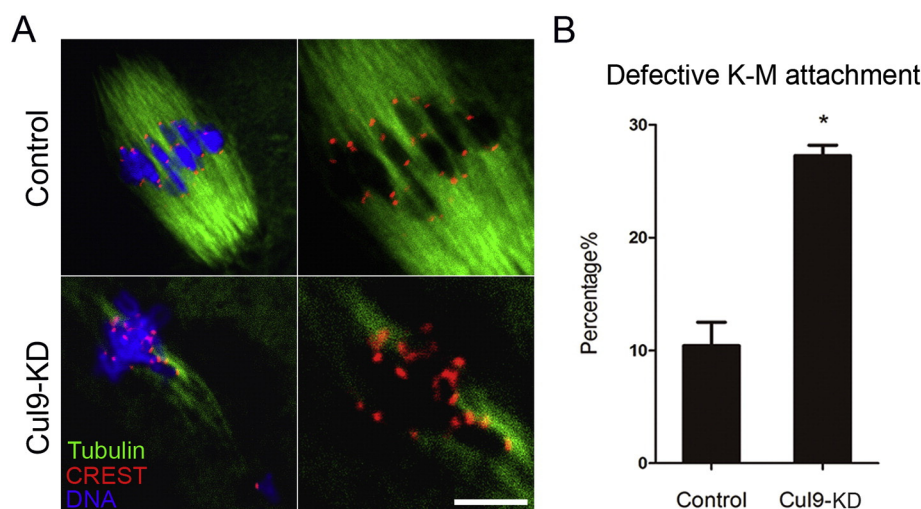


Fig. 3. Depletion of Cullin9 compromises kinetochore-microtubule attachments in mouse oocytes. (A) Representative images of normal and abnormal kinetochore-microtubule attachments in control and Cullin9-KD oocytes. Metaphase I oocytes were chilled at 4 °C for 15 min to depolymerize the unstable microtubules and then immunostained with α -tubulin-FITC antibody to visualize spindles (green), with CREST to detect kinetochores (red) and counterstained with Hoechst 33342 to observe chromosomes (blue). Scale bar, 10 μ m. (B) The rate of defective kinetochore-microtubule attachments was recorded in control and Cullin9-KD oocytes. Data were presented as mean percentage (mean \pm SEM) of at least three independent experiments. Asterisk denotes significant difference ($p < 0.05$).

downstream molecule that mediates the function of Cullin9 in this process. Collectively, the hyperacetylation of α -tubulin when depleted of Cullin9 shows the over-stabilization of microtubules, which thereby would disrupt microtubule dynamics, spindle organization and chromosome segregation.

To further confirm the role of Cullin9 in regulation of microtubule stability, the resistance of microtubules in oocytes to the microtubule depolymerizing drug nocodazole was tested. In controls, 10 min after nocodazole treatment, spindle apparatus was collapsed and microtubules were completely depolymerized (Fig. 6C). By contrast, although spindle was not observed, microtubules persisted at this time in Cullin9-depleted oocytes, showing the enhanced microtubule stability in these oocytes (Fig. 6C). Moreover, when co-depleted of Cullin9 and Survivin, the resistance of microtubules to nocodazole restored to the normal level as controls (Fig. 6C). Finally, we assessed the incidence of aneuploid eggs when knockdown of Survivin in Cullin9-depleted oocytes, and the rate of aneuploidy also restored to control levels

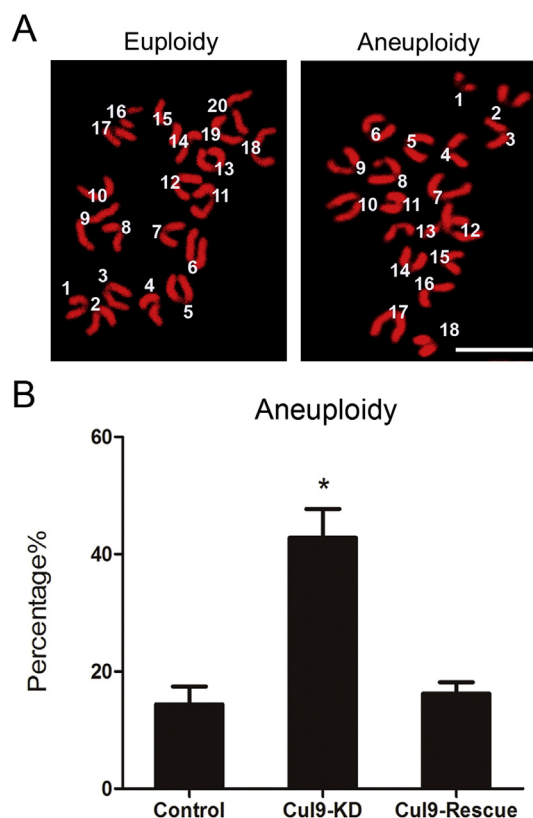


Fig. 4. Depletion of Cullin9 generates aneuploidy in mouse oocytes. (A) Representative images of euploid and aneuploid eggs in control, Cullin9-KD and Cullin9-rescue oocytes. Chromosome spreading was performed to count the number of chromosomes. Chromosomes were counterstained with PI. Scale bar, 5 μ m. (B) The rate of aneuploid eggs was recorded in control, Cullin9-KD and Cullin9-rescue oocytes. Data were presented as mean percentage (mean \pm SEM) of at least three independent experiments. Asterisk denotes significant difference ($p < 0.05$).

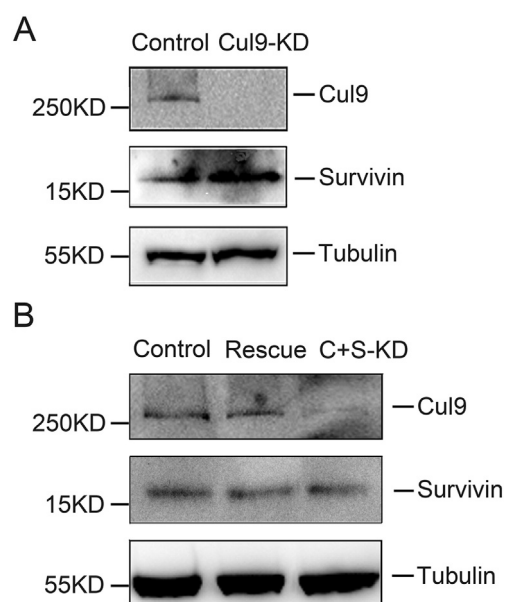


Fig. 5. Protein levels of Cullin9 and Survivin in Cullin9 and/or Survivin knockdown oocytes. (A) Protein levels of Cullin9, Survivin and tubulin in control and Cullin9-KD oocytes were determined by Western blotting. (B) Protein levels of Cullin9, Survivin and tubulin in control, Cullin9-rescue and Cullin9/Survivin-KD (Cullin9-MO/Survivin siRNA co-injected) oocytes were determined by Western blotting. The blots were probed with anti-Cullin9, anti-Survivin and anti-tubulin antibodies, respectively. The molecular weights of Cullin9, Survivin and tubulin are 282 kDa, 16 kDa and 55 kDa, respectively.

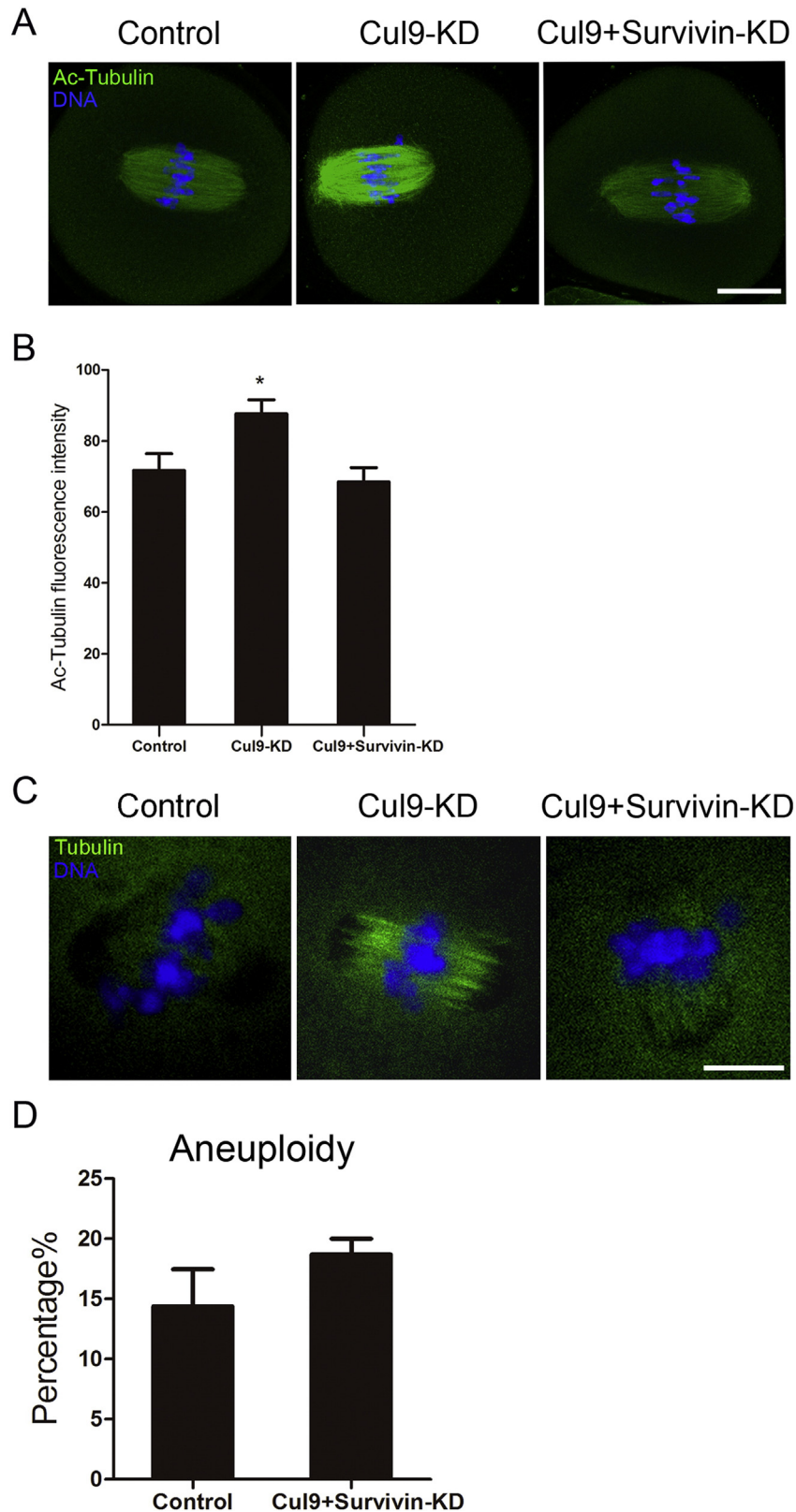


Fig. 6. Depletion of Cullin9 over-stabilizes microtubules. (A) Representative images of acetylated-tubulin in control, Cullin9-KD and Cullin9/Survivin-KD oocytes. Oocytes were immunolabeled with anti-acetylated α -tubulin antibody (green) and counterstained with Hoechst 33342 (blue). Scale bar, 20 μ m. (B) Quantitative analysis of acetylated α -tubulin fluorescence intensity in control, Cullin9-KD and Cullin9/Survivin-KD oocytes. Data were presented as mean percentage (mean \pm SEM) of at least three independent experiments. Asterisk denotes significant difference ($p < 0.05$). (C) The resistance of microtubules to the microtubule depolymerizing drug in mouse oocytes. After treatment in medium containing nocodazole for 10 min, control, Cullin9-KD and Cullin9/Survivin-KD MI oocytes were immunostained with α -tubulin-FITC antibody to visualize microtubules (green) and counterstained with Hoechst 33342 to observe chromosomes (blue). Scar bar, 10 μ m. (D) The rate of aneuploid eggs was recorded in control and Cullin9/Survivin-KD oocytes. Data were presented as mean percentage (mean \pm SEM) of at least three independent experiments.

(14.39% \pm 3.08%, n = 35 VS 18.70% \pm 1.31%, n = 38, Fig. 6D). Taken together, these results demonstrate that Survivin acts as a downstream effector of Cullin9 to regulate the microtubule stability and ensure euploidy during mouse oocyte meiosis.

4. Discussion

Previous studies in mitotic cells have shown that Cullin9 binds with p53 and is ubiquitously localized in the cytoplasm [12]. In our data, the immunofluorescent results show that Cullin9 is concentrated on the spindle and colocalized with microtubule fibers during oocyte meiosis, which predicts that Cullin9 might play a unique role in regulation of microtubule dynamics and spindle organization. This prediction is consistent with a recent report showing that Cullin9 is a critical downstream effector of the 3 M complex in the maintenance of microtubule and genome integrity in mitosis. Thus, to examine the specific functions of Cullin9 during mouse oocyte meiotic maturation, we employed morpholino-based gene-silencing approach to perturb Cullin9 expression in the protein level. As expected, depletion of Cullin9 resulted in a higher incidence of severely aberrant spindles and misaligned chromosomes with unattached kinetochores in MI oocytes, resultantly leading to aneuploidy in MII eggs.

The regulation of Cullin9 in the spindle assembly further prompted us to test its possible roles in microtubule dynamics. Tubulin acetylation is a post-translational modification that occurs on Lys-40 of the α -tubulin subunit [19,20]. Acetylated α -tubulin is abundant in stable microtubules but is absent in dynamic subcellular structures [21]. Recent studies have shown that acetylation of α -tubulin is involved in microtubule organization in nematode touch receptor neurons [22,23] and in the regulation of microtubule stability [20,24]. Also, acetylated α -tubulin is found in stabilized microtubules in mouse oocytes [25, 26]. Thus we detected acetylated α -tubulin as the indicator of microtubule stability in Cullin9-depleted oocytes. As our results revealed that the acetylation level of α -tubulin is significantly increased when depleted of Cullin9, indicating that microtubules are over-stabilized and lose the dynamics in this case, which might be the leading cause resulting in the defective spindle assembly we observed before. Another line of evidence we presented to confirm that microtubules are over-stabilized in Cullin9-depleted oocytes is their notably elevated resistance ability of microtubules to microtubule depolymerizing drug nocodazole. The microtubule fibers still persist in Cullin9-depleted oocytes following period of treatment with nocodazole, while they completely disappear in controls. Collectively, we demonstrate from different aspects that Cullin9 plays an important role in maintaining microtubule stability to ensure the normal spindle organization.

A recent report has proposed a 3 M-Cullin9-Survivin pathway in maintaining microtubule and genome integrity and verified that Cullin9 is an E3 ligase of Survivin for its ubiquitination [7]. Survivin shows multiple functions in various biological processes including inhibition of apoptosis and regulation of chromosome segregation, spindle formation, spindle checkpoint and cell division [27,28]. More importantly, Survivin has been reported to modulate microtubule dynamics and nucleation to exert microtubule-based functions [29]. In human RPE-1 cells depleted of Survivin, the decreased level of acetylated tubulin reveals the role of Survivin in regulation of microtubule stability [29]. To confirm whether Survivin is a downstream effector to mediate the functions of Cullin9 in meiotic cells, we detected the protein level of Survivin in Cullin9-depleted oocytes. In agreement with the findings in mitotic cells, Survivin protein level increases a lot in the absence of Cullin9. Additionally, inhibition of Survivin in Cullin9-depleted oocytes is able to, at least partially, rescue the phenotypes of over-stabilized microtubules and aneuploidy, suggesting that the relationship of Cullin9 and Survivin in regulation of microtubule dynamics is conserved between mitosis and meiosis.

In the present study, we investigate the localization and potential functions of Cullin9 during mouse oocyte meiotic maturation. We find

that Cullin9 is required for normal spindle assembly and proper chromosome alignment by controlling microtubule stability to maintain the euploidy in mouse eggs. Moreover, we discover that Cullin9 promotes these events by suppressing the protein level of Survivin in oocytes.

Conflicts of interest

The authors have no conflicts of interest to disclose.

The authors declare that they have no competing interests.

Transparency document

The [Transparency document](#) associated with this article can be found, in the online version.

Acknowledgements

This work was supported by the National Natural Science Foundation of China (31571545) and the Natural Science Foundation of Jiangsu Province (BK20150677).

References

- [1] S. Yin, X.F. Sun, H. Schatten, Q.Y. Sun, Molecular insights into mechanisms regulating faithful chromosome separation in female meiosis, *Cell Cycle* 7 (2008) 2997–3005.
- [2] A.F. Severson, G. von Dassow, B. Bowerman, Oocyte meiotic spindle assembly and function, *Curr. Top. Dev. Biol.* 116 (2016) 65–98.
- [3] S. Matsuura, E. Ito, H. Tauchi, K. Komatsu, T. Ikeuchi, T. Kajii, Chromosomal instability syndrome of total premature chromatid separation with mosaic variegated aneuploidy is defective in mitotic-spindle checkpoint, *Am. J. Hum. Genet.* 67 (2000) 483–486.
- [4] L.H. Hartwell, M.B. Kastan, Cell cycle control and cancer, *Science* 266 (1994) 1821–1828.
- [5] N.J. Ganem, Z. Storchova, D. Pellman, Tetraploidy, aneuploidy and cancer, *Curr. Opin. Genet. Dev.* 17 (2007) 157–162.
- [6] Z. Li, X.H. Pei, J. Yan, F. Yan, K.M. Cappell, A.W. Whitehurst, Y. Xiong, CUL9 mediates the functions of the 3 M complex and ubiquitylates Survivin to maintain genome integrity, *Mol. Cell* 54 (2014) 805–819.
- [7] S.L. Kline-Smith, C.E. Walczak, Mitotic spindle assembly and chromosome segregation: refocusing on microtubule dynamics, *Mol. Cell* 15 (2004) 317–327.
- [8] H.Y. Kueh, T.J. Mitchison, Structural plasticity in actin and tubulin polymer dynamics, *Science* 325 (2009) 960–963.
- [9] E. Logarinho, T. Resende, C. Torres, H. Bousbaa, The human spindle assembly checkpoint protein Bub3 is required for the establishment of efficient kinetochore-microtubule attachments, *Mol. Biol. Cell* 19 (2008) 1798–1813.
- [10] A. Musacchio, E.D. Salmon, The spindle-assembly checkpoint in space and time, *Nat. Rev. Mol. Cell Biol.* 8 (2007) 379–393.
- [11] J. Yan, F. Yan, Z. Li, B. Sinnott, K.M. Cappell, Y. Yu, J. Mo, J.A. Duncan, X. Chen, V. Cormier-Daire, A.W. Whitehurst, Y. Xiong, The 3 M complex maintains microtubule and genome integrity, *Mol. Cell* 54 (2014) 791–804.
- [12] X.H. Pei, F. Bai, Z. Li, M.D. Smith, G. Whitewolf, R. Jin, Y. Xiong, Cytoplasmic CUL9/ PARC ubiquitin ligase is a tumor suppressor and promotes p53-dependent apoptosis, *Cancer Res.* 71 (2011) 2969–2977.
- [13] P.K. Jackson, Regulating microtubules and genome stability via the CUL7/3 M syndrome complex and CUL9, *Mol. Cell* 54 (2014) 713–715.
- [14] Y. Watanabe, Temporal and spatial regulation of targeting aurora B to the inner centromere, *Cold Spring Harb. Symp. Quant. Biol.* 75 (2010) 419–423.
- [15] F. Li, E.J. Ackermann, C.F. Bennett, A.L. Rothermel, J. Plescia, S. Tognin, A. Villa, P.C. Marchisio, D.C. Altieri, Pleiotropic cell-division defects and apoptosis induced by interference with Survivin function, *Nat. Cell Biol.* 1 (1999) 461–466.
- [16] A. Giodini, M.J. Kallio, N.R. Wall, G.J. Gorbosky, S. Tognin, P.C. Marchisio, M. Symons, D.C. Altieri, Regulation of microtubule stability and mitotic progression by Survivin, *Cancer Res.* 62 (2002) 2462–2467.
- [17] S.M. Lens, R.M. Wolthuis, R. Klompmaier, J. Kauw, R. Agami, T. Brummelkamp, G. Kops, R.H. Medema, Survivin is required for a sustained spindle checkpoint arrest in response to lack of tension, *EMBO J.* 22 (2003) 2934–2947.
- [18] S.C. Sun, L. Wei, M. Li, S.L. Lin, B.Z. Xu, X.W. Liang, N.H. Kim, H. Schatten, S.S. Lu, Q.Y. Sun, Perturbation of Survivin expression affects chromosome alignment and spindle checkpoint in mouse oocyte meiotic maturation, *Cell Cycle* 8 (2009) 3365–3372.
- [19] J.C. Bulinski, J.E. Richards, G. Piperno, Posttranslational modifications of alpha tubulin: deetyrosination and acetylation differentiate populations of interphase microtubules in cultured cells, *J. Cell Biol.* 106 (1988) 1213–1220.
- [20] G. Piperno, M. LeDizet, X.J. Chang, Microtubules containing acetylated alpha-tubulin in mammalian cells in culture, *J. Cell Biol.* 104 (1987) 289–302.
- [21] S.J. Robson, R.D. Burgoyne, Differential localisation of tyrosinated, deetyrosinated, and acetylated alpha-tubulins in neurites and growth cones of dorsal root ganglion neurons, *Cell Motil. Cytoskeleton* 12 (1989) 273–282.

- [22] J.G. Cueva, J. Hsin, K.C. Huang, M.B. Goodman, Posttranslational acetylation of alpha-tubulin constrains protofilament number in native microtubules, *Curr. Biol.* 22 (2012) 1066–1074.
- [23] I. Topalidou, C. Keller, N. Kalebic, K.C. Nguyen, H. Somhegyi, K.A. Politi, P. Heppenstall, D.H. Hall, M. Chalfie, Genetically separable functions of the MEC-17 tubulin acetyltransferase affect microtubule organization, *Curr. Biol.* 22 (2012) 1057–1065.
- [24] L. Zhang, X. Hou, R. Ma, K. Moley, T. Schedl, Q. Wang, Sirt2 functions in spindle organization and chromosome alignment in mouse oocyte meiosis, *FASEB J.* 28 (2014) 1435–1445.
- [25] H. de Pennart, E. Houlston, B. Maro, Post-translational modifications of tubulin and the dynamics of microtubules in mouse oocytes and zygotes, *Biol. Cell.* 64 (1988) 375–378.
- [26] G. Schatten, C. Simerly, D.J. Asai, E. Szoke, P. Cooke, H. Schatten, Acetylated alpha-tubulin in microtubules during mouse fertilization and early development, *Dev. Biol.* 130 (1988) 74–86.
- [27] D.C. Altieri, The case for Survivin as a regulator of microtubule dynamics and cell-death decisions, *Curr. Opin. Cell Biol.* 18 (2006) 609–615.
- [28] S.M. Lens, G. Vader, R.H. Medema, The case for Survivin as mitotic regulator, *Curr. Opin. Cell Biol.* 18 (2006) 616–622.
- [29] J. Rosa, P. Canovas, A. Islam, D.C. Altieri, S.J. Doxsey, Survivin modulates microtubule dynamics and nucleation throughout the cell cycle, *Mol. Biol. Cell* 17 (2006) 1483–1493.



项目批准号	31571545
申请代码	C120202
归口管理部门	
依托单位代码	21009508A1649-1247



3 15715 45 1008 104

国家自然科学基金委员会 资助项目计划书

资助类别：面上项目

亚类说明：

附注说明：常规面上项目

项目名称：利用Ovastacin-mCherry转基因小鼠研究哺乳动物皮质颗粒的动态转运及调控机理

直接费用：60万元 间接费用：11.6万元

项目资金：71.6万元 执行年限：2016.01-2019.12

负责人：熊波

通讯地址：南京农业大学动物科技学院

邮政编码： 电 话：025-84399605

电子邮件：xiongbo@njau.edu.cn

依托单位：南京农业大学

联系人：张红霞 电 话：025-84395725

填表日期：2015年08月21日

国家自然科学基金委员会制

Version: 1.008.104



国家自然科学基金委员会资助项目计划书填报说明

- 一、项目负责人收到《关于国家自然科学基金资助项目批准及有关事项的通知》（以下简称《批准通知》）后，请认真阅读本填报说明，参照国家自然科学基金相关项目管理办法及《国家自然科学基金资助项目资金管理办法》（请查阅国家自然科学基金委员会官方网站首页“政策法规”-“管理办法”栏目），按《批准通知》的要求认真填写和提交《国家自然科学基金委员会资助项目计划书》（以下简称《计划书》）。
- 二、填写《计划书》时要求科学严谨、实事求是、表述清晰、准确。《计划书》经国家自然科学基金委员会相关项目管理部门审核批准后，将作为项目研究计划执行和检查、验收的依据。
- 三、《计划书》各部分填写要求如下：
 - （一）简表：由系统自动生成。
 - （二）摘要及关键词：各类获资助项目都必须填写中、英文摘要及关键词。
 - （三）项目组主要成员：计划书中列出姓名的项目组主要成员由系统自动生成，与申请书原成员保持一致，不可随意调整。如果批准通知中“项目评审意见及修改意见表”中“对研究方案的修改意见”栏目有调整项目组成员相关要求的，待项目开始执行后，按照项目成员变更程序另行办理。
 - （四）资金预算表：按批准资助的直接费用填报资金预算表和预算说明书，其中的劳务费、专家咨询费金额不应高于申请书中相应金额；间接费用及项目总经费由系统自动生成。国家重大科研仪器研制项目还应按照预算评审后批复的直接费用各科目金额填报资金预算表、预算说明书及相应的预算明细表。
 - （五）正文：
 1. 面上项目、青年科学基金项目、地区科学基金项目：如果《批准通知》中没有修改要求的，只需选择“研究内容和研究目标按照申请书执行”即可；如果《批准通知》中“项目评审意见及修改意见表”中“对研究方案的修改意见”栏目明确要求调整研究期限和研究内容等的，须选择“根据研究方案修改意见更改”并填报相关修改内容。
 2. 重点项目、重点国际（地区）合作研究项目、重大项目、国家重大科研仪器研制项目：须选择“根据研究方案修改意见更改”，根据《批准通知》的要求填写研究（研制）内容，不得自行降低、更改研究目标（或仪器研制的技术性能与主要技术指标以及验收技术指标）或缩减研究（研制）内容。此外，还要突出以下几点：
 - （1）研究的难点和在实施过程中可能遇到的问题（或仪器研制风险），拟采用的研究（研制）方案和技术路线；
 - （2）项目主要参与者分工，合作研究单位之间的关系与分工，重大项目还需说明课题之间的关联；
 - （3）详细的年度研究（研制）计划。



3. 国家杰出青年科学基金、优秀青年科学基金和海外及港澳学者合作研究基金项目：须选择“根据研究方案修改意见更改”，按下列提纲撰写：
 - (1) 研究方向；
 - (2) 结合国内外研究现状，说明研究工作的学术思想和科学意义（限两个页面）；
 - (3) 研究内容、研究方案及预期目标（限两个页面）；
 - (4) 年度研究计划；
 - (5) 研究队伍的组成情况。
4. 对于其他类型项目，参照面上项目的方式进行选择和填写。



简表

申请者信息	姓 名	熊波	性 别	男	出生年月	1980年05月	民 族	汉族
	学 位	博士			职称	教授		
	电 话	025-84399605		电子邮件	xiongbo@njau.edu.cn			
	传 真			个人网页				
	工 作 单 位	南京农业大学						
	所 在 院 系 所	动物科技学院						
依托单位信息	名 称	南京农业大学					代码	21009508A1649
	联 系 人	张红霞		电子邮件	kjcxm@njau.edu.cn			
	电 话	025-84395725		网站地址	http://www.njau.edu.cn			
合作单位信息	单 位 名 称							代 码
项目基本信息	项 目 名 称	利用Ovastacin-mCherry转基因小鼠研究哺乳动物皮质颗粒的动态转运及调控机理						
	资 助 类 别	面上项目			亚 类 说 明			
	附 注 说 明	常规面上项目						
	申 请 代 码	C120202:卵巢功能与卵子成熟						
	基 地 类 别	23269002. 动物生理生化实验室						
	执 行 年 限	2016.01-2019.12						
	直 接 费 用	60万元			间 接 费 用	11.6万元		
	项 目 资 金	71.6万元						



项目摘要

中文摘要(500字以内):

多精受精是指超过一个精子进入卵子形成多个原核的异常受精形式,最终会导致早期胚胎死亡。卵子防止多精受精的机制主要与一种被称为皮质颗粒的特殊细胞器有关,它是存在于未受精卵母细胞皮质区的一层分泌囊泡。受精后,皮质颗粒释放其内容物至卵周隙,修饰细胞外基质以阻止多精受精。目前有关皮质颗粒成分和功能的认识主要来自于海胆等无脊椎动物,对哺乳动物的皮质颗粒知之甚少。最近,在小鼠中Ovastacin首次被鉴定为哺乳动物的皮质颗粒成分,负责受精后切割卵透明带中的精子受体ZP2来防止多精受精。本项目将利用Ovastacin作为皮质颗粒的标识物,构建Ovastacin-mCherry转基因小鼠,探索皮质颗粒在卵子成熟和受精中的转运及调控机制,阐明皮质颗粒转运和释放异常导致受精失败和引起多精受精的根本原因,并分离鉴定皮质颗粒的其它未知成分和功能,为全面了解哺乳动物皮质颗粒在生殖生物学和生殖医学中的意义提供研究基础。

关键词: 小鼠; 卵母细胞; 卵子成熟; 减数分裂; 卵子质量

Abstract(limited to 4000 words):

Polyspermy, an abnormal fertilization, forms multiple pronuclei by allowing more than one sperm entry into the eggs, which would cause early embryonic lethality. The block to polyspermy is related to a unique organelle called cortical granules located in the cortex of unfertilized oocytes. Following fertilization, cortical granules undergo exocytosis to release their contents into the perivitelline space, and then modify the extracellular matrix to prevent polyspermy. The previous studies on the cortical granules mainly originate from invertebrates such as sea urchin, little is known about contents and functions of mammalian cortical granules. Not till recently, Ovastacin has been firstly identified as one of the components of cortical granules in the mouse. Thus, the present project will establish an Ovastacin-mCherry transgenic mouse model, taking advantage of Ovastacin as the marker of cortical granules to investigate its dynamic trafficking and regulatory mechanisms during mouse oocyte maturation and fertilization, explicating the molecular basis regarding the fertilization failure and polyspermy caused by the aberrant translocation and exocytosis of cortical granules. Also, density gradient centrifugation coupled with fluorescence-activated cell sorting will be used to isolate and identify more contents of cortical granules to discover their extra functions in the reproduction, providing fundamental basis to learn the significance of mammalian cortical granules in the reproductive biology and medicine.

Keywords: Mouse; Oocyte; Oocyte maturation; Meiosis; Oocyte quality



项目组主要成员

编号	姓名	出生年月	性别	职称	学位	单位名称	电话	证件号码	项目分工	每年工作时间（月）	
1	熊波	1980.05	男	教授	博士	南京农业大学	025-84399605	360102198005295810	项目负责人	10	
2	侯艳君	1985.10	女	博士后	博士	南京农业大学	025-84399605	410603198510121529	皮质颗粒的分离与鉴定	10	
3	代小新	1988.01	女	博士生	硕士	南京农业大学	025-84399605	372923198801012921	显微注射、小鼠模型构建等	10	
4	张冕群	1991.02	女	硕士生	学士	南京农业大学	025-84399605	341002199102129429	载体构建、活细胞观察等	10	
总人数			高级		中级		初级		博士后	博士生	硕士生
4			1				1		1	1	



国家自然科学基金项目资金预算表（定额补助）

项目名称： 利用Ovastacin-mCherry转基因小鼠研究哺乳动物皮质颗粒的动态转运及调控机理

项目负责人：熊波

金额单位：万元

序号	科目名称	金额	备注
	(1)	(2)	(3)
1	一、项目资金支出	71.6000	/
2	（一）直接费用	60.0000	
3	1、设备费	2.0000	
4	（1）设备购置费	2.0000	购买一台计算机和一台小型离心机
5	（2）设备试制费	0.0000	
6	（3）设备改造与租赁费	0.0000	
7	2、材料费	34.0000	生化试剂、抗体、实验动物、培养试剂等
8	3、测试化验加工费	4.0000	激光共聚焦、活细胞工作站等设备使用费
9	4、燃料动力费	0.0000	
10	5、差旅费	3.0000	参加国内学术会议注册费、差旅费
11	6、会议费	0.0000	
12	7、国际合作与交流费	4.0000	参加国际学术会议费用
13	8、出版/文献/信息传播/知识产权事务费	3.0000	发表SCI论文版面费、彩图费
14	9、劳务费	10.0000	直接参加项目的研究生劳务费
15	10、专家咨询费	0.0000	
16	11、其他支出	0.0000	
17	（二）间接费用	11.6000	管理费、绩效支出等
18	其中：绩效支出	2.9000	绩效支出
19	二、自筹资金	0.0000	



预算说明书

(请对各项支出的主要用途和测算理由及合作研究外拨资金等内容进行详细说明, 可根据需要另加附页。)

- 1) 设备费2万元, 购买一台计算机约5000元用于数据分析, 一台小型离心机约15000元供分子生物学实验用。
- 2) 材料费34万元, 包括: 实验小鼠的繁殖和饲养费用4年约为100000元(学校收费为每只每日1元, 按平均100只算), 利用Crispr/Cas9制作小鼠模型约80000元(小鼠模型制作成本高), 小鼠基因型鉴定所需试剂和试剂盒20000元(小鼠尾巴裂解液, Tag酶, DNA提取试剂盒等), 4年所需抗体约10支30000元(不同目的蛋白抗体以及各种marker级抗体), 制作用于显微注射的mRNA和sgRNA所需的载体、限制性内切酶等分子克隆试剂和各种试剂盒约40000元, 4年所需基因测序和引物合成费用20000元, 小鼠卵母细胞培养试剂和一次性消耗器材如培养皿等约50000元。
- 3) 测试费、差旅费共7万元, 包括: 大型公用仪器如激光共聚焦显微镜、活细胞工作站等使用费(学校内部使用费40元, 由于活细胞工作站需要长时间连续观察, 每年大约需要使用250小时, 4年费用为 $40 \times 250 \times 4 = 40000$ 元)。带领一至两名学生参加三次国内会议, 所需注册费10000元、差旅费20000元, 共30000元。
- 4) 国际合作费、出版费共7万元。发表3篇SCI论文所需的彩图费和版面费约30000元(每篇SCI论文版面和彩图费平均约为1500美元)。国际交流合作费约4万元, 包括参加两次国际学术会议展示研究成果: 一次美国生殖生物学年会SSR, 一次亚洲繁殖生物技术大会ARBS, 两次合计40000元。
- 5) 剩余费用为支付劳务费10万元(3名研究生4年每个月800元补助, $3 \times 4 \times 10 \times 800 \approx 100000$ 元)和自动生成的间接费用11.6万元。

项目负责人签字:

科研部门公章:

财务部门公章:



报告正文

研究内容和研究目标按照申请书执行。



国家自然科学基金资助项目签批审核表

	<p>我接受国家自然科学基金的资助，将按照申请书、项目批准意见和计划书负责实施本项目（批准号：31571545），严格遵守国家自然科学基金委员会关于资助项目管理、财务等各项规定，切实保证研究工作时间，认真开展研究工作，按时报送有关材料，及时报告重大情况变动，对资助项目发表的论著和取得的研究成果按规定进行标注。</p> <p>项目负责人（签章）： 年 月 日</p>	<p>我单位同意承担上述国家自然科学基金项目，将保证项目负责人及其研究队伍的稳定和研究项目实施所需的条件，严格遵守国家自然科学基金委员会有关资助项目管理、财务等各项规定，并督促实施。</p> <p>依托单位（公章） 年 月 日</p>					
本栏目由基金委填写	<p>科学处审查意见：</p>						
	<p>建议年度拨款计划（本栏目为自动生成，单位：万元）：</p>						
	年度	总额	第一年	第二年	第三年	第四年	第五年
	金额						
	<p>科学部审查意见：</p> <p>负责人（签章）： 年 月 日</p>						
本栏目主要用于重大项目等	<p>相关局室审核意见：</p> <p>负责人（签章）： 年 月 日</p>						
	<p>委领导审批意见：</p> <p>委领导（签章）： 年 月 日</p>						

江苏省科技项目合同

计划类别 基础研究计划（自然科学基金）--青年基金项目

项目编号 BK20150677

项目名称 哺乳动物皮质颗粒动态转运影响受精的机制研究

项目类别

起止年限 2015 年 7 月至 2018 年 6 月

项目负责人 熊波 电话及手机 15850502046 025-84399605

电话及手机

承担单位 南京农业大学

单位地址 南京市玄武区卫岗1号 邮政编码 210095

项目主管部门 南京农业大学

江苏省科学技术厅

二〇一五年

委托单位（甲方）： 江苏省科学技术厅

法定代表人： 王秦

地址： 南京市北京东路 39 号

邮政编码： 210008

承担单位（乙方）：

承担单位： 南京农业大学

法定代表人： 周光宏

地址： 南京市玄武区卫岗 1 号 邮政编码： 210095

项目负责人： 熊波

电话： 15850502046 传真：

电子邮件： kjcxmk@njau.edu.cn

保证单位（丙方、项目主管部门）： 南京农业大学

法定代表人（科技局局长）：

地址： 邮政编码：

甲方批准由乙方承担省科技计划《哺乳动物皮质颗粒动态转运影响受精的机制研究》项目的研究开发或建设任务。依据《中华人民共和国合同法》的规定，为明确甲、乙、丙三方的权利和责任，保证项目的顺利实施和科研经费的合理使用，签订本合同。

一、项目的目标和主要研究内容

要解决的主要技术难题和问题，项目研究的创新点和内容等。

- 1、利用微丝和微管的解聚剂，以及微丝成核因子和微管动力蛋白的抑制剂处理 Ovastacin-mCherry 转基因小鼠的卵母细胞，观察卵母细胞成熟过程中 mCherry 从胞质向皮质区的转运。
- 2、采用荧光漂白恢复术淬灭 Ovastacin-mCherry 在皮质区的荧光信号，实时记录信号的恢复情况，确定皮质颗粒在皮质区的定位是否是动态变化的。
- 3、利用细胞骨架解聚剂研究无皮质颗粒区的形成机制。
- 4、实时观察卵子受精后排放皮质颗粒的过程，确定皮质颗粒排放与卵子质膜及透明带对精子接受性的时空关系，以及实时记录卵子老化过程中皮质颗粒的动态变化，确定老化卵子中皮质颗粒提前释放与受精率下降的关系。

江苏省科学技术厅

二、项目验收内容和考核指标

包括 1、主要技术指标：如形成的专利、新技术、新产品、新装置、论文专著等数量、指标及其水平等；2、主要经济指标：如技术及产品所形成的市场规模、效益等；3、项目实施中形成的示范基地、中试线、生产线及其规模等；4、其他应考核的指标。

利用微丝和微管的解聚剂，以及微丝成核因子和微管动力蛋白的抑制剂处理 Ovastacin-mCherry 转基因小鼠的卵母细胞，观察卵母细胞成熟过程中 mCherry 从胞质向皮质区的转运。采用荧光漂白恢复术淬灭 Ovastacin-mCherry 在皮质区的荧光信号，实时记录信号的恢复情况，确定皮质颗粒在皮质区的定位是否是动态变化的。利用细胞骨架解聚剂研究无皮质颗粒区的形成机制。实时观察卵子受精后排放皮质颗粒的过程，确定皮质颗粒排放与卵子质膜及透明带对精子接受性的时空关系，以及实时记录卵子老化过程中皮质颗粒的动态变化，确定老化卵子中皮质颗粒提前释放与受精率下降的关系。1、明确哺乳动物皮质颗粒在保证成功受精和防止多精受精中的具体作用和调控机理。2、利用皮质颗粒作为衡量卵子质量的标准，设计和开发卵子质量评估试剂盒。3、在生殖生物学领域的国际知名期刊发表 SCI 学术论文 2-3 篇。4、推动和改善体外受精技术以及冷冻卵子技术。5、参加国际会议展示相关研究成果。6、培养研究生 2-3 名。

江苏省科学技术厅

三、项目进度及考核指标

时 间	考核指标
2015 年 7 月 至 2016 年 6 月	繁殖 Ovastacin-mCherry 转基因小鼠，确定 Ovastacin-mCherry 转基因的功能性；以活细胞成像平台为基础，利用细胞骨架抑制剂深入探究皮质颗粒的转运和释放过程及机制，以及对受精或多精受精的影响；
2016 年 7 月 至 2017 年 6 月	采用荧光漂白恢复术确定皮质颗粒在皮质区的动态变化。利用微丝、微管解聚剂，以及脂类运动抑制剂确认影响其动态定位的因素；利用显微注射结合活细胞成像探明无皮质颗粒区形成的分子基础以及在受精过程中所起的作用。
2017 年 7 月 至 2018 年 6 月	实时观察卵子受精后排放皮质颗粒的过程，确定皮质颗粒排放与卵子质膜及透明带对精子接受性的时空关系。同时观察皮质颗粒排放被抑制后卵子质膜及透明带对精子的接受性；实时记录卵子老化过程中皮质颗粒的动态变化，确定老化卵子中皮质颗粒提前释放与受精率下降的关系；撰写论文并投稿。

四、项目承担单位、参加单位及主要研究开发人员

[illegible]

五、项目经费预算

(一) 项目经费来源预算

经费单位：万元

	合计	2015 年	2016 年	2017 年	备注
合计	20				
1、省拨款	20	20	0		
2、部门、地方配套	0				
3、承担单位自筹	0				
4、其他来源	0				

(二) 项目经费支出预算

经费单位：万元

	预算数	其中：省拨款	备注
(一) 直接费用	17	17	
1、设备费	1	1	
(1) 购置设备费	1	1	购买一台计算机和一台数码相机
(2) 试制设备费	0	0	
(3) 设备改造与租赁费	0	0	
2、材料费	8	8	生化试剂、抗体、实验动物、培养试剂等
3、测试化验加工费	2	2	激光共聚焦、活细胞工作站等设备使用费
4、燃料动力费	0	0	
5、差旅费	2	2	参加国内学术会议注册费、差旅费
6、会议费	0	0	
7、国际合作与交流费	0	0	
8、出版/文献/信息传播/知识产权事务费	2	2	发表 SCI 论文版面费、彩图费
9、劳务费	2	2	直接参与项目的研究生劳务费

10、专家咨询费	0	0	
11、其他支出	0	0	
(二) 间接费用	3	3	管理费、绩效支出等
其中：绩效支出	0.8	0.8	绩效支出
合计	20	20	

六、其他条款

(一) 缔约各方的权利、义务

第一条 缔约各方均应共同遵守国家、省有关科技计划与经费管理的规定，严格遵守并认真履行本合同的各项条款。

甲方应按合同约定的金额提供项目研究开发经费，有权监督、检查合同履行情况。合同履行期间，甲方有权直接组织或委托丙方检查、监督乙方对本合同的履行情况。乙方完成项目研究开发任务后，由甲方负责进行验收。

乙方应严格履行合同义务，为项目实施提供承诺的技术与条件保障，以及财务管理、成果管理、科技档案管理服务合同约定的其他义务。项目申请验收前乙方应按照规定提交科技报告，未提交科技报告的项目不予验收。乙方应加强项目实施成果的转化，自项目验收后一年内未实施转化的项目，甲方有权责成乙方将成果交省内技术产权交易机构挂牌转让。

丙方应按合同约定的金额提供项目配套经费，并进行相关的协调和监督。

第二条 甲方有权根据乙方项目计划进度完成情况决定是否拨付后续经费。乙方使用项目经费应按照合同约定的支出范围执行，保证专款专用，并实行单独核算，严禁弄虚作假、截留和挪用项目经费等违反财经纪律的行为。

第三条 甲、乙、丙各方对项目合同及其他技术资料负有保密责任。

(二) 违约责任

第四条 甲方未能按合同约定的经费数提供经费，导致乙方研究开发工作延误的，应允许合同规定的研究开发工作完成期限相应顺延。

第五条 因乙方原因，导致研究开发工作未能达到合同约定指标的，乙方应采取措施尽快使项目达到合同预定要求，并承担由此而增加的费用。

第六条 乙方无正当理由未履行合同时，甲方有权停拨、追缴部分或全部省拨经费，由此造成的经济损失由乙方承担。对乙方在申报和实施项目中的失信行为，甲方将根据省科技信用管理的有关规定记入不良信用记录，并报送至省公共信用信息平台，列入乙方的社会信用记录。

第七条 乙方违反经费使用规定或经甲方检查确认计划进度不符合合同约定的，甲方有权减拨或停拨后续经费；情节严重的，甲方有权终止合同，乙方应返还甲方已拨付的全部经费。

第八条 乙方因不可抗力不能履行合同义务时，可以免除违约责任，但应及时通知甲、丙方，并在合理的期限内出具因不可抗力导致合同不能履行的证明。

第九条 在履行本合同过程中，确因在现有水平和条件下难以克服的技术困难，导致研究开发部分或全部失败造成损失的，经甲方确认风险责任后，甲方在其拨款额度范围内承担损失。

（三）合同的变更、解除和争议解决

第十条 合同的变更或解除，须经缔约各方协商一致，并签署书面文件。

第十一条 发生下列情况之一的，缔约方应当协商变更或解除合同：

（1）由于不可抗力或意外事故导致合同无法履行或部分无法履行；

（2）由于项目目标已被他人先行实现，有关成果已被申请专利或公开，继续履行合同已无必要；

（3）由于乙方未按合同要求履行合同，或是由于其他原因，导致项目在检查或评估中被淘汰的。

第十二条 合同一方发生合并、分立或更名时，由变更后的单位继受或分别继受变更一方在合同中的权利义务。

第十三条 合同在履行过程中发生争议的，缔约各方应通过友好协商的方式解决。如协商不成时，缔约各方有权向人民法院起诉或仲裁机构申请仲裁，但在有关司法、仲裁结果生效之前，乙方有义务按照甲方要求继续履行或终止履行本合同。

（四）附 则

第十四条 项目任务书、可行性论证报告作为合同附件。项目如涉及多家（包含两家）单位参加，乙方应在签订本合同前与有关单位就合作任务和知识产权分配等问题签订有关合同或协议（仅委托其他单位进行常规试验、提供社会化科技服务和少量辅助科研工作的情况除外），同时作为本合同的附件。

第十五条 有关合同的未尽事宜，按照国家、省有关科技计划与经费管理的规定执行。

第十六条 本合同正本一式六份（甲、乙、丙方各执2份），自缔约各方签章后生效。

第十七条 本合同的解释权归甲方享有。

七、附加条款

第十八条 省自然科学基金青年基金项目负责人在申报该类项目前，必须是未主持承担过省级或国家级科技计划项目（含国家自然科学基金项目）。否则，一经发现，按弄虚作假处理，取消该项目立项，并追究项目负责人、承担单位和科技主管部门责任。



江苏省科学技术厅

八、签订合同各方

甲方：

法定代表人或委托代理人（签字）

项目主管处室负责人（签字）

项目主管处室经办人（签字）

公 章

年 月 日

乙方：

承担单位法定代表人或委托代理人（签字）

项目负责人（签字）

公 章

开户银行、帐号

年 月 日

丙方：

法定代表人或委托代理人（签字）

公 章

年 月 日

说明：

1、本合同适用于省基础研究、科技支撑、科技基础设施、苏北发展、国际科技合作、软科学研究等计划。

2、合同条款中所有空项都需如实填写，确无此项的，请在该栏中打“/”或在空白处写“无”。

3、乙方盖章必须是单位公章，部门章无效。



江苏省科学技术厅